Trepça Yeraltı Ocağında Dolgulu Tavan Arınlı Ayak Yönteminde Üretim Topuklarının Duraylılığının Değerlendirilmesi

Gzim Ibishi

DOKTORA TEZİ

Maden Mühendisliği Anabilim Dalı

Mart 2019

Stability Assessment of Post Pillars in Cut-and-Fill Stoping Method at Trepça Underground Mine

Gzim Ibishi

DOCTORAL DISSERTATION

Department of Mining Engineering

March 2019

Stability Assessment of Post Pillars in Cut-and-Fill Stoping Method at Trepça Underground Mine

A thesis submitted to the Eskişehir Osmangazi University
Graduate School of Natural and Applied Sciences in partial
fulfillment of the requirements for the degree of Doctor of Philosophy
in Discipline of Mining of the Department of Mining Engineering
by
Gzim Ibishi

Supervisor: Prof. Dr. Mahmut Yavuz

This thesis was supported by ESOGU BAP within the framework of the project no.
``201715A238``

March 2019

APPROVAL OF THE THESIS

The thesis titled “Stability Assessment of Post Pillars in Cut-and-Fill Stoping Method at Trepça Underground Mine” and submitted by Gzim Ibishi has been accepted as satisfactory in partial fulfillment of the requirements for the degree of DOCTOR OF PHILOSOPHY in Department of Mining Engineering.

Supervisor **:** Prof. Dr. Mahmut Yavuz

Co-Supervisor **: -**

Examining Committee Members:

Member: Prof. Dr. Mahmut Yavuz

Member: Prof. Dr. Adnan Konuk

Member: Prof. Dr. Yasin Dursun Sarı

Member: Prof. Dr. Melih Geniş

Member: Prof. Dr. Melih İphar

Graduation of Gzim Ibishi was approved by the Graduate School Board Decision on............................ with the decision number of ....

Prof. Dr. Hürriyet ERŞAHAN
Director of the Institute

ETHICAL STATEMENT

I hereby declare that this thesis study titled “Stability Assessment of Post Pillars in Cut-and-Fill Stoping Method at Trepça Underground Mine” has been prepared in accordance with the thesis writing rules of Eskişehir Osmangazi University, Graduate School of Natural and Applied Sciences under academic consultancy of my supervisor Prof. Dr. Mahmut Yavuz. I hereby declare that the work presented in this thesis is original. I also declare that, I have respected scientific ethical principles and rules in all stages of my thesis study, all information and data presented in this thesis have been obtained within the scope of scientific and academic ethical principles and rules, all materials used in this thesis which are not original to this work have been fully cited and referenced, and all knowledge, documents and results have been presented in accordance with scientific ethical principles and rules. 11/04/2019

Gzim Ibishi

Signature

ÖZET

Sert kaya madenciliğinde, derin yeraltı açıklığı duraylılığının belirlenmesi kaya mekaniği tasarımlarında en önemli hususlardan biridir. Çok derin yeraltı ocaklarındaki madencilikle ilişkili duraylılık kavramı, maden mühendisleri ve araştırmacılar için daima bir araştırma konusu olmuştur. Bu durum, yerindeki arazi gerilmelerinin oldukça yüksek olmasından ve kaya kütlelerinin jeolojik anlamda oldukça karmaşık bir yapıya sahip olmasından kaynaklanmaktadır. Derin yeraltı kazılarında da (cevher üretimi yapıldıktan sonra açılan boşluklar gibi), açıklıkların etrafını çevreleyen kaya kütlelerindeki gerilmelerin neden olduğu duraysızlık problemleri ile karşılaşılabilmesi oldukça muhtemeldir. Söz konusu gerilmeler kaya kütlesinin dayanımını aştığında yenilmeler, kaya düşmeleri ve kavlaklanma gibi duraysızlık problemleri ile karşılaşılmaktadır. Bu nedenle; topukların üretilmesinde karşılaşılabilecek bu tür problemler, iş sağlığı ve güvenliği anlamında tehlikeli bir çalışma ortamının meydana gelmesine neden olmakta ve madencilik faaliyetlerinin aksamasına, yeraltı ekipmanlarının ve makinaların hasarlanmasına ve istenmeyen ölümcül olayların meydana gelmesine yol açmaktadır.

Bu çalışma kapsamında; üç boyutlu sayısal modelleme ve analiz sonuçları dikkate alınarak, değişen kazı yüksekliğine bağlı olarak en fazla kazı yüksekliğinin ve en düşük üretim topuğu boyutlarının belirlenmesi konusu araştırılmıştır. Tavan arınlı ayak ya da “kes ve doldur (*cut-and-fill*)” yeraltı üretim yönteminde tavan kontrolü genellikle üretim topukları yardımıyla sağlanır. Kalın cevher damarlarında uygulanan bu yeraltı üretim yönteminde, üretim topukları ocağın genel duraylılığında oldukça büyük bir öneme sahiptir. Bu araştırmada, kazı yüksekliği ve derinliğine göre statik yükleme koşulları altında üretim topuklarının duraylılıklarının belirlenmesi ve topuk davranışlarının anlaşılması üzerine yoğunlaşılmıştır. Kes-doldur yeraltı üretim yönteminin sayısal modeli FLAC^{3D} yazılımı kullanılarak oluşturulmuş, açılan açıklıkların etrafında ve üretim topuklarında meydana gelen en büyük asal gerilmelerin dağılımları ile yenilme zonları incelenmiştir. Üretim topuklarının, ilk kazı aşamasında geniş yenilme zonları oluşmayacak şekilde tasarlanması gerektiği sonucuna varılmıştır.

Ayrıca, üretim topuklarının duraylılıklarının belirlenmesinde kullanılabilecek Topuk Yenilme Oranı (PYR) gibi yeni bir indeks ile birlikte Topuk Duraylılık Grafiği (PSG) geliştirilmiştir. Önerilen bu yeni indeks ve grafik kullanılarak; Trepça Yeraltı Ocağındaki üretim topuklarının duraylılıkları ile ilgili duraylı, potansiyel olarak duraysız ve yenilmiş topuk durumları arasındaki sınır çizgi belirlenebilmektedir.

Anahtar kelimeler: Duraylılığın belirlenmesi, yeraltı kazıları, sert kaya madenciliği, üretim topuğu tasarımı, FLAC^{3D}.

SUMMARY

Stability assessment of deep underground excavations in hard rock mines is one of the most important issues in rock engineering design. Stability issues correlated with mining at great depth below the ground surface has become a challenge for researchers and engineers due to presence of high in situ stress state and complexity of geological rock mass conditions. Deep underground excavations (e.g. stopes) are more likely to suffer from ground falls since disturbed rock mass induce stresses which are usually high enough to exceed the strength of the rock mass causing failures which might be manifested in the form of rock fall and spalling. Hence, rock falling and/or spalling might affect the overall safety in production stopes causing of fatalities, damage of underground equipment and machinery, and cause delays to mining operations.

Within the scope of this thesis, the maximum mine excavation height and minimum required dimensions of post-pillar have been investigated varying mine excavation depth based on 3D numerical modeling and analysis. The support of overhand cut-and-fill stoping method is mainly provided by post-pillars. Post-pillars have great influence on overall stope stability in thick ore bodies. This research focuses on post-pillar stability assessment under static loading conditions to understand pillar behavior with respect to mine excavation height and depth. Numerical modeling of the whole mining method is simulated using FLAC^{3D} code, investigating extent of failure zones and distribution of maximum principal stresses around excavated stopes and in post-pillars. Design of post-pillars should be done in such a way that failure does not take place at the first excavation stage. A new assessment index i.e. Pillar Yield Ratio (PYR) and Pillar Stability Graph (PSG) investigating stability of post-pillars has been developed. Here, the objective is to determine a border line between stable, potentially unstable, and failed state of post-pillars at a specific mine site (e.g. Trepça Underground Mine).

Keywords: Stability assessment, underground excavations, hard rock mine, post-pillar design, FLAC^{3D}.

ACKNOWLEDGMENT

I would like to thank my committee members Prof. Dr. Adnan Konuk, Prof. Dr. Yasin Dursun Sarı, Prof. Dr. Melih Geniş and Prof. Dr. Melih İphar for serving as my committee members and letting my defense be a pleasant moment and for their useful critiques of this research work and suggestions.

My deep and sincere gratitude goes to my supervisor Prof. Dr. Mahmut Yavuz for his excellent and continuous guidance, patience, motivation, and friendly behavior. His guidance helped me in all the time of the research and writing of this thesis.

I would like to thank Prof. Dr. Melih Geniş for his continuous help, constructive criticism, enthusiastic encouragement, valuable advice and assistance during numerical modeling stage. It would be almost impossible to complete this task without his contribution. Great and useful knowledge he has shared with me, for his trust and friendship.

I am thankful to the Department of Mining Engineering at Zonguldak Bülent Ecevit University for their permission to use FLAC^{3D} software during my thesis.

I would like to express my gratitude and thanks to Yurtdışı Türkler ve Akraba Topluluklar Başkanlığı (YTB) of the Republic of Turkey and ESOGU BAP Project providing financial support to finish successfully my doctoral studies at ESOGU in Turkey.

Last but not the least, my special and the biggest thank you goes to my kind parents Rizah and Shaha, to my brother Zeqir and to my lovely fiancée Njomza for their sacrifice, patience, courage, motivation and support during my PhD research.

LIST OF CONTENTS

Page

ÖZET .... **vi**
SUMMARY .... **vii**
ACKNOWLEDGMENT .... **viii**
LIST OF CONTENTS .... **ix**
LIST OF FIGURES .... **xi**
LIST OF TABLES .... **xiv**
LIST OF ABBREVIATIONS AND SYMBOLS .... **xvi**
1. INTRODUCTION AND PURPOSE **1**
2. LITERATURE REVIEW **5**
  2.1. Introduction 5
  2.2. A Brief Review on the Effect of Dynamic Loading Conditions 10
  2.3. A Brief Review on Stope and Post-Pillar Stability Assessment 14
  2.4. Conclusion 19
3. MATERIALS AND METHODS **20**
  3.1. General Background of Trepça Underground Mine 20
    3.1.1. Geological settings 21
    3.1.2. Geotechnical studies 25
      3.1.2.1. Rock material properties 25
      3.1.2.2. Rock mass classification and characteristics 26
      3.1.2.3. Estimation of rock mass properties 32
  3.2. Current Mining Method at Trepça Underground Mine 39
  3.3. Reassessment of Underground Mining Method at Trepça Mine 42
    3.3.1. Multiple criteria decision-making techniques in mining 45
      3.3.1.1. The analytic hierarchy process (AHP) methodology 45
      3.3.1.2. The fuzzy multiple attribute decision making (FMADM) methodology .. 47
  3.4. Numerical Methods Applied in Mining Engineering 49
  3.5. Numerical Modeling - FLAC^{3D} 51
    3.5.1. Mining sequence simulation 53
  3.6. Numerical Analysis of Cut-and-Fill Stoping Method 62
    3.6.1. Post-pillar design for overhand cut-and-fill stoping method 62

LIST OF CONTENTS (continued)

Page

3.6.2. Rock mass properties......62
3.6.3. In situ stress state......63
3.6.4. Mesh and boundary conditions......63
4. RESULTS AND DISCUSSION......64
4.1. Assessment of Rock Mass Damage due to Blasting......64
4.1.1. Blast vibration measurements and predictor equation......65
4.1.2. Extrapolation of the far-field PPV predictor equation......67
4.1.3. The assessment of maximum charge per delay......69
4.2. Post-Pillar Performance Assessment Index......69
4.2.1. Development of failure zones......69
4.2.2. Pillar Yield Ratio (PYR)......70
4.3. Numerical Analysis Results......74
4.3.1. Stability assessment of post-pillars at different mine excavation heights using hydraulic fill material......76
4.3.2. Stability assessment of post-pillars at different mine excavation heights using cemented rock fill material......78
4.3.3. Stability assessment of post-pillars at different mine excavation depths using hydraulic filling material......81
4.3.4. Stability assessment of post-pillars at different mine excavation depths using cemented rock fill material......83
5. CONCLUSION AND RECOMMENDATIONS......87
5.1. Recommendations for Future Work......88
5.2. Statement of Contributions......89
REFERENCES......90
APPENDIXES......102
APPENDIX –A......103
APPENDIX –B......113
APPENDIX –C......117

LIST OF FIGURES

Figure **Page**

2.1. Outline flowchart for mine design (Brady and Brown, 2007) 6
2.2. Flowchart for rock mechanics modeling (Hudson and Feng, 2007) 7
2.3. Blast-induced spalling close to blast source (Zhang, 2017) 11
2.4. Span definition (Hughes et al., 2017) 16
2.5. Updated Span Design Curve. Based on 292 observations (Wang et al., 2000) 17
2.6. Underground Pillar Stability Graph.178 observations. (Lunder, 1994) 18
3.1. Locations of study area of Trepça mine 21
3.2. Geological settings of Vardar zone and Trepça mineralization belt (Hyseni et al., 2010) 22
3.3. a) Longitudinal geological cross-section of central ore body illustrating associated b) Surface geological map of the Trepça mineral deposit hanging wall and footwall rock formations (after Forgan, 1936) 24
3.4. Geological factors influencing the engineering behavior of a rock mass (Villaescusa, 2014) 27
3.5. Rock mass characterization based on Geological Strength Index (Hoek, 2007) 31
3.6. Overhand cut-and-fill stoping method layout (Atlas Copco, 2007) 39
3.7. Post-pillar and overhand cut-and-fill stoping method layout (Atlas Copco, 2007) 40
3.8. Hydraulic backfilling being poured in the mined-out stope at TUM 41
3.9. Basic explicit calculation cycle in FLAC (Itasca, 2005) 52
3.10. Typical post-pillar and overhand cut-and-fill stoping method a) Longitudinal cross-section of central ore body, b) cross-section of the ore body I-I, c) cross-section of the ore body II-II. Not to scale 54
3.11. Schematic representation of rock falling of blocks from the sidewalls and back of the stope in central ore body at TUM 55
3.12. Rock falling of blocks from the back of the stope close to post-pillar in central ore body at a mining depth of 693 m 56

LIST OF FIGURES (continued)

Figure **Page**

3.13. Rock falling of blocks from the back of the stope in central ore body at a mining depth of 693 m 57
3.14. Hydraulic fill – Model 1 (O'Toole et al., 2011) 58
3.15. Cured cemented rock fill– Model 2 (Dorricott and Grice, 2002) 59
3.16. Numerical modeling of central ore body at TUM. a) represent half of the model in y-direction, b) represent front view model in y-direction....60
4.1. Micromate® and triaxial geophone....65
4.2. Blast vibration predictor for blast at Trepça underground mine....67
4.3. Extrapolated PPV values with varying distances....68
4.4. A few cubic meters of rock fallen of block from the roof of the stope due to rock blasting at TUM 68
4.5. Post-pillar model cross-section view. a) Post-pillar plan view – CC, b) Post-pillar side view – BB, c) Post-pillar front view – AA....71
4.6. Pillar Stability Graph (PSG) for Trepça Underground Mine (TUM) 73
4.7. Case study post-pillar assessment based on maximum principal stress obtained from numerical analysis FLAC^{3D} 74
4.8. FLAC^{3D} numerical model setup of post-pillar and overhand cut-and-fill stoping method. a) three-dimensional perspective view of the stope and post-pillars with delayed backfill, b) two-dimensional cross section view of the modeled stope and post-pillars with delayed backfill....75
4.9. Extent of failure zones with modeling mine excavation height and delayed backfill (e.g. hydraulic fill material). a) mine excavation height is 4 m, b) mine excavation height is 8 m, and c) mine excavation height is 12 m 77
4.10. Mine excavation height vs. extent of failure zones in post-pillars using hydraulic fill material 78

LIST OF FIGURES (continued)

Figure **Page**

4.11. Extent of failure zones with modeling mine excavation height and delayed backfill (e.g. cemented rock fill material). a) mine excavation height is 4 m, b) mine excavation height is 8 m, and c) mine excavation height is 12 m.............................79

4.12. Mine excavation height vs. extent of failure zones in post-pillars using cemented rock fill material...80

4.13. Extent of failure zones in post-pillars with modeling mine excavation depths and delayed backfill (e.g. hydraulic fill material). a) mine excavation depth is 453 m, b) mine excavation depth is 573 m, c) mine excavation depth is 693 m, d) mine excavation depth is 813 m, e) mine excavation depth is 933 m 82

4.14. Mine excavation depth vs. extent of failure zones in post-pillars using hydraulic fill material 83

4.15. Extent of failure zones in post-pillars with modeling mine excavation depth and delayed backfill (e.g. cemented rock fill material). a) mine excavation depth is 453 m, b) mine excavation depth is 573 m, c) mine excavation depth is 693 m, d) mine excavation depth is 813 m, e) mine excavation depth is 933 m 84

4.16. Mine excavation depth vs. extent of failure zones in post-pillars using cemented rock fill material...85

LIST OF TABLES

Table **Page**

2.1. Summary of the main rock engineering design methodologies used in mining applications (Cepuritis, 2010; Pakalnis, 2015 and Hughes et al., 2017)........................8
2.2. Peak Particle Velocity criterion for blast-induced damaged 12
3.1. Mechanical and physical properties of the rock materials for different geological rock units at TUM (modified from Hetemi, 2013) 26
3.2. RMR values of hanging wall (e.g. volcanic breccia), ore body (e.g. sulfide mineralization), and footwall (e.g. limestone)...28
3.3. Q values of hanging wall (e.g. volcanic breccia), ore body (e.g. sulfide mineralization), and footwall (e.g. limestone) 29
3.4. GSI values for hanging wall (e.g. volcanic breccia), ore body (e.g. sulfide mineralization), and footwall (e.g. limestone)...30
3.5. Rock mass classification ratings for TUM 32
3.6. List of empirical equations for determining deformation modulus of the rock mass (Geniş et al., 2007; Basarir et al., 2010; Geniş and Çolak, 2015 and Hughes et al., 2017)..33
3.7. Calculated rock mass deformation modulus...35
3.8. List of empirical equations for determining strength of the rock mass (Genis et al., 2007; Basarir et al., 2010; Geniş and Çolak, 2015 and Hughes et al., 2017)...............36
3.9. Calculated strength of the rock mass..38
3.10. Geotechnical properties of rock mass for different geological rock units at TUM 38
3.11. Classification of underground mining methods (Tatiya, 2005) 43
3.12. Pair-wise comparison scale for AHP (Saaty, 1980)...46
3.13. Random indices of randomly generated reciprocal matrices (Saaty, 2000) 47
3.14. The advantages and disadvantages of numerical methods (Hoek et al., 1991) 50
3.15. Mechanical properties of hydraulic filling (Naung et.al. 2018; Abdellah, 2015).......57
3.16. Mechanical properties of cemented rock filling (Abdellah et al., 2012; Yang et al., 2015; Emad 2017; Deng 2017; Naung et al., 2018; Zhou et al., 2019)......................58

LIST OF TABLES (continued)

Table **Page**

3.17. Mining stages and sequences carried out in numerical modeling.............................61
3.18. In situ stress state for numerical modeling 63
4.1. General specification of triaxial geophone(www.instantel.com) 65
4.2. Blast vibration monitoring details at Trepça underground mine 66
4.3. Maximum allowable charge per delay with distance...69
4.4. Pillar Yield Ratio (PYR) classification index..72
4.5. Stoping design parameters...72
4.6. Extent of failure zones in post-pillars at different mine excavation heights using hydraulic fill material 77
4.7. Extent of failure zones in post-pillars at different mine excavation height using cemented rock fill material...80
4.8. Extent of failure zones in post-pillars at different mine excavation depth using hydraulic fill material 82
4.9. Extent of failure zones in post-pillars at different mine excavation depth using cemented rock fill material...85

LIST OF ABBREVIATIONS AND SYMBOLS

Symbols	**Descriptions**
γ	Unit weight of rock
E_i	Deformation modulus of rock material
E_{mass}	Deformation modulus of rock mass
c_i	Cohesion of rock material
c_{mass}	Cohesion of rock mass
ϕ_i	Internal friction angle of rock material
ϕ_{mass}	Internal friction angle of rock mass
ν_i	Poisson’s ratio value of rock material
ν_{mass}	Poisson’s ratio value of rock mass
s, a	Hoek-Brown rock mass constants
σ_{ci}	Uniaxial compressive strength of rock material
σ_{cmass}	Uniaxial compressive strength of rock mass
σ_{ti}	Tensile strength of rock material
σ_1	Principal stress
σ_{tmass}	Tensile strength of rock mass
P_v	Vertical in situ stress
P_h	Horizontal in situ stress
w_p	Pillar width
h_p	Pillar height
σ_{max}	Maximum principal stress
P_s	Pillar strength
K, α	Dynamic site specific constants
λ_{max}	Maximum Eigen value

LIST OF ABBREVIATIONS AND SYMBOLS (continued)

Abbreviations	**Descriptions**
AHP	Analytic Hierarchy Process
CRF	Cemented Rock Fill
CPF	Cemented Paste Fill
CR	Consistency Ratio
CI	Consistency Index
FMADM	Fuzzy Multiple Attribute Decision Making
GSI	Geological Strength Index
HF	Hydraulic Fill
MADM	Multiple Attribute Decision Making
PPV	Peak Particle Velocity
PYR	Pillar Yield Ratio
PSG	Pillar Stability Graph
Q	Rock Quality Index
RI	Random Index
RMR	Rock Mass Rating
RQD	Rock Quality Designation
RSS	Rock Substance Strength
SD	Scaled Distance
SRF	Stress Reduction Factor
TUM	Trepça Underground Mine
USBM	United State Bureau of Mines
UBC	University of British Colombia
UMMS	Underground Mining Method Selection

1. INTRODUCTION AND PURPOSE

The exploitation of deeper mineral resources has become a crucial, tough and challenging task for geotechnical engineers to design a mining method in such a way that warns of consequences and instabilities in deep underground excavations (e.g. stopes), as mineral resources located at shallow depths have been already exploited all over the world. Mining accidents and fatal injuries occurring in deep underground production stopes are increasing from time to time and half of the related fatalities have been occurred due to rocks falling of blocks and spalling from the back of the stope and hanging wall or footwall. The cause of these failures can be from different origins such as the presence of high in situ stress state, large excavation geometry, poor design of post-pillars, and excessive vibration levels induced by blasting practices. Reducing mining accidents and fatal injuries still remain the major challenge in the mining industry.

In a study by Aydan et al. (1997), Martin et al. (2003) and Kulatilake et al. (2013) is concluded that stability assessment of deep underground excavations requires detailed information of in situ stress state and strength of the rock mass parameters. Deep underground excavations are more likely to suffer from ground control problems since disturbed rock mass induce stresses which are usually high enough to exceed the strength of the rock mass causing failures which might be manifested in the form of rock falling and spalling (Brady and Brown, 1985; Ortlepp and Stacey, 1994).

From the rock mechanics point of view, it is well known the fact that, as mining depth increases, the in situ stress state increase meaning that the rock mass is highly stressed in deeper production levels. Thus, this leads to a concern whether the stope could sustain stable or suffer from any potential rock failures affecting the safety to workers, damaging underground equipment and causing delays to mining operations. Rock failures can be restrained by applying different rock support systems used in production stopes (e.g. post-pillars, rock/cable bolting systems and backfilling materials) to prevent potential instabilities and, the degree of rock mass damage triggered by cyclic loading conditions (e.g. blasting source) must be investigated optimizing the charge weight per delay.

Rock falling is a big risk for deep hard rock mines. Rock falling of block occur after many successive blasts where the rock mass experiences cyclic loading making it weakened (e.g. rock mass strength become lower) and as a result of failure on discontinuities within the rock mass due to rock block structures failing under gravity when discontinuity boundaries become unstable (Kabongo and Bron, 1999; Zhang, 2017). Hence, rock falling in deep hard rock mines is mainly aggravated by blasting practices and stress concentration becomes more and more present in the post-pillars between. Therefore, providing a ground vibration predictor equation correlating the Peak Particle Velocity (PPV) and Scaled Distance (SD) enables practical assessment of rock mass damage due to blasting practices in deep hard rock mines. Additionally, optimization of stoping excavation height and dimensions of post-pillar when the stope has large geometry (i.e. strike length, width, and height), is necessarily required for preventing possible rock failures. In a study by Sjöberg (1993), it was noted that post-pillars in overhand cut-and-fill stoping method play a key role in the prevention of rock falling and spalling because it provides support to the roof of the stope and sidewalls, respectively.

Exploitation of mineral resources in central ore body at Trepça Underground Mine (TUM) with any condition leads to different stability problems. Serious ground control problems have been reported in recent years between levels +195 m and +15 m. There have been many cases reported of injuries and fatalities due to rock falling of blocks and spalling. Actually, this research is unique for the fact that more than 25 years not a single detailed study has been carried out to investigate stope and post-pillar stability. Thus, what makes unique this study is that numerous field measurements and investigations have been carried out till now to better understand the problem of rocks falling and spalling from back of the stope and sidewalls (e.g. hanging walls and footwalls). For modeling purposes, the mine excavation height adapted from mining practice at TUM is 12 m, the stope geometry is approximately 72 m in length, 48 m in width and 60 m in height, and mine excavation depth is 693 m below the ground surface.

The primary objective of this study is to characterize geological rock units surrounding the main ore body and ore body itself, then classify geological rock units based on rock mass classification systems such as Rock Mass Rating (RMR), Rock Quality

Index (Q) and Geological Strength Index (GSI) and determine geotechnical properties of rock mass for modeling purposes.

The second objective is to monitor blasting events and provide a ground vibration predictor equation correlating PPV and SD parameters for the mine site trying to get the answer, which charge weight per delay is much more likely to produce some damage in the rock mass (e.g. ore body) during ore recovery process. In this way, the potential risk of rock falling/spalling is practically assessed.

The third and the main objective of this research is to develop a new assessment index evaluating stability of post-pillars and pillar stability graph. This graph can be used by geotechnical engineers to evaluate post-pillar stability based mainly on maximum principal stress acting on the pillar to uniaxial compressive strength of intact rock ratio and pillar width to height ratio varying mine excavation height. Thus, the assessment index enables post-pillars to be classified into three groups, stable, potentially unstable and failure state.

This research has attempted for the first time to investigate the interaction of the excavation stage, post-pillar, and backfilling materials with respect to mining depth as a whole mining method modeled by FLAC^{3D} numerical modeling technique. Numerical analysis results are discussed in terms of expanded failure zones and maximum principal stress with respect to mine excavation height and mining depth.

The thesis is organized in 5 chapters, including this chapter which presents the importance of the proposed research, scope and objectives of the research and thesis outline.

Chapter 2, presents a general design process in rock engineering describing chronological essentials steps in mine design. Brief information on the effect of blasting induce-vibrations is summarized. Also, a brief review on stope and post-pillar stability assessment and factors affecting the stability were discussed.

Chapter 3, describes the general background, geological settings and geotechnical studies, and current mining method used at Trepça underground mine. Reassessment of current mining method used at Trepça underground mine using University of British Columbia (UBC) mining method selection tool and multiple criteria decision-making techniques. Finally, the numerical modeling and analysis of overhand cut-and-fill stoping method is described.

Chapters 4, presents blast field data collection and analysis, a new assessment index i.e. Pillar Yield Ratio (PYR) and Pillar Stability Graph (PSG) is practically illustrated based on numerical analysis.

Chapter 5, presents conclusion, recommendations for future work, and statement contribution of this thesis.

2. LITERATURE REVIEW

A brief literature review will be presented in a well-organized manner where several publications have been selected for review. A literature review is divided into three parts; Introduction, including the general overview of rock engineering design process. Body text includes literature review on the effect of dynamic and static loading conditions in deep hard rock mines. The last part is the conclusion, summarizing major contributions of studies and pointing out gaps.

2.1. Introduction

Rock engineering as a scientific discipline has made a significant contribution for solving of complex underground rock excavation problems in mining operations, including dimensions of deep underground excavations (e.g. stopes) and post-pillars, excavation sequences of stopes and evaluation of backfill strength parameters.

One thing should be kept in mind that underground excavations in mining engineering remarkably differ from underground excavations in civil engineering due to the nature of the structure. Where, structures in civil engineering and other fields alike are basically fixed, whereas, structures in mining engineering proceed along to develop during the whole life of the mine. Moreover, Brady and Brown (2007) provided a generalized outline for mine design comprises of five essentials steps such as; site characterization, mine model formulation, design analysis, rock performance monitoring and retrospective analysis, as shown in Figure 2.1. The objective of the first step is to determine geotechnical properties such as strength and deformability of rock, in-situ stress state and investigate the hydrogeology of the ore body and environment. The objective of the second step is to formulate a mining model based on data generated from site characterization. The objective of the third step is to predict underground excavation geometry and mechanical performance of the mining layout using numerical modeling techniques. The objective of the fourth step is to describe rock mass response to mining activity. Monitoring rock mass performance is enabled by the use of instruments.

And the last objective is the measurement of in situ rock mass properties and recognition principal modes of underground structure response. Even though the general design process in rock engineering recommended by Brady and Brown (2007) does not really equip with precise information data necessarily required in rock engineering design.

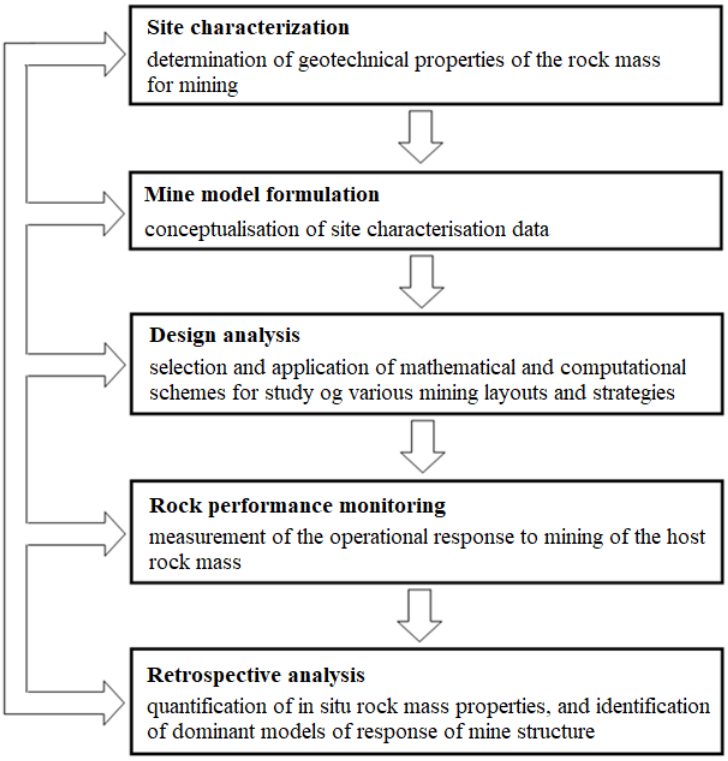
Site characterization
determination of geotechnical properties of the rock mass for mining
Mine model formulation
conceptualisation of site characterisation data
Design analysis
selection and application of mathematical and computational schemes for study og various mining layouts and strategies
Rock performance monitoring
measurement of the operational response to mining of the host rock mass
Retrospective analysis
quantification of in situ rock mass properties, and identification of dominant models of response of mine structure

Figure 2.1. Outline flowchart for mine design (Brady and Brown, 2007)

In a study by Hudson and Feng (2007) provided a flowchart for selecting a design methodology, as shown in Figure 2.2. The proposed flowchart helps to demonstrate that problems encountered in rock engineering might be evaluated using different methodologies. According to the authors, the modeling flowchart comprises of eight fundamental categories of modeling within the project objective, site investigation, design, and construction. The design methodology mainly increases in complexity from the left to the right i.e. Method A → Method B → Method C → Method D increase from simple to complicated. First three categories are broadly used in rock engineering design. Later on, in another study by Feng and Hudson (2010) is highlighted that at the beginning of the design stage is really important to have a look on these questions; how much information is needed and is that data enough for modeling in rock engineering design?

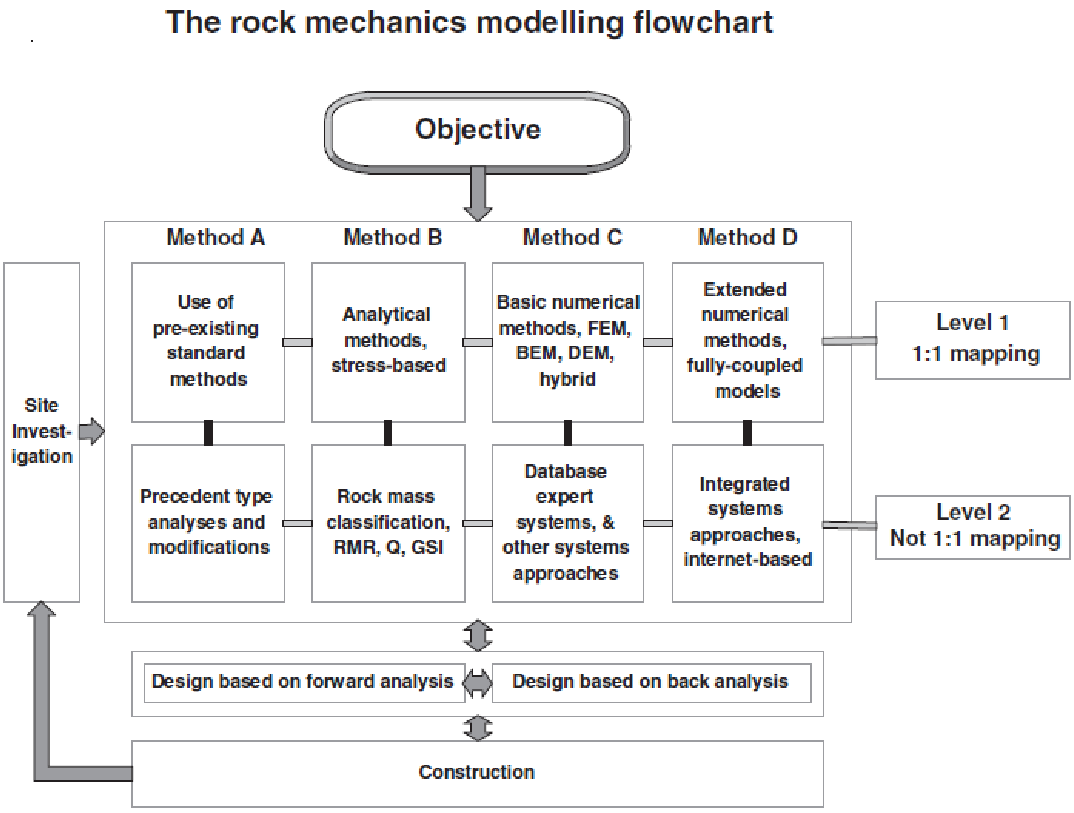
The rock mechanics modelling flowchart
Objective
Method A
Method B
Method C
Method D
Use of pre-existing standard methods
Analytical methods, stress-based
Basic numerical methods, FEM, BEM, DEM, hybrid
Extended numerical methods, fully-coupled models
Level 1 1:1 mapping
Site Invest-igation
Precedent type analyses and modifications
Rock mass classification, RMR, Q, GSI
Database expert systems, & other systems approaches
Integrated systems approaches, internet-based
Level 2 Not 1:1 mapping
Design based on forward analysis
Design based on back analysis
Construction

Figure 2.2. Flowchart for rock mechanics modeling (Hudson and Feng, 2007)

At the very beginning of underground rock excavation design, site investigation has to be carried out to characterize the rock mass. Also, in a study by Potvin et al. (2012) is noted that a detailed site characterization process is required to calculate the intrinsic properties of rock mass required in modeling stage.

Stability analysis and design of underground excavations in rock engineering can be assessed by applying different approaches as presented in Table 2.1. Analyzing deep underground complex problems by employing analytical methods are not the appropriate methods to be used. Such methods are applicable to simple geometric shapes (i.e. circular or elliptical), with the help of these analytical approaches are possible to determine stresses and strains around an underground opening (Brady and Brown, 2007). Stability assessment is one of the most important issues in mining ground control. Solving complex mining problems analytical methods are not adequate to provide a solution (Zhang and Mitri, 2008).

Table 2.1. Summary of the main rock engineering design methodologies used in mining applications (Cepuritis, 2010; Pakalnis, 2015 and Hughes et al., 2017)

Rock Engineering Design Methodologies	Empirical design methods	Rock mass characterization	Rock Quality Designation (RQD) Rock Mass Rating (RMR) Rock Quality Index (Q) Rock Mass index (RMi) Geological Strength Index (GSI)
		Mine stope stability graph Mine entry span stability Pillar stability Underhand cut-and-fill sill beam stability	
	Observational method	Monitoring rock mass performance	
	Analytical design methods	Classical stress analysis Voussoir beams Block theory	Closed-form solutions
	Numerical methods	Continuum methods	Finite Difference Method (FDM) Finite Element Method (FEM) Boundary Element Method (BEM)
		Discontinue methods	Discrete Element Method (DEM) Discrete Fracture Network (DFN)
		Hybrid continuum/discontinue methods	Hybrid FEM/BEM Hybrid FEM/DEM

A general methodology for stability assessment of an underground excavation design in mining engineering consists of input parameters, including geotechnical properties of an ore body and its host rock masses, information on in situ stress state, underground excavation geometry, and rock mass failure criteria.

Empirical methods have been widely used in many underground mines for design purpose. These methods are based on past experiences and rock mass classification system. Nowadays, empirical and numerical methods together have broadly been used in mine designs. Empirical design techniques are widely used in mining engineering due to the simplicity of use and well-suited to the initial design of underground excavation. Additionally; these techniques are developed based on experiences, reported and documented histories, and understanding fundamental concepts of rock mechanics. Empirical design techniques are based on an evaluation of the constitutive properties of rock masses (Hughes et al., 2017).

Numerical modeling techniques have successfully been used to investigate and solve complex mining and tunneling problems. Applying numerical techniques, it is possible to understand, assess geotechnical risks and generate practical solutions for concerned mining problems in an effective way. Also, numerical modeling techniques have been widely used to design all underground mining methods based on experience and empirical methods (Zhang and Mitri, 2008; Aksoy and Genis, 2010). Numerical modeling techniques are based on the constitutive behavior of rock mass including Heok-Brown and Mohr-Coulomb failure criteria (Hughes et al., 2017). Using the presented methods in Table 2.1 is possible to understand the response of any underground excavation designed in mining engineering.

Applying numerical modeling techniques, it is possible to investigate stope design parameters such as stope dimensions with respect to ore body geometry, in situ pillars, and stoping and backfilling sequences for safety conditions and effective mining operation. Optimal design for various stope conditions can be reached by assessing stresses, displacements, and yield zones (Himanshu and Kushwaha, 2015).

2.2. A Brief Review on the Effect of Dynamic Loading Conditions

In underground hard rock mines, drilling and blasting is the most common excavation technique and widely used due to its production efficiency and economic cost. Rock excavation by blasting operation produces vibrations which propagate through the rock mass in terms of seismic waves and reach out the free surface. Generally, in mining and tunneling engineering dynamic behavior of underground excavations has been investigated over the years in terms of Peak Particle Velocity (PPV), assessing the rock mass damage caused by rock blasting. Thus, the maximum ground particle velocity is indicated as the PPV and ground motions created by blasting are recorded with the help of seismographs (Dowding, 1985).

Rock mass damage due to blast-induced vibrations have been investigated over the years by different researchers. Rajmeny et al. (1995) investigated rock mass damage scale in an underground lead-zinc mine. The goal of this investigation was to monitor ground vibrations from blasting source to limit damage to main mine structures (e.g. main shaft, underground structures etc.). Also, rock damage was evaluated by visual observation and concluded that the extent of the rock damage decreases with increasing of distance from the blasting site. Kabongo and Bron (1999) investigated the rock falls in deep underground excavations and emphasized that rocks fall are generally exacerbated by blasting practices due to failure on discontinuities within the rock mass.

Rock damage occurs as a result of quality of rock mass and quantity of explosive detonates per delay. Drilling long holes are correlated with higher explosive charge per delay and hole, as well. Hence, contributing to roof rock damages in stopes. According to Caceres (2011), the higher the amount of explosives detonated per delay, the higher the effect of seismic vibration. Nateghi (2012) noted that two main parameters such as PPV and frequency are necessarily required to be known to determine the response of the rock mass due to blasting source. The level of ground vibrations caused by blasting load depends on rock medium, heterogeneity of rock mass at the site, distance from the blasting source, characteristics of wave propagation at a site, and dynamic characteristics of the rock.

Yugo and Shin (2015) assessed the influence of blast-induced seismic waves on adjacent mining excavations and concluded that decreasing the round length seems to be an effective way of limiting potential rock mass damage. In underground hard rock mines, many safety problems are linked to rock blasting (e.g. spalling and rock fall) directly or indirectly. According to Zhang (2017) blast-induced spalling occurs in the area close to blast source such as in the back of the underground excavations (e.g. stopes, tunnels), as seen in Figure 2.3. However, investigation of the local rock mass together with the blast design is strongly recommended. Because spalling could be more serious when blasting is not well designed.

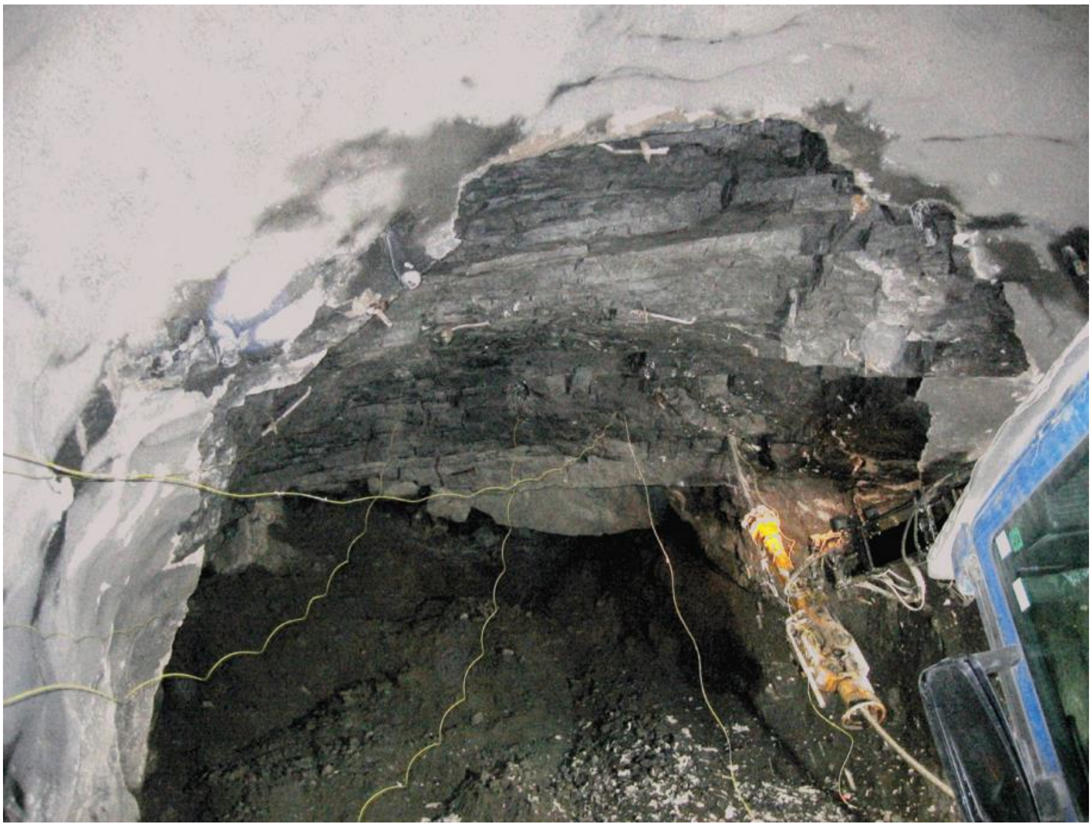

Figure 2.3. Blast-induced spalling close to blast source (Zhang, 2017)

The control of rock mass damage due to blasting source is very important when it comes to underground excavation design, safety and cost. Damage to the host rock mass due to a production blast could result in ground failures (e.g. rock spalling and/or rock fall) causing serious safety hazards and production losses. The main objective during ore exploitation process is to excavate only the desired profile of the ore as safely as possible leaving the rest of the ore with minor damages.

Hence, rock mass fails as a result of blast-induced crack increase and widening due to expanding gases. Knowing how far fractures will be created into the unexcavated rock mass is very important for blast engineer to design a safe recovery process. Being aware of the rock mass damage limit due to blasting will make safer and more productive mines and construction operations. Further, threshold levels of rock mass damage have been proposed by different researchers based on vibration measurements and extrapolation of the PPV predicators. Hence, a brief review of the proposed threshold levels is given in Table 2.2.

Table 2.2. Peak Particle Velocity criterion for blast-induced damaged

Researcher	PPV based damage estimation
Bauer and Calder (1970)	PPV < 254 mm/s – No fracturing occurred PPV of 254 – 635 mm/s – Minor tensile slabbing PPV of 635 – 2540 mm/s – Strong tensile/radial cracking PPV >2540 mm/s – Break up of rock mass occurred
Langerfors and Kihlström (1973)	PPV of 305 – 610 mm/s – New cracks and fall of rock respectively in unlined excavations (e.g. tunnels)
Holmberg and Persson (1979)	PPV of 700 – 1000 mm/s – Rock damage occur
Oriard (1982)	PPV > 635 mm/s – Rock damage occur
Rustan et al., (1985)	PPV of 1000 – 3000 mm/s – Rock damage occur
Meyer and Duun (1995)	PPV > 300 mm/s – Minor damage occur PPV of 600 mm/s – Rock damage occur
McKenizie and Holley (2004)	PPV > 700 mm/s – Intense damage PPV > 400 mm/s – Significant damage PPV > 350 mm/s – Open cracking PPV > 300 mm/s – Fine cracking in wall blasting
Silva et al., (2018)	PPV < 250 mm/s – No fracturing of intact rock PPV of 250 – 635 mm/s – Minor tensile slabbing occurs PPV of 635 – 2540 mm/s – Strong tensile/radial cracking occur PPV >2540 mm/s – The complete break up of rock mass occurred

In an effort to manage and decrease blast-induced rock mass damage, assessment of the extent of damage is extremely important. Hence, it is essential to survey the blast-induced rock mass damage prediction methods and correlate the extrapolated blast vibration measurements with actual overbreak. Providing the ground vibration propagation equation blast monitoring and measurement must be conducted. Blast-induced vibration data are meant to be collected regarding Peak Particle Velocity (PPV) values and Scaled Distance (SD) factor, as given in equation (2.1) and is widely used in the literature. The aim of SD is to monitor blasts at different distances and for different maximum charge per delay (Dowding, 1985).

$$\mathrm{SD} = \left(\frac{\mathrm{D}}{\sqrt{\mathrm{W}}}\right) \tag{2.1}$$

There are several PPV predictors used in the literature by many researchers, but the most broadly PPV predictor equation used is the one proposed by United States Bureau of Mines (USBM), as given in equation (2.2). Resende et al. (2014) have described the factors affecting the ground vibration. They said that the dominant outcome of the equation (2.2) is that requires a sufficient number of blasts records before it can offer statistically sound results and cannot cope with variables other than charge and distance, such as geological environment or excavation shape effects.

$$\mathrm{PPV} = \mathrm{K}(\mathrm{SD})^{-\alpha} \tag{2.2}$$

Where:

D, is the distance from the blast source
W, is the maximum charge weight per delay
K, α, are dynamic site constants.

In this research, the assessment of rock mass damage due to blasting has been briefly investigated. Reviewed published articles have been evaluated with a special care trying to understand rock mass damage due to blast-induced vibrations. Each published article presents a special importance to current problems in deep hard rock mines.

2.3. A Brief Review on Stope and Post-Pillar Stability Assessment

Due to the continuous exploitation of shallow mineral resources and with the growing demand for mineral resources for industrial needs, many metal mines are progressively turning to deep level mining. In some parts of the world, the mining depth varies approximately from 600 m to 4000 m below the ground surface. In South Africa, Tau Tona gold mine is a part of deep underground mines located at deep production levels with a maximum depth of 3456 m below the ground surface (Murphy, 2012). In China, metal mines are being exploited and constructed at an approximately 800 m depth below ground surface (Li et al., 2017). In Kosovo, Trepça underground mine is becoming part of deep underground mines in the world; currently, the production process is being carried out at an approximate depth of 800 m and is planning to extend to a depth of 1000 m below the ground surface (Hetemi, 2013).

Deep underground mines could suffer from serious ground control problems. Since disturbed rock mass induce stresses which are usually high enough to exceed the strength of the rock mass causing failures which might be manifested in the form of rock fall and spalling (Brady and Brown, 1985; Ortlepp and Stacey, 1994). Accordingly, it is necessary to carry out investigations to optimize stope production in stages concerning safety during exploitation of mineral resources. Stability of deep underground excavations is affected by several factors such; mechanical properties of the rock mass, geometrical properties of stoping, in situ stress state in rock mass and mining depth (Heidarzadeh et al., 2019).

During exploitation of an ore body in deep underground mines, the span of the stope excavation sometimes is as wide as the ore body it is. But in thick ore bodies for safety purposes, post pillars are left in situ to prevent any possible instability within the stope. Therefore, it is convenient to investigate the performance of stope boundary excavation and host rock mass during the excavation process in terms of magnitudes of displacements. Displacements in ore body and host rock mass are controlled by an increase of stress state around the support units. Ore bodies located at great depths are fully supported by pillars (Brady and Brown, 2007).

Stability of deep underground excavations relies upon several important factors such as geotechnical properties of rock masses, discontinuity rock properties, in situ stress state, excavation geometry and hydrological conditions (Chen et al., 1997). Numerical modeling techniques have successfully been used to evaluate the stability of concerning different problems (e.g. post-pillars, sill pillars, crown pillars, stoping and backfilling sequence etc.), for overhand cut-and-fill stoping method. Several studies on numerical modeling for cut-and-fill stoping method are reviewed with respect to extraction stage height, post-pillars dimensions, and backfilling stage with the intention of prediction of mining conditions in varying depth.

In a study by Sulistianto et al. (2009), stope stability was investigated with respect to rock falling from the roof stope due to extensive jointed rock mass along the ore body. Authors suggested applying frictional bolt support system to maintain the roof of stope stable. Furthermore, in a study by Li et al. (2011) the stope stability has been investigated due to excavation height for overhand cut-and-fill stoping method. Preventing rocks of falling and roof collapse for deep underground mines is necessarily required to install an appropriate long anchor cable reinforcement system based on rock mass condition of the stope. They concluded that as the excavation height advance, the displacements increase gradually. Also, with the advance of excavation height, the failure regions increase for non-reinforcement stopes.

Himanshu and Kushwaha (2015) illustrated a case study on post-pillar design for overhand cut-and-fill stoping method at Bagjata underground uranium mine. Investigation on post pillar design was carried out for different dimensions. They proposed an optimum dimension of post-pillars for overhand cut-and-fill stoping method (e.g. 4 m x 4m). It is noted from the authors that application of backfilling materials is necessarily required in stopes because increase the strength factor of post-pillars.

In order to provide support for deep underground excavations, post-pillars are often left within the ore body maintaining overall stope stability. The role of post-pillar is to support the hanging wall, the roof of stope, and footwall for a certain period of time during the exploitation stage. Due to economic conditions, it is necessarily required to design post pillars in that way that fulfill the load bearing requirements (Sjöberg, 1993; Lunder, 1994).

Design of post-pillars for overhand cut-and-fill stoping method used in deep underground mines from day to day has become a very tough and challenging task for geotechnical engineers since post-pillars will eventually fail as mining advances upwards. Such a method is applied in the thick and inclined ore bodies. Post-pillars provide additional support to the hanging wall, the roof of the stope and footwall. Design of post-pillars should be done in such a way that failure does not take place at the first excavation stage. Post-pillars are predicted to fail as mining operation advance upwards but be confined by backfilling materials. Post-pillars should be designed using empirical deterministic and numerical modeling methods (Thibodeau and Yao, 2015).

The design of excavation and post-pillars dimensions for overhand cut-and-fill stoping method is described by Thibodeau and Yao, (2015) using a combination of empirical design method (e.g. span stability graph method), deterministic analysis (e.g. tributary area method), and numerical modeling technique (e.g. Map3D). Authors used span graph method to determine maximum allowable span (e.g. slot and cross-out intersection span) from average RMR values which fall within the stable domain. Then the tributary area method was used to determine the possible range of post-pillar dimensions and numerical modeling using Map3D has been carried out in order to investigate post-pillar failure for different dimensions based on elastic solution. To design post-pillars, the critical span is determined based on the largest circle that can be drawn within the boundaries of the exposed back as shown in plan (Figure 2.4).

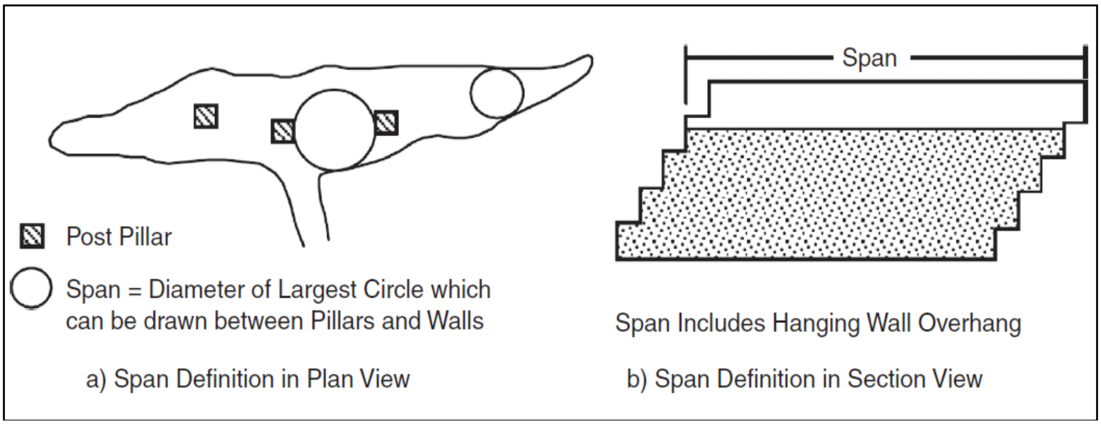
Post Pillar
Span = Diameter of Largest Circle which can be drawn between Pillars and Walls
a) Span Definition in Plan View
Span
Span Includes Hanging Wall Overhang
b) Span Definition in Section View

Figure 2.4. Span definition (Hughes et al., 2017)

The measured exposed span is then related to the rock mass rating in the immediate back to determine the stability of the span. According to Kumar et al. (2002), Hughes et al. (2017) the Rock Mass Rating (RMR) proposed by (Bieniawski, 1976) is used to assess the rock mass in the immediate back with following corrections:

1. Reducing the RMR rating by (10) if shallow joints (dip < 30°) are present
2. Reducing the RMR rating by (10) if there are signs of high stress such as corner spalling
3. Reducing the RMR rating by (20) if bursting conditions are present.

When the maximum span and the RMR are obtained, the stability of underground mine excavations is classified into three main categories: stable excavation, potentially unstable excavation, and unstable excavation.

Stability of the span is determined based on the measured exposed span and related to RMR (Bieniawski, 1989). The allowable unsupported span of underground excavation is determined using empirical unsupported design curve span, as shown in Figure 2.5.

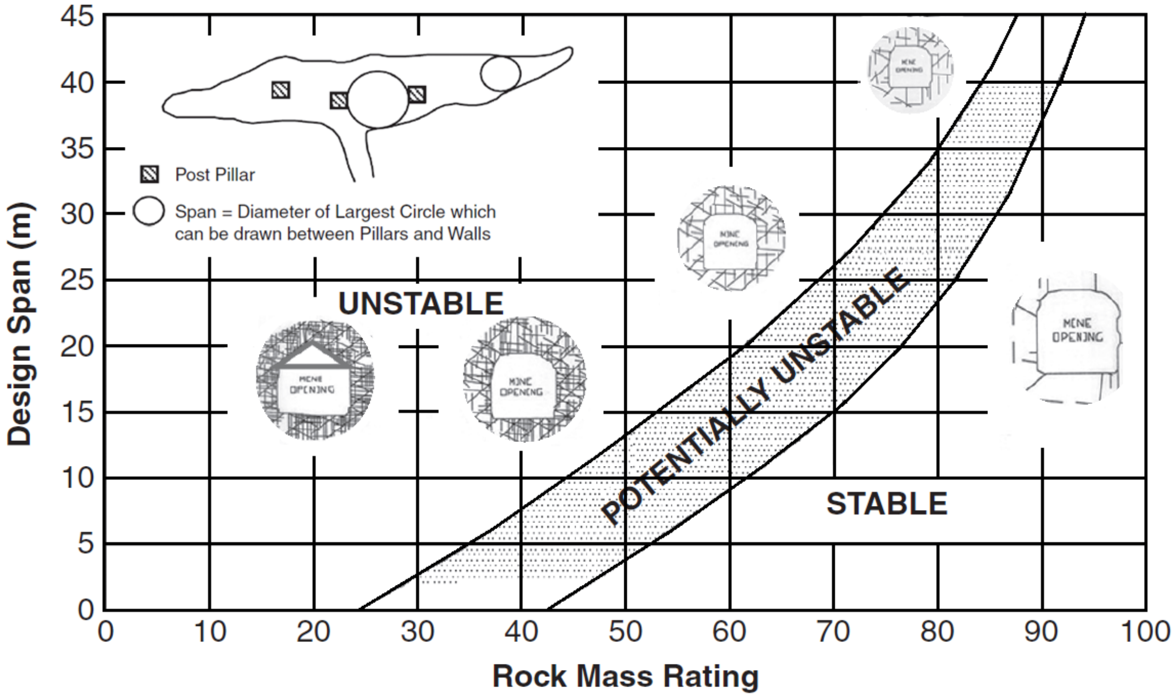

Figure 2.5. Updated Span Design Curve. Based on 292 observations (Wang et al., 2000)

The database for span stability was originally a site-specific database from the Detour Lake Mine including 172 unique points that had RMR (Bieniawski, 1976) values ranging between 60 and 80 (Lang, 1994; Hughes et al., 2017). Then, the database was expanded to 292 observations that had RMR (Bieniawski, 1976) values ranging between 24 and 87, including six underground mines, as shown in Figure 2.5 (Wang et al., 2000; Brady et al., 2003; Hughes et al., 2017). At the time of determining the rock mass rating in a potential excavation, a geotechnical engineer can easily determine the maximum allowable span that is possible for miner-entry opening using Figure 2.5. The use of span design curve involves the mapping of all available headings and faces with RMR updated by Bieniawski (1976) (Brady et al., 2003; Hughes et al., 2017).

Lunder (1994) developed a comprehensive pillar database considering pillar geometry, in-situ rock strength, loading conditions, and stability conditions. Developing pillar stability graph (Figure 2.6) a total of 178 stability cases from hard rock mines have been analyzed where each case is classified as a failed pillar, an unstable pillar and/or stable pillar.

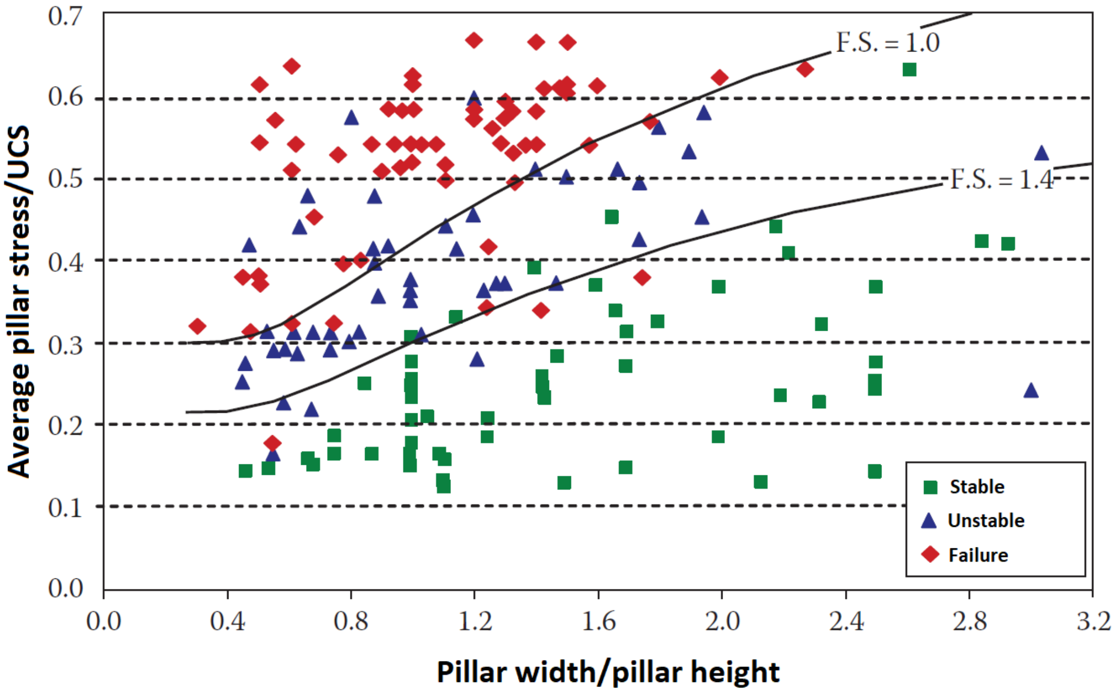

Figure 2.6. Underground Pillar Stability Graph.178 observations. (Lunder, 1994)

Developing this methodology, seven (7) individual pillar stability database published worldwide were used. Where, five of seven databases originate from massive sulfide deposits and the entire database have reported RMR in excess of 65% representing good to very good quality rock mass conditions. In this design methodology, two factors are used. The first factor relates to pillar shape and intact rock strength and the second factor is related to predicted pillar stress. The pillar stability graph was developed by plotting the ratio of pillar stress/unconfined compressive strength ratio and pillar width/pillar height ratio (Pakalnis, 2014; Hughes et al., 2017).

For deep hard rock mines backfilling material is an important component providing support to hanging wall and footwall and confinement to post-pillars. The use of backfilling materials helps to prevent any potential failures of the surrounding rock mass. After the mine excavation stage is completed at a certain mining height ground control problems tend to occur due to the large opening created and jointed rock mass conditions. Tahzibi et al. (2016) assessed the strength properties of backfilling materials depending on the function it is designed for. Backfilling materials used for ground support purpose the strength properties should be at least 5MPa, if the backfilling material is supposed to be used as a working platform strength parameter is usually 1MPa.

2.4. Conclusion

Surveying of available researches on overhand cut-and-fill stoping method and post-pillar stability assessment have been evaluated with special care. Each published article presents a special importance to current problems in underground mines but compared to our case study there are differences in what is being considered so far and how to solve such complex ground control problems at TUM.

In comparison with other researches in this study, the following issues will be addressed. Stope stability has been investigated with respect to mine excavation heights varying depth of underground excavation, stoping dimensions are larger comparing to surveyed researches, and post-pillars were evaluated with a new developed assessment index in various dimensions at different mine excavation height and depth.

3. MATERIALS AND METHODS

In this chapter, the general background, geological settings, geotechnical studies, and current mining method used at Trepça Underground Mine (TUM) will be discussed. Currently, applied mining method at TUM for ore recovery has been reassessed using UBC underground mining method selection tool and multiple criteria decision-making techniques to prove the application of overhand cut-and-fill stoping method for such ore body characteristics. Thereafter, the numerical modeling and analysis of overhand cut-and-fill stoping method will be described.

3.1. General Background of Trepça Underground Mine

Mining activities in Kosovo date back to pre-Roman times up to nowadays. That makes it one of the oldest mine in Balkans. Whereas, the modern history of mining activities started in 1925 when a British company (i.e. Selection Trust Ltd.) initially started an exploration of the deposit. Afterward, mine development begun in 1926-1927 and at the same period Trepça Mines Ltd., was founded. Trepça underground mine is a poly-metallic underground mine, located near Stan Trg village in the Trepça valley of Mitrovica municipality, roughly 7.5 km east and 9 km northeast of Mitrovica and approximately 40 km northwest of Pristine capital city of Kosovo, as seen in Figure 3.1. Trepça underground mine has access to all local and regional roads.

Hence, the exploitation stage started in 1930 until the Second World War was ended. Currently, Trepça mine operates under the Privatization Agency of Kosovo (PAK). Trepça underground mine is the most well-known mine of the Eastern part of Europe. Currently, ore reserves of the TUM are supposed to be roughly 20.7 Mt of ore with 4.02% Pb, 4.02% Zn, and 76g/t Ag (Hetemi, 2013).

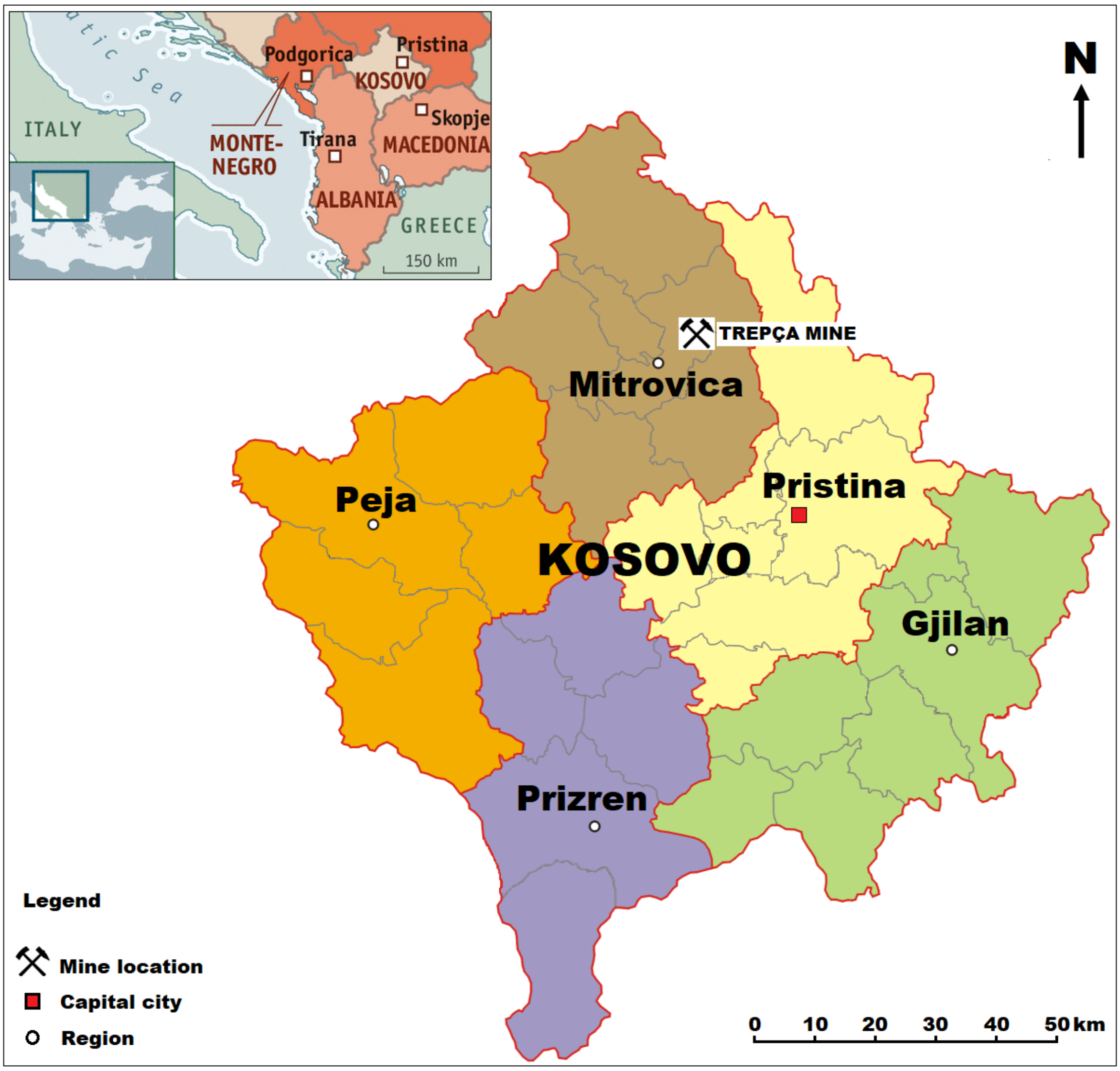
Podgorica
Pristina
KOSOVO
Skopje
ITALY
MONTE-NEGRO
Tirana
MACEDONIA
ALBANIA
GREECE
150 km
N
TREPÇA MINE
Mitrovica
Peja
Pristina
KOSOVO
Gjilan
Prizren
Legend
Mine location
Capital city
Region
0 10 20 30 40 50 km

Figure 3.1. Locations of study area of Trepça mine

3.1.1. Geological settings

Trepça mineral deposit is located in the Kopaonik block of the western Vardar zone in the further east part of the Dinarides. The Vardar zone comprises of large cost-effective significant mineral deposits of Pb-Zn-Ag-Bi-Mo and small mineral deposit of Cu-Fe-Au (Palinkas et al., 2013). Trepça mineralization belt extends approximately 80 km in northern Kosovo and hosts several mines and mineral occurrences, as shown in Figure 3.2 (Hyseni et al., 2010).

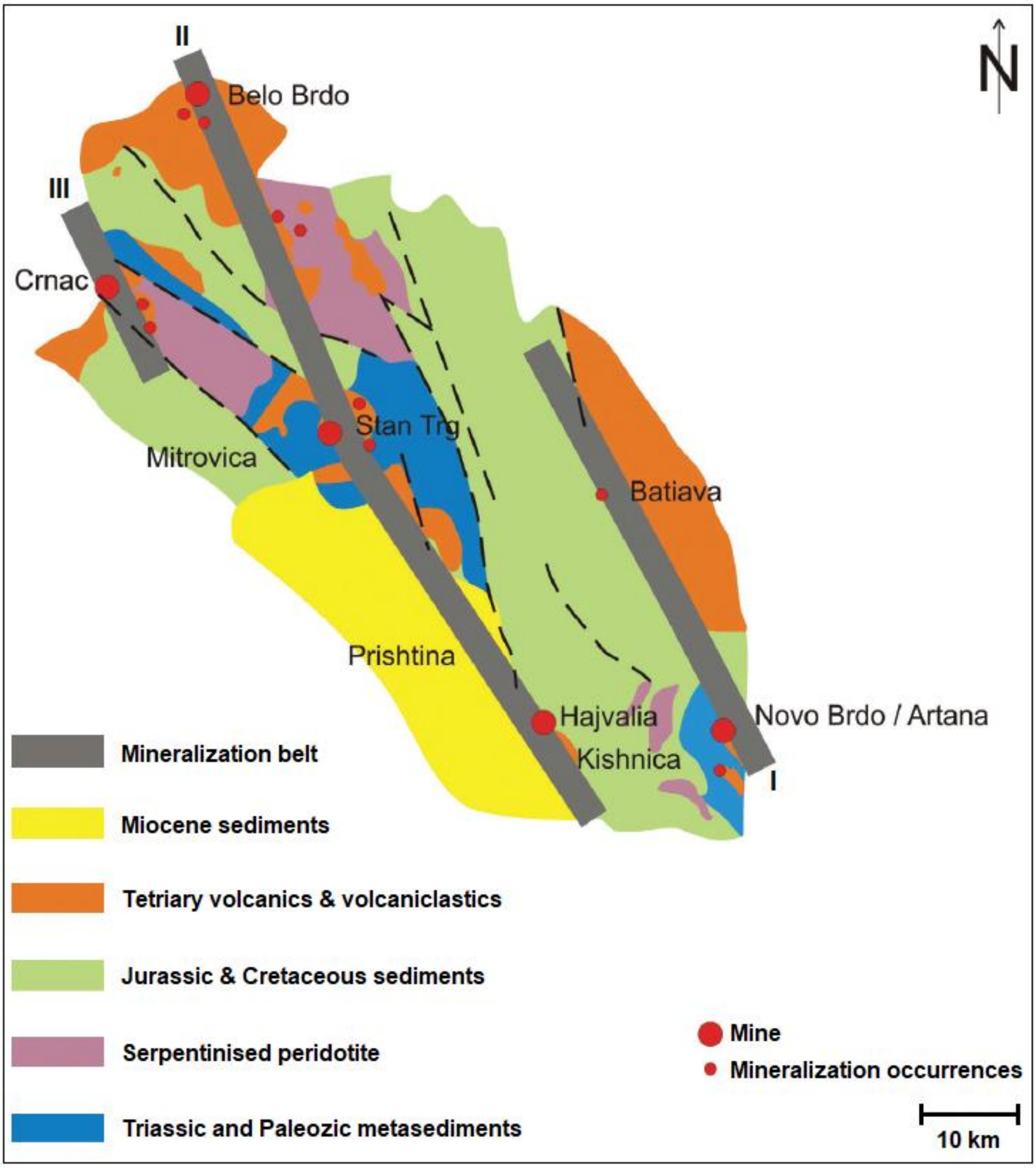
II
III
I
N
Belo Brdo
Crnac
Stan Trg
Mitrovica
Batiava
Prishtina
Hajvalia
Kishnica
Novo Brdo / Artana
Mineralization belt
Miocene sediments
Tetriary volcanics & volcaniclastics
Jurassic & Cretaceous sediments
Serpentinised peridotite
Triassic and Paleozic metasediments
Mine
Mineralization occurrences
10 km

Figure 3.2. Geological settings of Vardar zone and Trepça mineralization belt (Hyseni et al., 2010)

Trepça mineral deposit has been an interesting research area for geologist from national and international universities across Europe due to its complexity and geological formation process. Several studies have been conducted from (Forgan, 1936; Forgan, 1950; Schumacher, 1950; Dimitrijevic, 1995; Maliqi, 2001; Hyseni and Large, 2003; Palinkas et al., 2013).

The Vardar zone contains fragments of Paleozoic crystalline schist and phyllite with unconformable overlying Triassic clastics, phyllites, volcano clastic rocks, and upper Triassic carbonate. It is clearly seen from Figure 3.2 that within the Vardar zone three main mineralization zones are distinguished;

- 1st zone of mineralization consists of Batlava and Artana mineralization deposit,
- 2nd zone of mineralization consists of Trepça, Hajvalia-Kishnica, and Belo Brdo mineralization deposit, and
- 3rd zone of mineralization consists of Crnac mineralization deposit.

Trepça mineralization deposit belongs to the second zone, as shown in Figure 3.2. Central ore body of Trepça Underground Mine (TUM) consists of pyrite, pyrrhotite, sphalerite, and galena with typical carbonate gangue minerals and minor quartz (Palinkas et al., 2013). Trepça mineralization deposit belongs to a hydrothermal-metasomatic type of deposit. Hydrothermal minerals are characterized by sulfides (i.e. galenite, sphalerite, pyrite, arsenopyrite etc.), carbonates and oxides. Whereas, as supporting elements of sulfide mineralization appears to be dolomite, calcite, quartz, and rhodochrosite (Hyseni and Large, 2003).

The principal mineralized host rock is recrystallized upper Triassic limestone with a developed karst system. The host limestone is placed within the core of an anticline and roofed by schist, as shown in Figure 3.3. In a review by Palinkas et al. (2013) has illustrated that Trepça, Belo Brdo, Crnac, Hajvalia, Kishnica, and Novo Brdo are considered the most productive mines in the past with total production of 60.5 Mt of 8%Pb+Zn and more than 4,500t of Ag.

Trepça mineral deposit is originated by the metasomatic replacement of limestone and consists mainly of an intimate mixture of sulfides associated with little admixed gangue. Structural and lithological control on mineralization process by the longitudinal cross-section of the Trepça mineral deposit. Trepça mineralization deposit has been considered as the best and largest lead-zinc-silver mine in Kosovo and Europe (Palinkas et al., 2013).

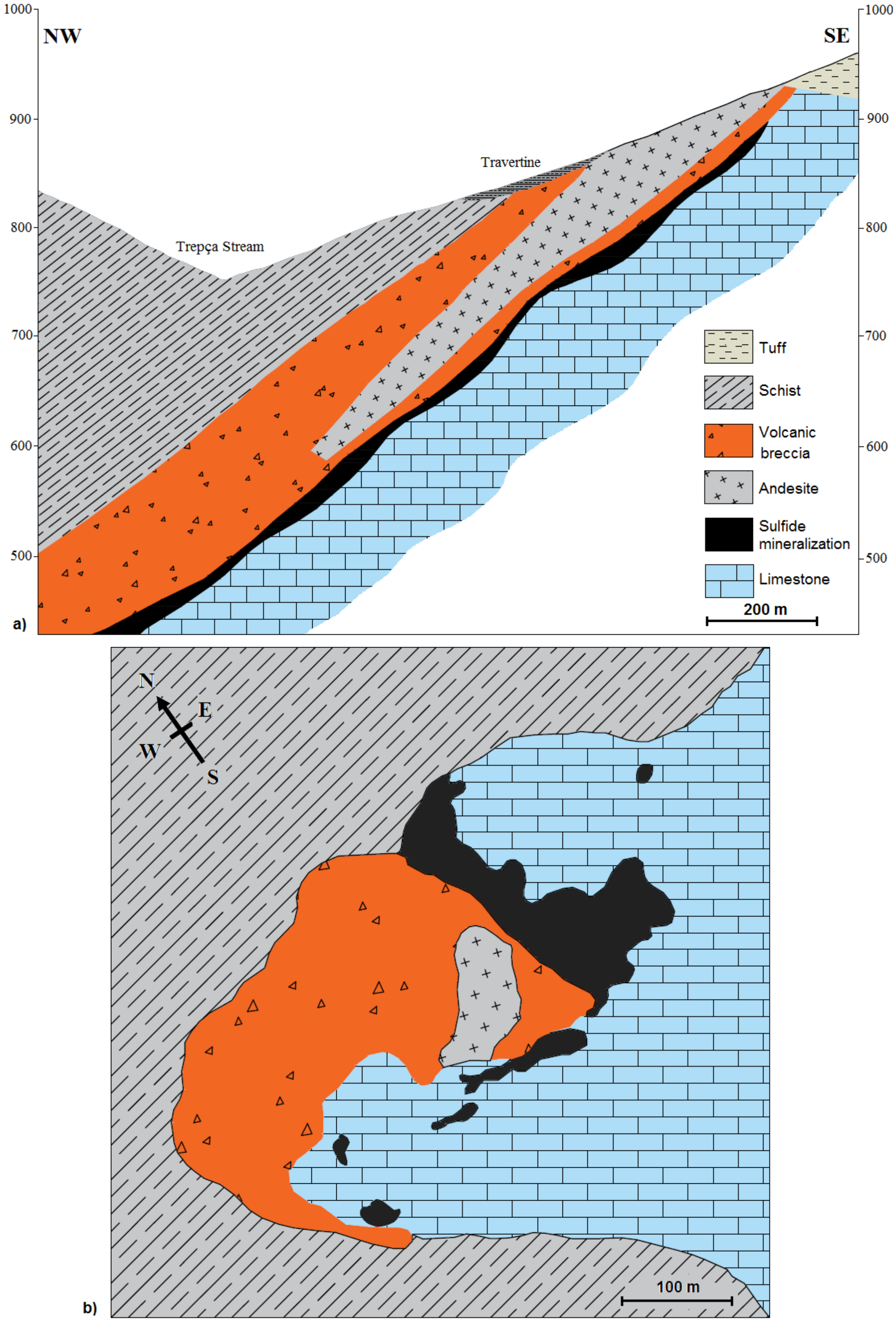
1000
900
800
700
600
500
NW
SE
Travertine
Trepça Stream
1000
900
800
700
600
500
Tuff
Schist
Volcanic breccia
Andesite
Sulfide mineralization
Limestone
200 m
a)
N
E
W
S
100 m
b)

Figure 3.3. a) Longitudinal geological cross-section of central ore body illustrating associated b) Surface geological map of the Trepça mineral deposit hanging wall and footwall rock formations (after Forgan, 1936)

The TUM consists of south ore bodies, north ore bodies, and central ore body. Among them, central ore body is the greatest and main ore body of the mine. These ore bodies are identified during the exploration stage. The central ore body extends along a strike length of 1200 m below the ground surface. Available data shows that the ore body has been explored up to 925 m in depth below the ground surface. The central ore body is in contact with volcanic breccia (i.e. hanging wall) and limestone (i.e. footwall), the ore body geometry ranges from 2000 up to 10000 m^2. The ore body has a strike of N45°W and with a general dipping angle of 40-45° as given in Figure 3.3a (Maliqi, 2001).

3.1.2. Geotechnical studies

In the preliminary stages of rock engineering design, field investigations including discontinuities surveys and laboratory studies are necessarily required for the approximate calculations of rock mass strength parameters for modeling purposes (Genis et al., 2007). Section 3.1.2.1 provides with mechanical properties of rock material for different geological rock units based on laboratory tests, whereas, Section 3.1.2.2 provides with rock mass classification systems and characteristics of different geological rock units, and Section 3.1.2.3 provides with geotechnical rock mass properties of TUM for modeling purpose.

3.1.2.1. Rock material properties

Mechanical properties of rock materials for different geological rock units are necessarily required during rock mass characterization and classification stage (e.g. Rock Mass Rating - RMR). Moreover, rock material properties (e.g. intact strength of rock material) help to investigate stability of deep underground excavations (e.g. stopes) and post-pillars.

Mechanical and physical properties of rock material, including unit weight of the rock material (γ), uniaxial compressive strength (σ_{ci}), young modulus (E_i), indirect tensile strength (σ_{ti}), cohesion (c_i), internal friction angle (ϕ_i) were obtained from laboratory tests. The average values of laboratory tests were considered and provided by Hetemi (2013), as given in Table 3.1.

Table 3.1. Mechanical and physical properties of the rock materials for different geological rock units at TUM (modified from Hetemi, 2013)

Parameters	Geological rock units		
	Volcanic breccia	Sulfide mineralization	Limestone
Unit weight of the rock, $\gamma(\mathrm{kN/m^3})$	28.4	36.3	27.3
Uniaxial compressive strength, $\sigma_{ci}(\mathrm{MPa})$	60.9	78.0	59.5
Tensile strength, $\sigma_{ti}(\mathrm{MPa})$	6.4	5.9	5.0
Young's modulus, $E_i(\mathrm{GPa})$	49.9	63.7	40.2
Cohesion, $c_i(\mathrm{MPa})$	11.0	12.2	8.8
Internal friction angle, $\phi_i(°)$	51.6	56.4	51.3
Poisson's ratio, ν_i	0.17	0.19	0.17

3.1.2.2. Rock mass classification and characteristics

In this study, the most widely used rock mass classification systems such as the Rock Mass Rating (RMR) (Bieniawski, 1989), the Rock Quality Index (Q) (Barton et al., 1974; Grimstad and Barton, 1993), and the Geological Strength Index (GSI) (Hoek et al., 1995) were employed to characterize the rock mass and estimate rock mass strength parameters. All three rock mass classification systems have a quantitative estimation of the rock mass quality (Palmstrom, 2009).

According to Potvin et al. (2012), rock mass characterization should be used to determine the intrinsic properties of the rock mass, characterization should be compatible with the aforementioned rock mass rating tools. Hence, rock mass strength parameters were obtained with the use of the empirical equations, developed by different researchers based on RMR, Q, and GSI values. Moreover, these empirical equations have been proposed in an effort to assist geotechnical engineers during the early stages of design (Basarir et al., 2010).

Villaescusa (2014) noted that, rock mass is affected by several geological factors including intact rock, rock stress, number of discontinuity sets, discontinuity orientation, discontinuity frequency, and spacing, discontinuity persistence and termination, block shape and size, discontinuity roughness and planarity, aperture, wall strength, infill, and water seepage, as seen in Figure 3.4.

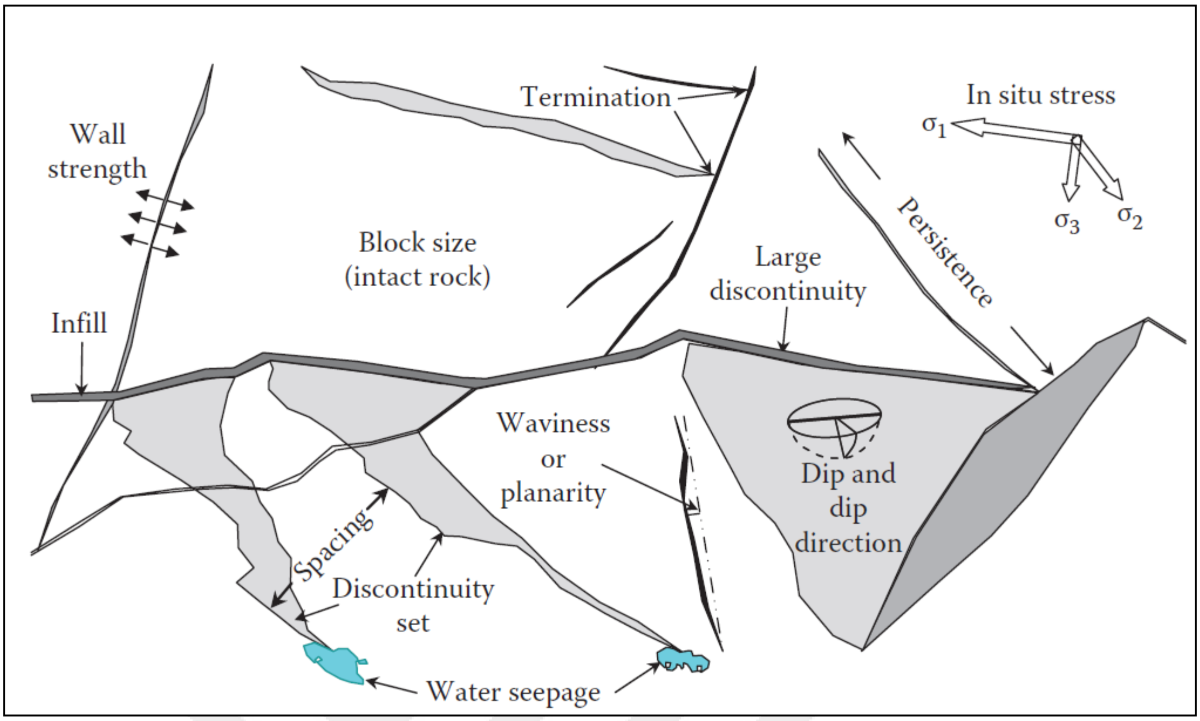
Wall
strength
Termination
In situ stress
σ_1
σ_3
σ_2
Persistence
Block size
(intact rock)
Large
discontinuity
Infill
Waviness
or
planarity
Dip and
dip
direction
Spacing
Discontinuity
set
Water seepage

Figure 3.4. Geological factors influencing the engineering behavior of a rock mass (Villaescusa, 2014)

However, rock mass characterization for hanging wall, ore body and footwall has been completed at the mine site based on field measurements and observations, where Rock Quality Designation (RQD) and discontinuity data were investigated with scan line length as a common way since there weren't any boreholes logs available. Thus, results from field investigation of rock mass characterization and classification for different geological rock units based on Rock Mass Rating (RMR) system are summarized in Table 3.2.

Table 3.2 shows the average RMR values of different geological units, where 57.4 refers to medium rock mass for the hanging wall, 72.2 refers to good rock mass for the ore body, and 65.4 refers to good rock mass for the footwall, as well.

Table 3.2. RMR values of hanging wall (e.g. volcanic breccia), ore body (e.g. sulfide mineralization), and footwall (e.g. limestone)

Rock condition	Hanging wall	Ore body	Footwall
A. General conditions:			
Intact rock strength (MPa)	60.90 (6.5)	78 (8)	59.5 (6.5)
RQD (%)	60 (12) 68(13.6)	88 (17.8) 98 (20)	75 (15) 85 (17)
Discontinuity spacing (cm)	5 (5.1) 10(6)	20-60 (6) 10-60 (11.5)	6 (5.2) 30 (8.5)
Groundwater conditions	Damp (10)	Damp (10)	Damp (10)
B. Discontinuity conditions:			
Discontinuity length (m)	1-3 (2) 3-10 (4)	<1 (4) 1-3 (6)	<1 (4) 1-3 (6)
Discontinuity separation (mm)	<0.1 (4) 0.1-1.0 (5)	None (6)	None (6)
Roughness	Slightly rough (3)	Slightly rough (3) Rough (5)	Slightly rough (3) Rough (5)
Infilling (mm)	None (6)	None (6)	None (6)
Weathering	Unweathered (6)	Slightly weathered (5) Unweathered (6)	Slightly weathered (5)
Rock mass rating (RMR)	RMR_{MIN} = 54.6 RMR_{MAX} = 60.1 RMR_{AVG} = 57.4	RMR_{MIN} = 65.8 RMR_{MAX} = 78.5 RMR_{AVG} = 72.2	RMR_{MIN} = 60.7 RMR_{MAX} = 70.0 RMR_{AVG} = 65.4

Values in the parentheses refer to rating values.

Results from field investigation of rock mass characterization and classification for different geological rock units based on Rock Quality Index (Q) are summarized in Table 3.3. Hence, each parameter is rated and the Q values are determined using equation (3.1) as given in classification system proposed by Barton et al., (1974).

$$Q = \frac{RQD}{J_n} \times \frac{J_r}{J_a} \times \frac{J_w}{SRF} \tag{3.1}$$

Where;

RQD – is the Rock Quality Designation
J_n – is the joint set number
J_r – is the joint roughness number
J_a – is the joint alteration number
J_w – is the joint water reduction factor
SRF – is the Stress Reduction Factor

Table 3.3. Q values of hanging wall (e.g. volcanic breccia), ore body (e.g. sulfide mineralization), and footwall (e.g. limestone)

	Hanging wall	Ore body	Footwall
Rock condition	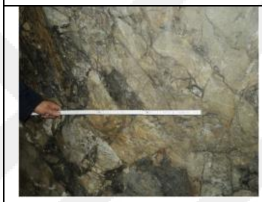		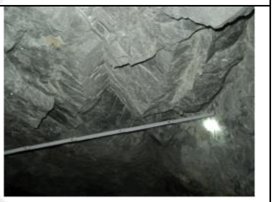
General conditions:			
RQD (%)	60 (60) 68 (68)	88 (88) 98 (98)	75 (75) 85 (85)
Number of joint sets	Three joint sets plus random joints (12)	Three joint sets (9)	Three joint sets (9)
Joint roughness	Rough or irregular, planar (1.5)	Rough or irregular, undulating (3)	Rough or irregular, planar (1.5)
Joint alteration	Slightly altered joint walls (2)	Slightly altered joint walls (2)	Slightly altered joint walls (2)
Joint water reduction number	Dry excavation or minor flow (1)	Dry excavation or minor flow (1)	Dry excavation or minor flow (1)
Stress reduction factor (SRF)	Moderate slabbing after > 1 hour in a massive rock (5) (50)	Moderate slabbing after > 1 hour in a massive rock (5) (50)	Moderate slabbing after > 1 hour in a massive rock (5) (50)
Rock quality rating (Q)	$Q_{MIN} = 0.08$ $Q_{MAX} = 0.85$ $Q_{AVG} = 0.5$	$Q_{MIN} = 0.3$ $Q_{MAX} = 3.3$ $Q_{AVG} = 1.8$	$Q_{MIN} = 0.1$ $Q_{MAX} = 1.4$ $Q_{AVG} = 0.8$

Values in the parentheses refer to rating values.

Table 3.3 shows the average Q values of different geological units, where 0.5 refers to very poor rock mass for the hanging wall, 1.8 refers to poor rock mass for the ore body, and 0.8 refers to poor rock mass for the footwall, as well.

Rock mass characterization and classification based on the Geological Strength Index (GSI), as illustrated in Figure 3.5 and GSI values are summarized in Table 3.4. The GSI system is mainly based on the geological description of the rock mass and blocks surface conditions at the face of an underground excavation. Table 3.4 shows the average GSI values of different geological units, where 60 refers to good rock mass for the hanging wall, 75 refers to very good rock mass for the ore body, and 70 refers to good rock mass for the footwall, as well.

Table 3.4. GSI values for hanging wall (e.g. volcanic breccia), ore body (e.g. sulfide mineralization), and footwall (e.g. limestone)

Geological rock units	Rock type	GSI value	Rock class
Hanging wall	Volcanic breccia	$GSI_{MIN} = 55$ $GSI_{MAX} = 65$ $GSI_{AVG} = 60$	Good rock mass
Ore body	Sulfide mineralization	$GSI_{MIN} = 70$ $GSI_{MAX} = 80$ $GSI_{AVG} = 75$	Very good rock mass
Footwall	Limestone	$GSI_{MIN} = 65$ $GSI_{MAX} = 75$ $GSI_{AVG} = 70$	Good rock mass

RMR, Q, and GSI values of different geological rock units are presented in Table 3.5. To overcome some of the uncertainties of the classification systems, a range of rock mass values was estimated rather than a single value Geniş and Çolak, (2015).

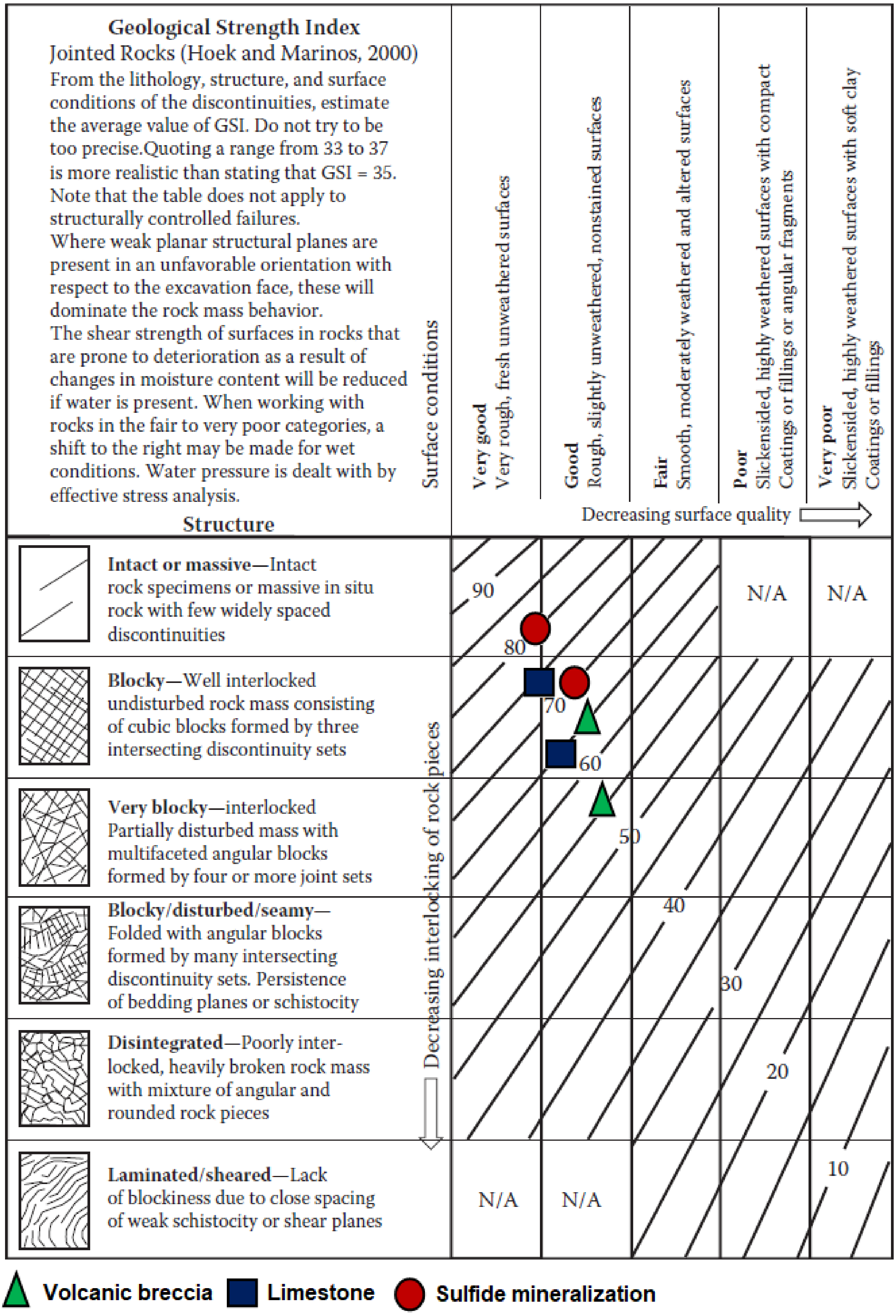

Figure 3.5. Rock mass characterization based on Geological Strength Index (Hoek, 2007)

Table 3.5. Rock mass classification ratings for TUM

Rock type	RMR Values		Q Values		GSI Values	
Hanging wall	57.4	Medium rock mass	0.5	Very poor rock mass	60	Good rock mass
Ore body	72.2	Good rock mass	1.8	Poor rock mass	75	Very good rock rock mass
Footwall	62.4	Good rock mass	0.8	Poor rock mass	70	Good rock mass

Rock mass classification values presented in table refer to average rating values.

3.1.2.3. Estimation of rock mass properties

Rock mass properties such as Mohr-Coulomb parameters, deformation modulus and uniaxial compressive strength of the rock mass parameters were calculated by using of empirical equations based on RMR, Q, and GSI. Rock mass parameters required for the numerical analysis such (e.g. deformation modulus, tensile strength, cohesion, friction angle). To calculate the uniaxial tensile strength (σ_{tmass}), cohesion (c_{mass}), and internal friction angle (ϕ_{mass}) of the rock mass surrounding the central ore body at TUM. Thus, the following empirical equations (3.2), (3.3), and (3.4) recommended by Aydan et al., (2012) were used.

$$\sigma_{tmass} = \frac{RMR}{RMR+6(100-RMR)} \times \sigma_{ti} \tag{3.2}$$

$$c_{mass} = \frac{RMR}{RMR+6(100-RMR)} \times c_i \tag{3.3}$$

$$\phi_{mass} = \left(0.3 + 0.7\frac{RMR}{100}\right) \times \phi_i \tag{3.4}$$

In situ measurements of the rock mass deformation modulus (E_{mass}) are costly, time consuming and very difficult. Hence, estimating the deformation modulus of rock masses by the means of empirical equations is recommended by (Basarir et al., 2005). In Table 3.6 are given proposed equations by different researchers based on RMR, Q, and GSI rating systems. Results of the rock mass deformation modulus for different geological rock units are presented in Table 3.7.

Table 3.6. List of empirical equations for determining deformation modulus of the rock mass (Geniş et al., 2007; Basarir et al., 2010; Geniş and Çolak, 2015 and Hughes et al., 2017)

Researchers	Equation	Equation no.
Empirical equations based on Rock Mass Rating (RMR) system:		
Bieniawski (1978)	$E_{mass} = 2 \cdot \mathrm{RMR} - 100$	(3.5)
Serafim and Pereira, (1983)	$E_{mass} = 10^{\left(\frac{\mathrm{RMR}-10}{40}\right)}$	(3.6)
Nicholson and Bieniawski, (1990)	$E_{mass} = \frac{E_i}{100}\left[0.0028 \cdot \mathrm{RMR}^2 + 0.9 \cdot \mathrm{e}^{\left(\frac{\mathrm{RMR}}{22.82}\right)}\right]$	(3.7)
Aydan et al. (1997)	$E_{mass} = 0.0097 \cdot \mathrm{RMR}^{3.54}$	(3.8)
Read et al. (1999)	$E_{mass} = 0.1 \cdot (\mathrm{RMR}/10)^3$	(3.9)
Aydan and Kawamoto, (2000)	$E_{mass} = \frac{\mathrm{RMR}}{\mathrm{RMR} + 6(100 - \mathrm{RMR})} \times E_i$	(3.10)
Gokceoglu et al. (2003)	$E_{mass} = 0.0736\mathrm{e}^{0.0755 \times \mathrm{RMR}}$	(3.11)
Ramamurthy (2004)	$E_{mass} = E_i \cdot \mathrm{e}^{\left(\frac{\mathrm{RMR}-100}{17.40}\right)}$	(3.12)
Galera et al. (2005)	$E_{mass} = 0.0876 \cdot \mathrm{RMR}$	(3.13)
	$E_{mass} = 0.0876\mathrm{RMR} + 1.056(\mathrm{RMR} - 50) + 0.015(\mathrm{RMR} - 50)^2$	(3.14)
Sonmez et al. (2006)	$E_{mass} = E_i \times 10^{[(\mathrm{RMR}-100)(100-\mathrm{RMR})/4000 \times \mathrm{e}^{(-\mathrm{RMR}/100)}]}$	(3.15)
Khawar (2013)	$E_{mass} = 1.35 \times \mathrm{e}^{0.047\ \mathrm{RMR}}$	(3.16)
Vasarhelyi and Kovacs, (2017)	$E_{mass} = E_i \times \mathrm{e}^{\left(\frac{\mathrm{RMR}-100}{22.94}\right)}$	(3.17)

Table 3.6. List of empirical equations for determining deformation modulus of the rock mass (Geniş et al., 2007; Basarir et al., 2010; Geniş and Çolak, 2015 and Hughes et al., 2017) (continued)

Researchers	Equation	Equation no.
Empirical equations based on Rock Quality Index (Q) system:		
Barton (1995)	$E_{mass} = 10 \times \mathrm{Q}^{1/3}$	(3.18)
Barton (2002)	$E_{mass} = 10 \times \mathrm{Q}_{\mathrm{c}}^{1/3} = 10 \times \left(\mathrm{Q} \times \frac{\sigma_{\mathrm{ci}}}{100}\right)^{1/3}$	(3.19)
	$E_{mass} = 10^{\left(\frac{15 \log \mathrm{Q} + 40}{40}\right)}$	(3.20)
Ramamurthy (2004)	$E_{mass} = E_i \times \mathrm{e}^{0.8625 \times \mathrm{Q} - 2.875}$	(3.21)
Empirical equations based on Geological Strength Index (GSI) system:		
Hoek and Brown (1998)	$E_{mass} = 10^{\left(\frac{\mathrm{GSI}-10}{40}\right)} \sqrt{\frac{\sigma_{\mathrm{ci}}}{100}}$	(3.22)
Hoek et al. (2002)	$E_{mass} = \left(1 - \frac{\mathrm{D}}{2}\right) \sqrt{\frac{\sigma_{\mathrm{ci}}}{100}}\, 10^{\left(\frac{\mathrm{GSI}-10}{40}\right)}$	(3.23)
Gokceoglu et al. (2003)	$E_{mass} = 0.1451\mathrm{e}^{0.0654 \times \mathrm{GSI}}$	(3.24)
Sonmez et al. (2004)	$E_{mass} = E_i \times \left(\mathrm{e}^{\left(\frac{\mathrm{GSI}-100}{9}\right)^{a}}\right)^{0.4}$	(3.25)
Hoek (2004)	$E_{mass} = 0.33\mathrm{e}^{0.064 \times \mathrm{GSI}}$	(3.26)
Hoek and Diederichs (2006)	$E_{mass} = E_i \times \left(0.02 + \frac{1 - \mathrm{D}/2}{1 + \mathrm{e}^{(60 + 15\,\mathrm{D} - \mathrm{GSI})/11}}\right)$	(3.27)

Average value of the rock mass is calculated by excluding the minimum and the maximum values of the rock mass deformation modulus, as seen in Table 3.7. Strength of the rock mass (σ_{cmass}) was calculated with the use of empirical equations proposed by different researcher. The most widely used empirical equations are presented in Table 3.8.

Table 3.7. Calculated rock mass deformation modulus

Parameter	Equation no.	Hanging wall	Ore body	Footwall
$E_{mass}, (GPa)$	(3.5)	14.8	44.4	24.8
	(3.6)	15.31	35.89	20.41
	(3.7)	10.16	22.85	9.96
	(3.8)	16.34	36.81	21.96
	(3.9)	18.91	37.63	24.29
	(3.10)	9.15	19.23	8.71
	(3.11)	5.61	14.14	8.18
	(3.12)	4.31	12.88	4.63
	(3.13)	5.02	6.32	5.46
	(3.14)	15.28	29.41	14.15
	(3.15)	7.81	25.48	13.02
	(3.16)	20.04	40.18	25.35
	(3.17)	7.79	18.95	7.81
	(3.18)	7.93	12.16	9.28
	(3.19)	6.72	11.19	7.81
	(3.20)	7.71	12.46	9.19
	(3.21)	4.33	16.96	4.52
	(3.22)	13.87	37.24	24.39
	(3.23)	8.32	22.34	14.63
	(3.24)	7.34	19.58	14.12
	(3.25)	20.51	36.53	30.54
	(3.26)	15.35	40.19	29.12
	(3.27)	8.52	22.96	17.42
Σ/n		226.32/21	525.06/21	309.05/21
Average		10.77	25.0	14.71

Table 3.8. List of empirical equations for determining strength of the rock mass (Genis et al., 2007; Basarir et al., 2010; Geniş and Çolak, 2015 and Hughes et al., 2017)

Researchers	Equation	Equation no.
Empirical equations based on Rock Mass Rating (RMR) system:		
Hoek and Brown, (1980)	$\sigma_{cmass} = \sigma_{ci} \times \sqrt{\mathrm{e}^{(\mathrm{RMR}-100/9)}}$	(3.28)
Yudhbir and Prinzl (1983)	$\sigma_{cmass} = \sigma_{ci} \times \mathrm{e}^{\left(\frac{\mathrm{RMR}-100}{13.07}\right)}$	(3.29)
Ramamurthy (1986)	$\sigma_{cmass} = \sigma_{ci} \times \mathrm{e}^{\left(\frac{\mathrm{RMR}-100}{18.75}\right)}$	(3.30)
Trueman (1998)	$\sigma_{cmass} = 0.5 \cdot \mathrm{e}^{0.06\ \mathrm{RMR}}$	(3.31)
Hoek et al. (1995)	$\sigma_{cmass} = \sigma_{ci} \times \mathrm{e}^{\left(\frac{\mathrm{RMR}-100}{18}\right)}$	(3.32)
Kalamaras and Bieniawski (1995)	$\sigma_{cmass} = \sigma_{ci} \times \mathrm{e}^{\left(\frac{\mathrm{RMR}-100}{24}\right)}$	(3.33)
Aydan et al. (1997)	$\sigma_{cmass} = 0.0016 \cdot \mathrm{RMR}^{2.5}$	(3.34)
Sheorey (1997)	$\sigma_{cmass} = \sigma_{ci} \times \mathrm{e}^{\left(\frac{\mathrm{RMR}-100}{20}\right)}$	(3.35)
Aydan and Dalgic (1998)	$\sigma_{cmass} = \dfrac{\mathrm{RMR}}{\mathrm{RMR} + 6(100 - \mathrm{RMR})} \times \sigma_{ci}$	(3.36)
Empirical equations based on Rock Quality Index (Q) system:		
Barton (1995)	$\sigma_{cmass} = 18.2 \cdot \mathrm{Q}^{1/3}$	(3.37)
Bhasin and Grimstad (1996)	$\sigma_{cmass} = \sigma_{ci} \times 0.07 \times \gamma \times \mathrm{Q}^{1/3}$	(3.38)
Singh et al. (1997)	$\sigma_{cmass} = 7 \times \gamma \times \mathrm{Q}^{1/3}$	(3.39)

Table 3.8. List of empirical equations for determining strength of the rock mass (Genis et al., 2007; Basarir et al., 2010; Geniş and Çolak, 2015 and Hughes et al., 2017) (continued)

Researchers	Equation	Equation no.
Barton (2002)	$\sigma_{cmass} = 5 \cdot \gamma \cdot \mathrm{Q}_{\mathrm{c}}^{1/3}$	(3.40)
Empirical equations based on Geological Strength Index (GSI) system:		
Ramamurthy et al. (2004)	$\sigma_{cmass} = \sigma_{ci} \times \mathrm{e}^{\left(\frac{\mathrm{GSI}-100}{18.5}\right)}$	(3.41)
Hoek (2004)	$\sigma_{cmass} = \sigma_{ci} \times 0.036\mathrm{e}^{\frac{\mathrm{GSI}}{30}}$	(3.42)

Calculated strength of the rock mass (σ_{cmass}) is given in Table 3.9. The average value of the rock mass is calculated by excluding the minimum and the maximum values of the rock mass strength. Finally, results of geotechnical properties of the ore body and other geological rock units surrounding the ore body are tabulated in Table 3.10.

Table 3.9. Calculated strength of the rock mass

Parameter	Equation no.	Hanging wall	Ore body	Footwall
σ_{cmass}, (MPa)	(3.28)	5.71	16.64	7.36
	(3.29)	2.33	9.29	3.35
	(3.30)	6.27	17.71	8.00
	(3.31)	15.65	38.04	21.13
	(3.32)	5.71	16.64	7.36
	(3.33)	10.32	24.49	12.42
	(3.34)	39.93	70.87	49.21
	(3.35)	7.23	19.42	9.07
	(3.36)	11.16	23.56	12.89
	(3.37)	14.44	22.13	16.89
	(3.38)	9.81	24.56	10.82
	(3.39)	16.11	31.50	18.19
	(3.40)	9.75	20.71	10.92
	(3.41)	7.00	20.19	11.75
	(3.42)	16.20	34.20	22.08
Σ/n		135.36/13	342.62/13	168.88/13
Average		10.41	26.35	12.99

Table 3.10. Geotechnical properties of rock mass for different geological rock units at TUM

Parameters	Geological rock units		
	Volcanic breccia	Sulfide mineralization	Limestone
Deformation modulus, $E_{mass}(GPa)$	10.77	25.0	14.71
Rock mass strength, $\sigma_{cmass}(MPa)$	10.41	26.35	12.99
Tensile rock strength, $\sigma_{tmass}(MPa)$	1.1	1.7	1.1
The cohesion of rock mass, $c_{mass}(MPa)$	2.01	3.6	1.9
Friction angle, $\phi_{mass}(°)$	36.2	45.4	37.7

3.2. Current Mining Method at Trepça Underground Mine

Post-pillar and overhand cut-and-fill stoping method is employed at Trepça Underground Mine (TUM) for ore recovery process, as shown in Figure 3.6. Cut-and-filling stoping method is applicable for steeply dipping ore bodies as well as large and irregularly mineral deposit having good to moderate stability and comparatively high-grade mineralization. The ore body is developed by incline, ramps, and shaft in the footwall from which several crosscuts are constructed to reach production levels for exploitation of mineral deposit. The crosscuts are driven by jacklegs and/or jumbos. Hence, from the crosscuts stopes are exploited by breasting and retreating with uppers using drill jacklegs sometimes jumbos and Load-Haul-Dump (LHD) loaders. The production cycle is as follows; the ore is drilled, blasted, loaded and removed from the stope, as shown in Figure 3.6 (Atlas Copco, 2007).

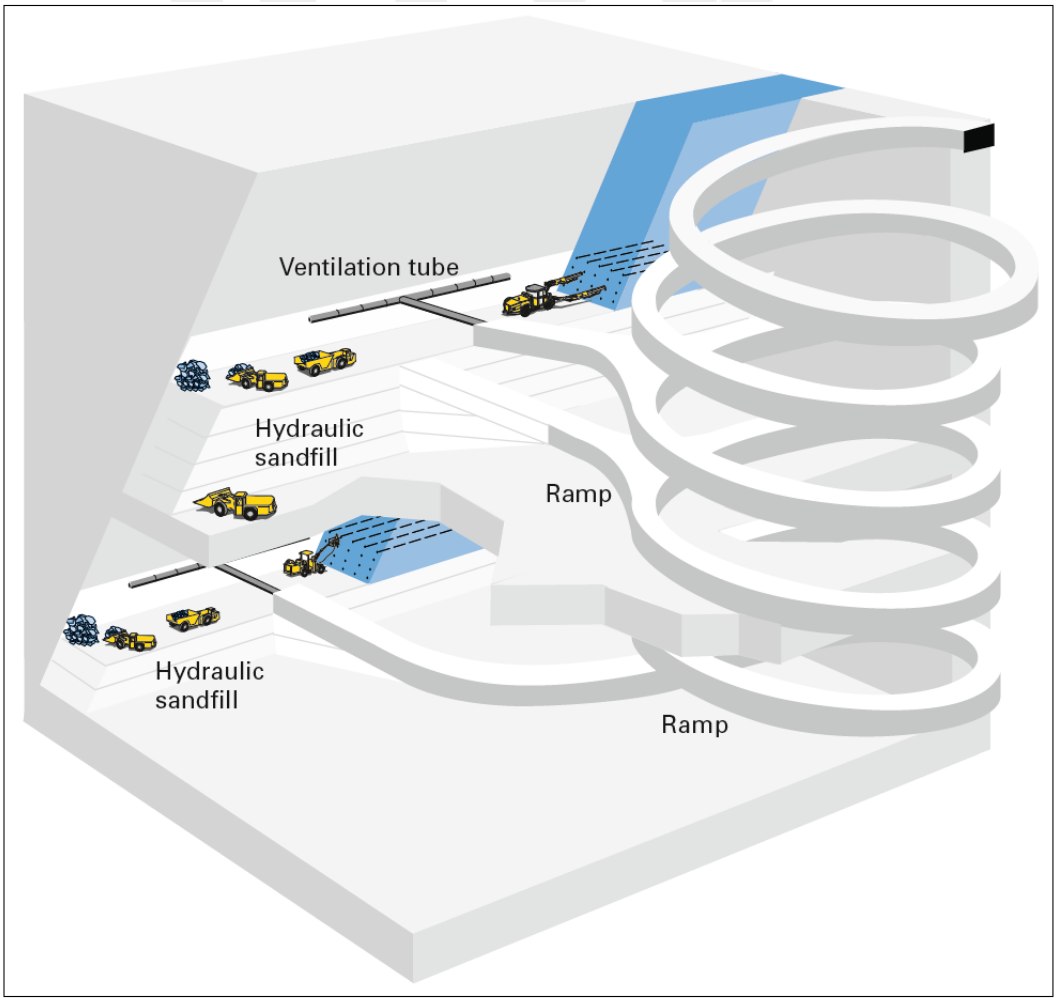

Figure 3.6. Overhand cut-and-fill stoping method layout (Atlas Copco, 2007)

The incline access is used for miners and materials transportation, exploited ore is transported by underground trucks and battery-powered locomotives. Whereas, ramp access is used to connect crosscuts and inclines also serve as a way for transportation of workers, material and for excavated ore. The shafts are designed for ventilation purposes.

Around 85% of the ore is exploited and the rest of the ore reserve will remain in place for stability purposes (e.g. post-pillars), and safety to workers and equipment, as seen in Figure 3.7. The production of sulfide mineralization is being recovered in horizontal slices from the lower levels to the upper levels of the mine. The mineral recovery process is repeated until stoping operation reaches up to the full height of the stope. During this operation, the unit operations are carried out in a cyclic order i.e. drilling, blasting, mucking, transportation and filling the stope.

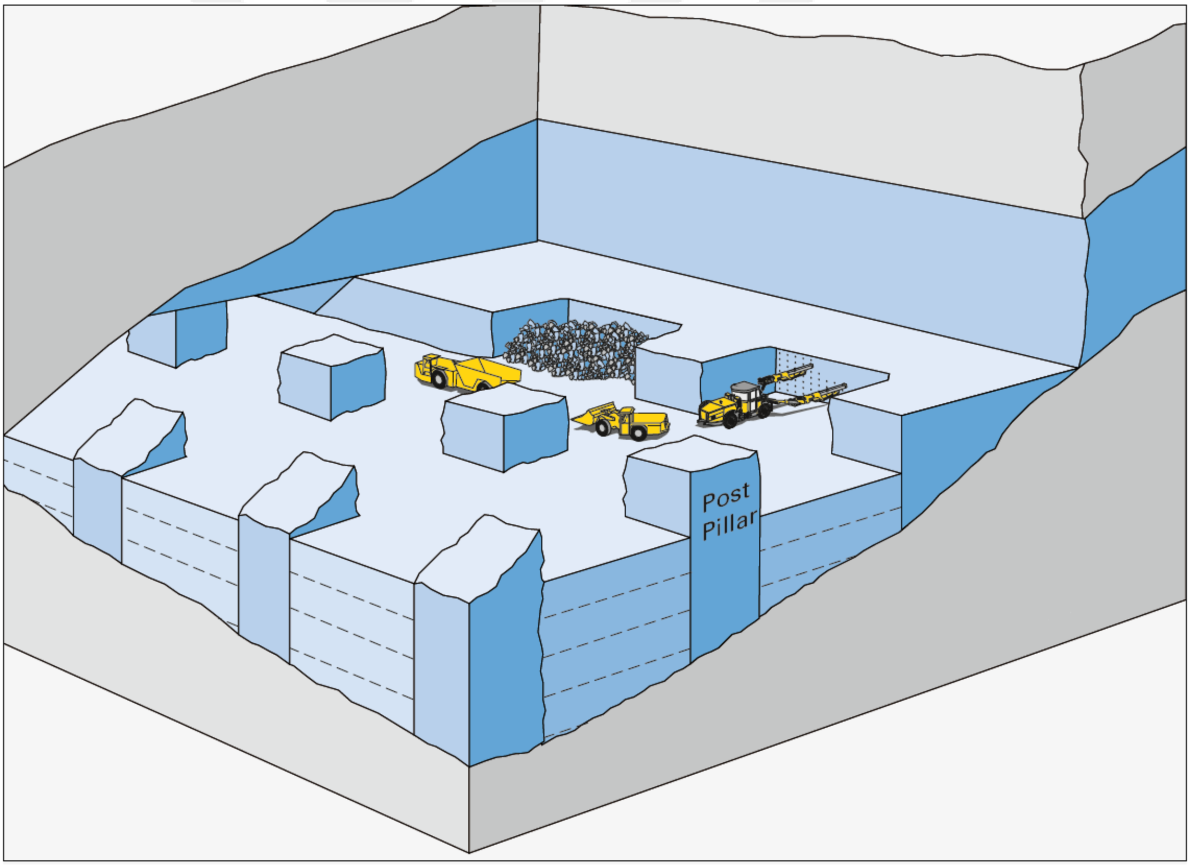

Figure 3.7. Post-pillar and overhand cut-and-fill stoping method layout (Atlas Copco, 2007)

At TUM post-pillars are left due to thick ore body and weak hanging wall in order to prevent collapsing within the working stope. Current practice is to begin growing post-pillars on the footwall side of the stope and as the stope boundary after each excavation stage shifts due to the plunge and ore body dip. Hence, post-pillars advance vertically from footwall to the hanging wall, as shown in Figure 3.7. Rock/Cable bolting is strongly recommended due to wide ore body and presence of fractures, cracks, and geological disturbance (Hamrin, 2001; Hartman and Mutmansky, 2002; Tatiya, 2005; Bullock, 2011).

The ore body is recovered in slices/cuts starting from the bottom of the stope (just above the sill pillar) and proceeding upward. Once the stope has been excavated, voids are backfilled with hydraulic filling material, as shown in Figure 3.8. The backfill material serve both as a working platform for miners and equipment because the hydraulic fill is smooth and suitable for rubber-tired equipment and at the same time provide support to hanging wall and footwall and provide confinement to post-pillars when mining the next slice/cut. Before backfilling stage takes place, stope entries are barricaded and drainage tubes installed.

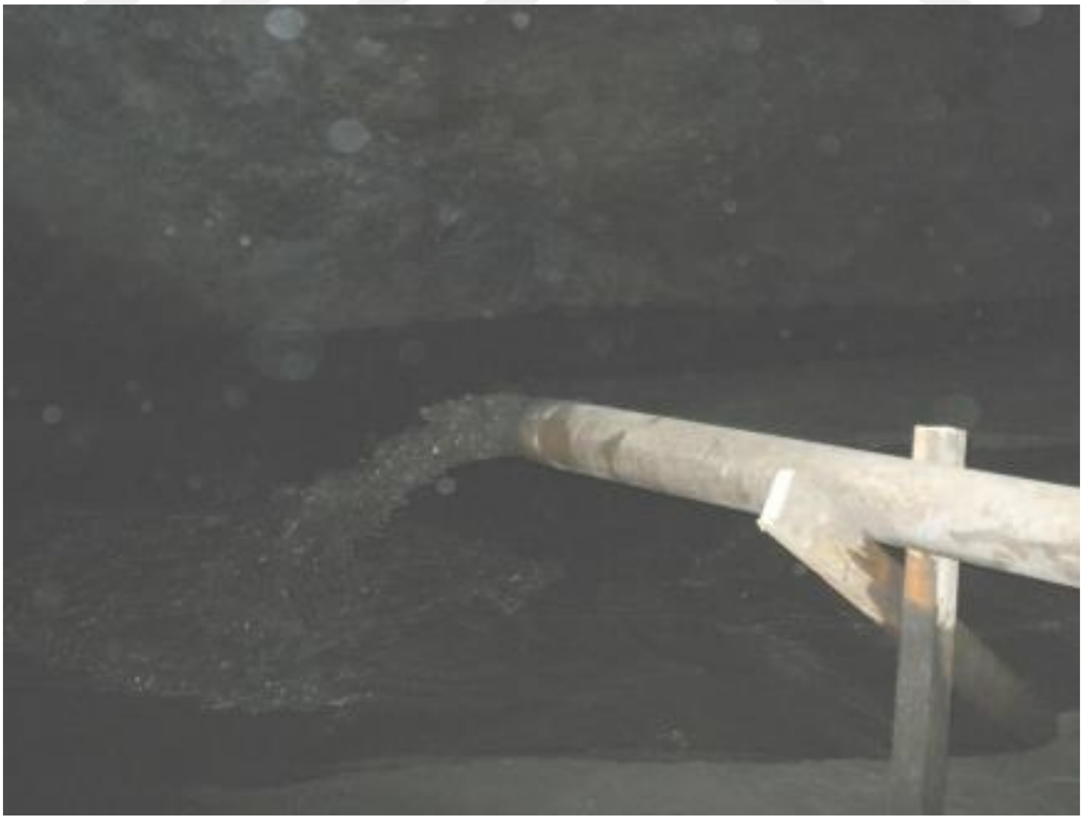

Figure 3.8. Hydraulic backfilling being poured in the mined-out stope at TUM

3.3. Reassessment of Underground Mining Method at Trepça Mine

Once an ore body has been explored and outlined and sufficient information has been collected to warrant further analysis, the most important process of selecting the most appropriate mining method can begin (Hustrulid and Bullock, 2001). Mineral exploitation in which all extraction is being carried out beneath the earth’s surface is termed underground mining. Underground mining methods presented in Table 3.11 are employed when the depth of the deposit, the stripping ratio of overburden to ore (or coal or stone) or both become excessive for surface exploitation (Hartman and Mutmansky, 2002). Regardless of the mining method used for mineral recovery three main conditions should be fulfilled, these are; to guarantee safe production, minimize dilution, and maximize recovery with low operating cost (Brady and Brown, 2007). Underground mining method selection is generally based on geology of the deposit and the degree of ground support necessary to make the methods productive and safe (Hartman and Mutmansky, 2002).

Boshkov and Wright, (1973) proposed one of the first qualitative classification schemes to be used as underground mining method selection (UMMS) tool. Factors influencing the selection method are physical characteristics and geotechnical properties of the ore body and its host rock masses. Morrison (1976) proposed a selection chart for mining method selection; this classification system divides underground mining into three fundamental groups such as rigid pillar support, controlled subsidence and caving. Factors influencing the selection method are ore width, support type, and strain energy accumulation. Laubscher (1981) proposed a selection methodology of an appropriate mass underground mining method based on RMR. Laubscher (1990) modified the selection system including Hydraulic Radius (HR). Including such parameter, cavability becomes feasible for more competent rock when the undercut area is being large. Hartman (1987) developed a mining method selection flow chart based on the geometry of the deposit and the ground conditions of the ore zone. This mining method selection tool is also qualitative and includes surface and underground methods for both soft and hard rock. Nicholas (1981) developed a quantitative mining method selection tool which determines an appropriate mining method by numerical ranking. In this classification several factors are being considered such as rock mass characteristics of the ore body, hanging wall and footwall in addition to ore geometry and grade distribution (Carter, 2011).

Table 3.11. Classification of underground mining methods (Tatiya, 2005)

	Ore strength Rock strength	Class	Deposits’ geometry	Stoping method
MINING METHODS IN UNDERGROUND MINING	Strong to moderate Competent	Unsupported	Tabular, flat, thin, large size	Room & pillar
			Tabular, flat, thick, large size	Stope & pillar
			Tabular, steep, thin, any size	Shrinkage stoping
			Tabular, steep, thick, large size	Sublevel stoping
	Moderate to weak Incompetent	Supported	Variable shape, steep, thin, any size	Cut & fill stoping
			Tabular, steep, thin, small size	Stull stoping
			Any shape, any dip, thick, any size	Square set stoping
	Moderate to weak Cavable	Caving	Tabular, flat, thin, large size	Longwall mining
			Tabular or massive, steep, thick, large size	Sublevel caving
			Massive, steep, thick, large size	Block caving

Miller-Tait et al. (1995) modified the Nicholas' classification system due to an erroneous definition of some ratings and small domain between favorable and unfavorable ratings and developed the UBC method to target underground mining methods (Peskens, 2013).

Currently applied mining method at Trepça underground mine for ore recovery process has been reassessed to understand whether the mining method was properly selected in the past as one of the most suitable underground mining method for such ore body characteristics. Reassessment of underground mining method for Trepça mine has been carried out based on decision-making tools to prove the application of overhand cut-and-fill stoping method. Making the right decision during Underground Mining Method Selection (UMMS) process, all known criteria related to the problem should be taken into consideration. The approach to selection of mining method can be classified in three groups as qualitative and quantitative ranking methods, numerical ranking methods, and decision-making methods. Different qualitative and quantitative ranking methods have been developed to assess appropriate mining method for an ore deposit based on physical characteristics of the deposit (e.g. thickness, dip, depth, grade distribution, and geotechnical properties of ore body and its host rock mass).

Increasing the number of criteria in decision-making process make the problem more complex but the accuracy of the decision also increases. Because of arising complexity in the decision process, many conventional methods consider only limited number of criteria. Thus, the need for alternative methods, which consider all known criteria related to UMMS in the decision-making process. Selection of mining method is the first and one of the most important and complex decision issue in mine design that a mining engineer have to make by harmonizing input criteria (Alpay and Yavuz, 2007).

Each underground mining method presented in Table 3.11 require specific mine infrastructure. Hence, developing mine infrastructure for a particular mining method and produce the ore will generate a certain amount of costs, but on the other hand generate certain revenue. Keeping the cost low and the revenue high will maximize economic return while regarding a high standard of safety for employees and low environment impact (Peskens, 2013). Also, in a study by Yavuz (2015) is noted that selection of underground mining method is straightforwardly associated with ground control, planning the ventilation system, decreasing the maintenance cost of the gallery, developing new mining panels and preparing the underground production schedule.

3.3.1. Multiple criteria decision-making techniques in mining

Underground Mining Method Selection (UMMS) is a very important process in mine design and at the same time is a very tough and complex issue due to many criteria handled in the selection process of decision making. Hence, the number of criteria applied in a particular problem of decision making is very important and should not exceed the number of criteria '9' or saying in another word the maximum number of criteria should be seven plus two due to general limitations on human performance.

When the number of elements is seven or less the inconsistency measurement is relatively large with respect to the number of elements involved, when the number is more than seven it is relatively small (Saaty and Ozdemir, 2003; Yavuz, 2015). In a study by Yavuz (2015) it is noted that those limits are broadly known as 'memory span' and if the pair-wise comparison matrixes are set up without taking into account just above mentioned limits, inconsistency might probably occur even the pair-wise comparison matrix is consistent it will probably be not valid. Accordingly, the use of appropriate decision making method is extremely important in order to make the right decision.

3.3.1.1. The analytic hierarchy process (AHP) methodology

Thomas Saaty (1980) developed the Analytic Hierarchy Process (AHP) method. The AHP is an adequate technique dealing with complex multiple attribute decision making (MADM) helping mining engineers to make the most appropriate mining method by setting up priorities. The AHP method is based on the pair-wise comparison of components with respect to attributes and alternatives and is applied for the hierarchy problem structuring (Alpay and Yavuz, 2007; Yavuz, 2015). A pair-wise comparison matrix $(n \times n)$ is constructed, where (n) is the number of elements to be compared. The problem is divided into three levels: problem statement, object identification to solve the problem and selection of evaluation criteria for each object.

After the hierarchy structuring the pair-wise comparison matrix is constructed for each level where a nominal discrete scale 1 to 9 is used for the evaluation as shown in Table 3.12 (Saaty, 1980; Saaty, 2000). In order to find the relative properties of criteria or alternatives implied by this comparison. The relative properties are calculated using the theory of eigenvector and values. Considering A as the pair comparison matrix in equation (3.43), then;

$$(A - \lambda_{max} \times I) \times w = 0 \tag{3.43}$$

To calculate the Eigen value (λ_{max}) and Eigen vector $(w = w_1, w_2, \dots, w_n)$, weights can be estimated as relative properties of criteria or alternatives.

Table 3.12. Pair-wise comparison scale for AHP (Saaty, 1980)

Definition	Relative intensity	Explanation
Equally preferred	1	sub/criteria$(j)$and$(k)$are equally important
Slightly preferred	3	sub/criteria(j) is slightly more important than sub/criteria (k)
More preferred	5	sub/criteria(j) is more important than sub/criteria (k)
Strongly preferred	7	sub/criteria(j) is strongly more important than sub/criteria (k)
Absolutely preferred	9	sub/criteria(j) is absolutely more important than sub/criteria (k)
Intermediate values	2,4,6,8	When compromise is needed

Since the comparison is based on the subjective evaluation, a consistency ratio (CR) is required to ensure the selection accuracy (λ_{max}) is given in equation (3.44);

$$\lambda_{max} = \frac{1}{n} \sum_{i=1}^{n} \left(\frac{\sum_{j=1}^{n} a_{ij} \times w_j}{w_i} \right) \tag{3.44}$$

Where,(λ_{max}) is the maximal eigenvalue, and (n) is the matrix size, (a_{ij}) is an element of pair-wise comparison matrix, (w_j) and (w_i) is the j^{th} and i^{th} element of Eigen value. The Consistency Index (*CI*) of the comparison matrix is computed using the following equation (3.45):

$$CI = \frac{\lambda_{max} - n}{n-1} \tag{3.45}$$

The Consistency Ratio (*CR*) is calculated as:

$$CR = \frac{CI}{RI} \tag{3.46}$$

Where, (*RI*) is the Random Index. Random consistency indices are given in Table 3.13.

Table 3.13. Random indices of randomly generated reciprocal matrices (Saaty, 2000)

Order of the matrix													
1,2	3	4	5	6	7	8	9	10	11	12	13	14	15
RI values													
0.0	0.58	0.90	1.12	1.24	1.32	1.41	1.45	1.49	1.51	1.48	1.56	1.57	1.59

To determine whether the resulting *CI* is acceptable, the *CR* should be calculated. The *RI* values are given in Table 3.13. As a general rule, a consistency ratio of 0.10 is considered acceptable. In practice, however, consistency ratios exceeding 0.10 occur frequently. If the maximum Eigen value, *CI* and *CR* are satisfactory then the decision is taken based on the normalized values, else the procedure is repeated till these values lie in the desired range (Yavuz, 2015).

3.3.1.2. The fuzzy multiple attribute decision making (FMADM) methodology

The (FMADM) methods have been developed due to the lack of precision in assessing the relative importance of attributes and the performance ratings of alternatives with respect to an attribute. The imprecision may come from a variety of sources such as unquantifiable information, incomplete information, non-obtainable information and partial ignorance (Chen and Klein, 1997; Yavuz, 2015).

The main problem of a fuzzy multiple attribute decision making is to prioritize a finite number of sequences of alternatives by evaluating a set of predetermined criteria. Hence, to solve this problem, an evaluation procedure to rate and rank, in order of preference, the set of alternatives must be constructed (Yavuz, 2015). The FMADM problem is described below:

1. A set of (m) possible alternatives, $A = \{A_1, A_2, \dots, A_i, \dots, A_m\}$;

2. A set of (n) criteria, $C = \{C_1, C_2, \dots, C_j, \dots, C_n\}$ with which alternative performances are measured;

3. A performance rating of alternative (A_i) with respect criterion (C_j), which is given by the $(n \times m)$ fuzzy decision matrix $\breve{R} = \{\breve{R}_{ij} | i = 1,2, \dots, m; j = 1,2, \dots, n\}$, where $(\breve{R}_{ij})$ is a fuzzy number; and

4. A set of (n) fuzzy weights $\breve{W} = \{\breve{W}_j | j = 1,2, \dots, n\}$, where $(\breve{W}_j)$ a fuzzy number is also and denotes the importance of criterion the n (j), (C_j) in the evaluation of the alternatives (Chen and Klein, 1999; Yavuz, 2015).

Although a large number of FMADM method have been addressed in the literature, the focus of this study is mainly on Yager's method. This is general enough to deal with both multiple objectives and multiple attribute problems. The Yager's method (1978) follows the max-min method of Bellman and Zadeh (1970), with the improvement of Saaty's method which considers the use of a reciprocal matrix to express the pair-wise comparison criteria and the resulting eigenvector as subjective weights. The weighting procedures used exponentials based on the definition of linguistic hedges proposed by Zadeh (1973). Otherwise, because of the limitations mentioned in the AHP method, the total number of criteria for the Yager's method should also be less than 9 (Yavuz et al., 2008; Yavuz, 2015)

On describing multi-attribute decision-making problems only, a single objective is considered namely the selection of the best alternative from a set of alternatives.

Yager's method suspects the max-min principle approach. The fuzzy set decision is the intersection of all criteria;

$$\mu D(A) = Min\,\{\mu C_1(A_i), \mu C_2(A_i), \dots, \mu C_n(A_i)\} \tag{3.47}$$

For all $(A_i) \in A$, and the optimal decision is yielded by,

$$\mu D(A^*) = Max\big(\mu D, (A_i)\big) \tag{3.48}$$

Where, (A^*) is the optimal decision.

The prime distinctness in this method is that the importance of criteria is signified as exponential scalars. This is based on the idea of linguistic hedges. The principle behind using weights as exponents is that the higher the importance of criteria the larger should be the exponent giving the minimum rule. Conversely, the less important a criterion the smaller its weight for $(\alpha > 0)$ (Kesimal and Bascetin, 2002; Yavuz, 2015).

$$\mu_D(A_i) = Min\left\{\left(\mu_{C_1}(A_i)\right)^{\alpha_1}, \left(\mu_{C_2}(A_i)\right)^{\alpha_2}, \dots, \left(\mu_{C_n}(A_i)\right)^{\alpha_n}\right\} \tag{3.49}$$

This section demonstrates the application of two classes of Underground Mining Method Selection (UMMS) namely the numerical ranking and decision-making methods. The results of the AHP and the Yager’s FMADM technique showed that the Cut-and-Fill Stoping Method is the most optimal mining method for Trepça Underground Mine (TUM). The detailed calculations of the decision-making techniques used in this research to reassess the current mining method at TUM have been provided in Appendix A.

3.4. Numerical Methods Applied in Mining Engineering

Numerical modeling techniques have successfully been used to investigate and solve complex mining and tunneling problems. In rock engineering design, the design methods include empirical methods, closed form solutions and numerical methods as are summarized in Table 3.14.

Table 3.14. The advantages and disadvantages of numerical methods (Hoek et al., 1991)

Numerical methods	Advantages	Disadvantages
Finite Difference Method (FDM) Finite Element Method(FEM)	Material heterogeneity easily handled. Material and geometric non-linearity handled efficiently, especially when explicit solution technique is used. When implicit solution techniques are used matrices are banded. When explicit solution techniques are used less skill is required of user in assessing numerical convergence.	Entire volume must be discretized, resulting in larger number of solution variables than for boundary element methods. Far-field boundary conditions must be approximated. For linear problems explicit solution techniques are relatively slow. Solution time increases exponentially with number of elements used for implicit solution techniques.
Boundary Element Method (BEM)	Far-field conditions inherently represented. Only boundaries require discretization, resulting in smaller number of solution variables than for finite element methods.	Coefficient matrix fully populated. Solution time increases exponentially with number of elements used. Limited potential for handling heterogeneous and non-linear materials.
Distinct Element Method (DEM)	Data structures well suited to modeling systems with high degree of non-linearity resulting from multiple intersecting joints. Very general constitutive relations may be used with little penalty in terms of computational expense. Solution times increase only linearly with number of elements used.	Solution times seem much slower than for linear problems. Results can be sensitive to assumed values of modeling parameters (these ‘disadvantages’ are natural consequence of nature of system being modeled; as there is currently no modeling alternative for such problems, the term ‘disadvantage’ must be interpreted accordingly).

With a rapid growth in the development of computers and software, powerful and adaptable numerical methods are progressively employed in design of underground rock excavations and analysis. The computer based numerical methods provide the means for obtaining approximate solutions to such problems. These methods facilitate modeling of a wide range of behavior related to rock mass characteristics.

The attractive feature of these methods is that practically any complex behavior including elastic and elasto-plastic behavior illustrated by materials can be easily integrated. Another different characteristic of numerical methods is that various mining sequences of excavations can be simulated (Hoek et al., 1991; Sharma, 2009).

Numerical models can be considerable assistance to geotechnical engineers in designing underground excavations. Underground rock excavations (e.g. stopes, ramps, x/cuts, galleries, inclines and shafts) result in significant changes in the stresses in the surrounding and an understanding of the behavior of such excavations requires that the stresses, the displacements and the failure zones in this rock mass be analyzed. The approach adopted in all of the numerical methods is to divide the problem into smaller physical and mathematical components and then sum the influence of the components to approximate the behavior of the whole system. Numerical methods used in rock engineering design can be divided into two classes; boundary and domain methods. In the first method, only the boundary of the excavation is divided into elements and the interior of the rock mass is represented mathematically as an infinite continuum. In the second method, domain methods divide the interior of the rock mass into geometrically simple zones, each with assumed properties. The collective behavior and interaction of these simplified zones model the more complex and otherwise unpredictable overall behavior of the rock mass. Finite Difference Method (FDM) and Finite Element Method (FEM) are domain methods that treat the rock mass as a continuum and the Distinct Element Method (DEM) is a domain method that models each individual block of rock as a unique element (Hoek et al., 1991).

Table 3.14 gives information on advantages and disadvantages of different types of numerical methods and the selection of appropriate models for the analysis of the problems that arise at different stages in the life of a mine have been discussed (Hoek et al., 1991).

3.5. Numerical Modeling - FLAC^{3D}

Numerical modeling of overhand cut-and-fill stoping and post-pillar was performed using the finite difference modeling software FLAC^{3D} (Fast Lagrangian Analysis of Continua) version 3.0 of Itasca.

FLAC^{3D} was developed by Dr. Peter Cundall in 1986, originally for geotechnical and mining engineering applications (Itasca, 2005). FLAC version 3.0 is used for this study. The reason why FLAC^{3D} has been selected for this study is that compared to other software, FLAC is more powerful since you can implement more complex constitutive models, can deal with huge and more complex geometries, and large strain problems very well comparatively through writing you own codes. Moreover, generating a null model of any geometry to represent an underground excavation is much more easily compared to other software. This program simulates the behavior of three-dimensional structures of rock as their yield limits are reached.

In FLAC, materials are presented by elements/zones which, together, form a grid. This grid can be shaped to fit the geometry of the object to be modeled. Each element is then given a constitutive model based on which its response to the applied forces or boundary restraints. As the stresses and forces are initialized within the model structure, the FLAC calculation sequence is started; the equations of motion are invoked to drive the velocities and displacements from applied stresses and forces, as illustrated in Figure 3.9. The velocities are then used to calculate the strain rates. The new stresses are finally derived from strain rates based on the prescribed stress/strain law (constitutive model) in the elements. This cycle is then repeated until the initially applied forces are approaching zero i.e. the model reaches the equilibrium

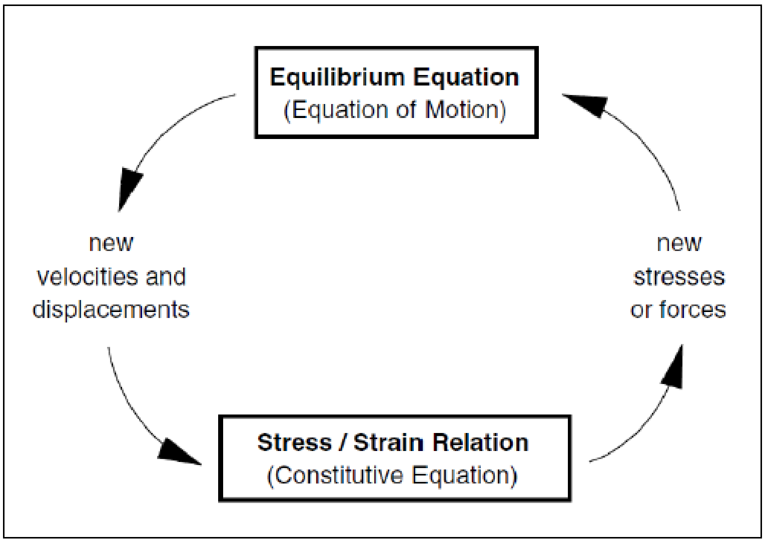

Figure 3.9. Basic explicit calculation cycle in FLAC (Itasca, 2005)

3.5.1. Mining sequence simulation

A multi-stage simulation of cut-and-fill sequence and dimensions of post-pillar are investigated to analyze post-pillar stability for deep hard rock mine i.e. Trepça Underground Mine. Mining sequences are simulated from lower to upper level. The mine excavation height is as practiced in the case study mine. Appropriately the geometry of the conceptual model is built in FLAC^{3D}. The model geometry assuming the inclined ore body is illustrated in Figure 3.10.

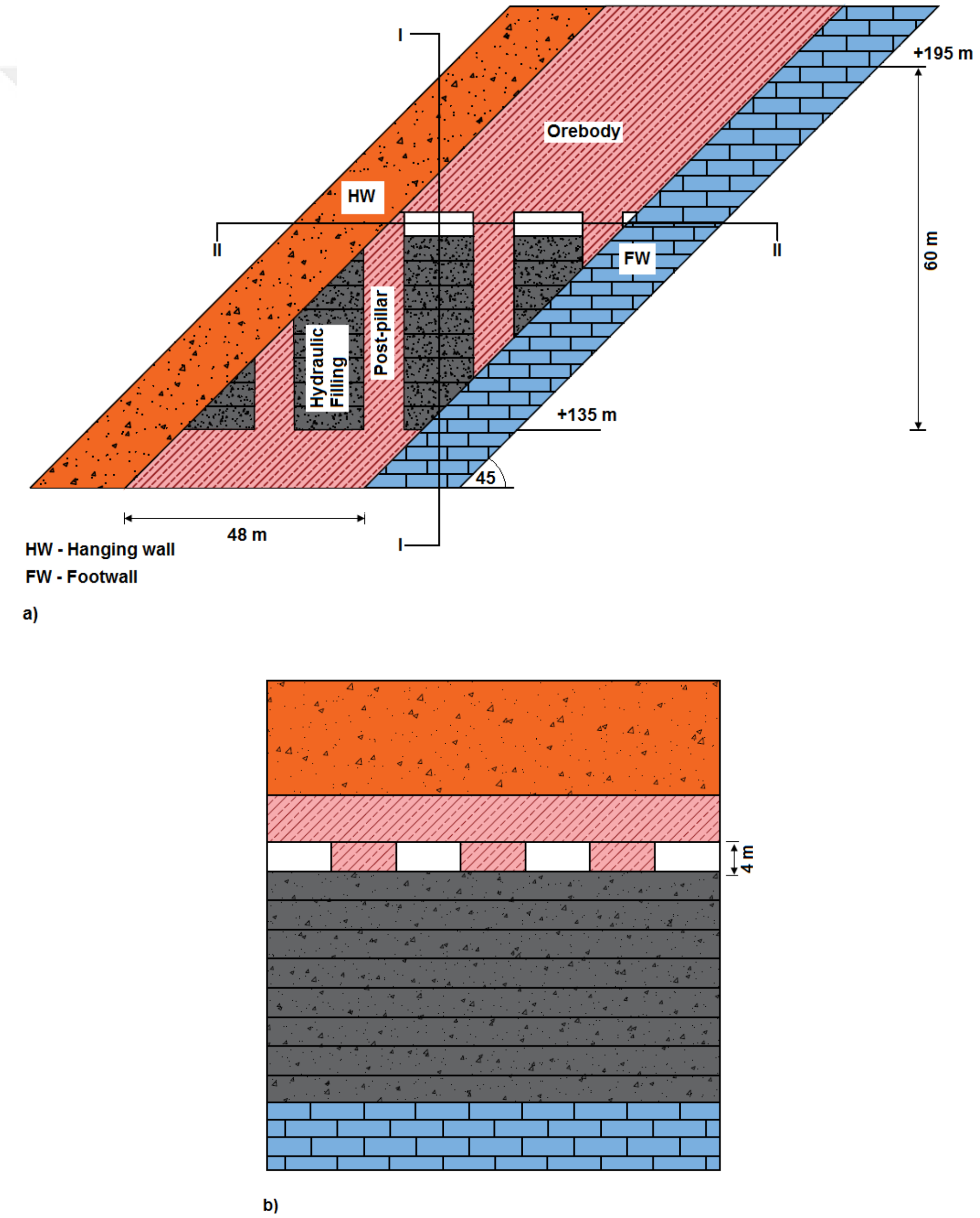
I
+195 m
Orebody
HW
II
FW
II
60 m
Hydraulic Filling
Post-pillar
+135 m
45
48 m
I
HW - Hanging wall
FW - Footwall
a)
4 m
b)

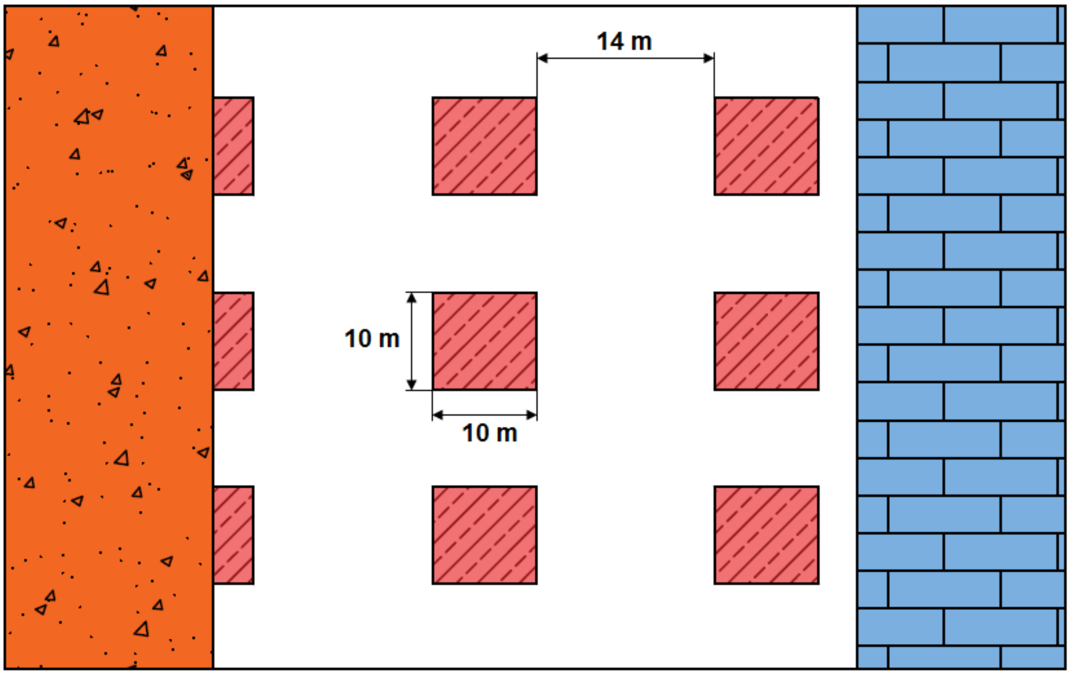

c)

Figure 3.10. Typical post-pillar and overhand cut-and-fill stoping method a) Longitudinal cross-section of central ore body, b) cross-section of the ore body I-I, c) cross-section of the ore body II-II. Not to scale

Overhand cut-and-fill stoping geometry for central ore body at TUM is modeled based on a typical overhand cut-and-fill stopping method with following parameters such as; vertical stope height is 60 m, ore body width is 48 m, the average length of the ore body is 72 m, the ore body has a dipping angle of 45 (degree), as seen in Figure 3.10.

In overhand cut-and-fill stoping method, the support is usually provided by key-block support such are post-pillars, cable bolting and backfilling materials. Applying various supporting tools could prevent rock failures in stopes manifested in terms of rock falling of blocks and spalling as illustrated in Figure 3.11. Rock failures are caused due to influence of complexity of geological conditions surrounding the ore body, wide span width, less and irregular post-pillars left in stopes, high in situ stress state, low post-pillar width to height ratio and most influenced parameter mining depth. Recently, in central ore body at TUM, there are many cases reported of injuries and fatalities to workers from rock falling of blocks and spalling between levels +195 m and +15 m varying mining depth i.e. 693 m, 813 m, and 933 m below the ground surface.

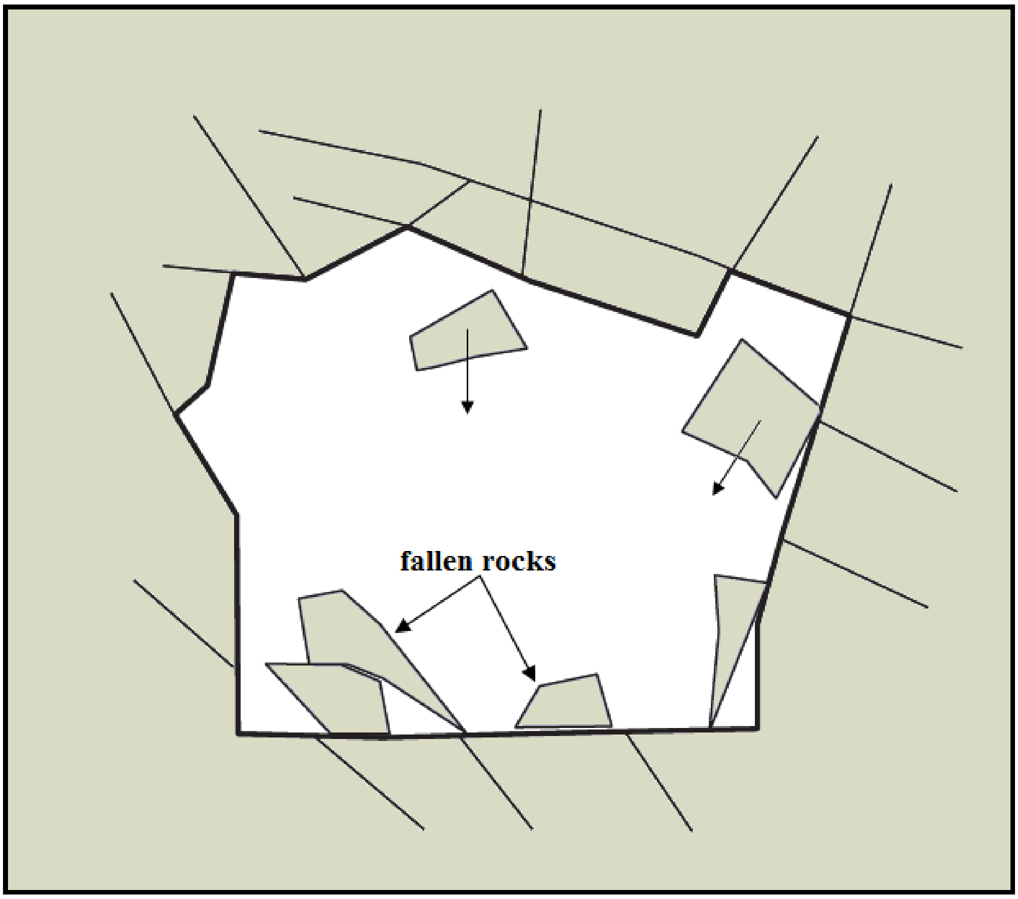

Figure 3.11. Schematic representation of rock falling of blocks from the sidewalls and back of the stope in central ore body at TUM

During field measurements and investigations at TUM, it is observed that post-pillars in large spans created from ore recovery process are not designed properly; as a result, rock falling phenomenon is now more present than ever, as shown in Figure 3.12, and Figure 3.13. Such rock failure phenomenon is occurring repeatedly at TUM and is also affected by low dipping angle of the ore body.

It is pretty well noted by Lang (1994) that post-pillars do not provide many benefits when they are located near/close to the sidewalls of the stope since the walls provide support, as well. Therefore, the maximum benefit of post-pillar is when located at the center of the exposed span yet by the time they reach the center of the span their width to height ratio is 4:1 to 5:1. If post-pillars fail the overall stability of the stope is in a question mark. It is expected that the post-pillars will yield as the width to height ratio decreases, however, experience demonstrate that the post-yield strength of the pillar is still capable of providing support to the immediate back.

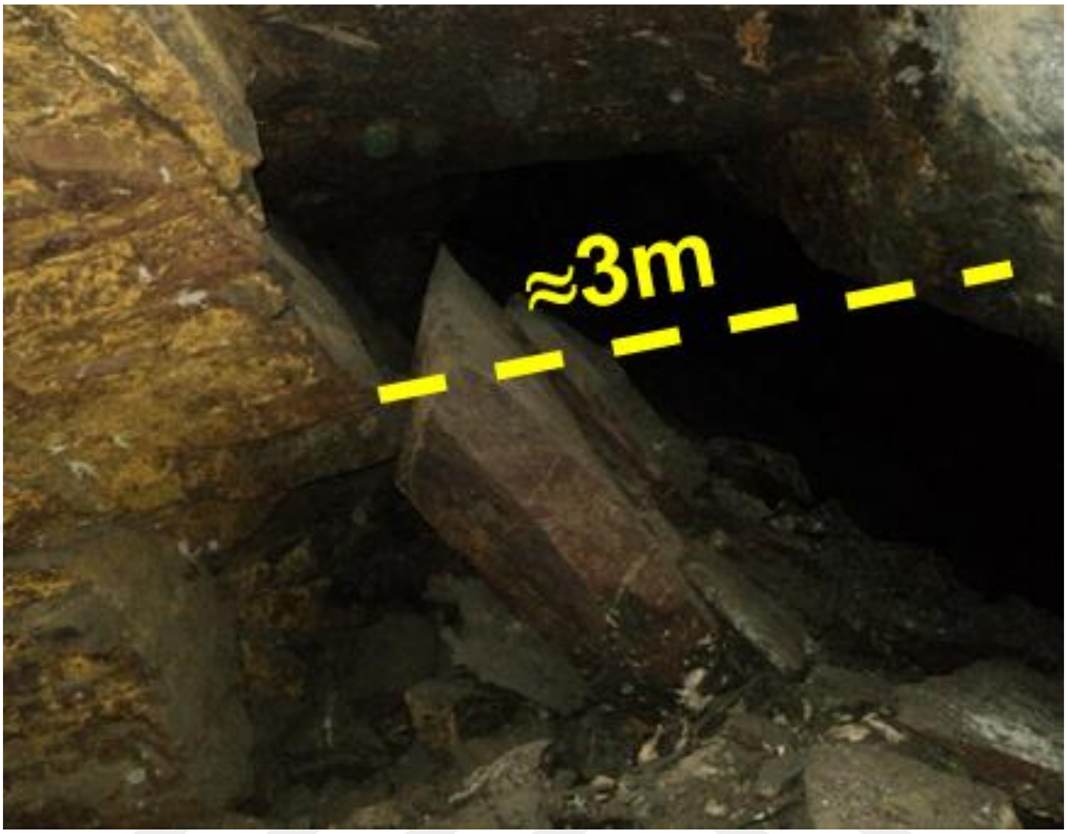

Figure 3.12. Rock falling of blocks from the back of the stope close to post-pillar in central ore body at a mining depth of 693 m

The presence of jointed rock masses in central ore body at TUM is another significant factor influencing the stability of blocks in jointed rock. It is well known the fact that jointed rock masses are characterized by the common occurrence of rock discontinuities with variable length and separation. The stability of blocks in jointed rock is controlled by the forces acting on the blocks and the shear strength of the joints that form the faces. Once the stope is excavated, blocks in jointed rock are not fully created so the face of the blocks has intact rock bridges. Hence, the rock bridges may be strong enough to manage the stability of the blocks right now. Nevertheless, excavation of deep underground stopes might provoke stresses in the preexisting discontinuities propagating through the rock bridges to create fully formed blocks. After a time, the stability of the created block is controlled by the orientations of the faces and the shear strength of the fully formed faces. It could be understood that the shear stresses resisting rock falling are not enough in order to prevent the failure mode given in Figure 3.12. Hence, according to

Figure 3.12 and Figure 3.13, the discontinuities could be only controlled by reinforcement techniques (Villaescusa, 2014).

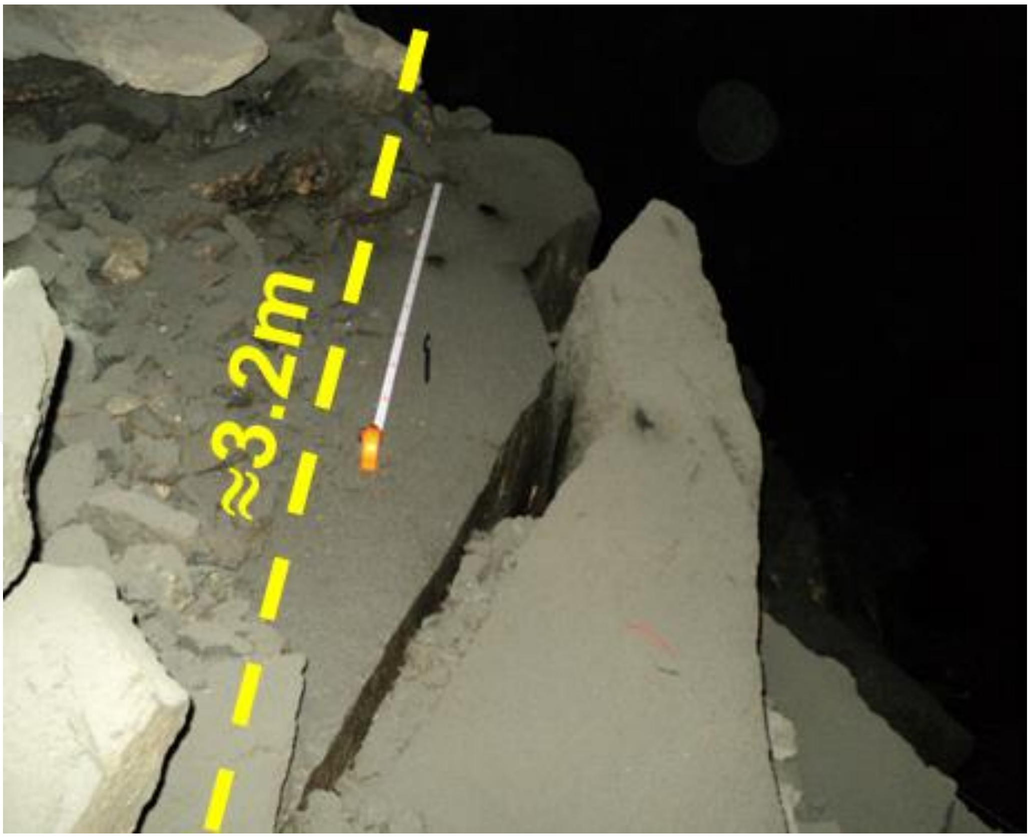

Figure 3.13. Rock falling of blocks from the back of the stope in central ore body at a mining depth of 693 m

As mining depth increase, production stopes and post-pillars are expected to experience high stress levels as a result rock falling of blocks is inevitable. In this study, two numerical models were developed to simulate mining sequences and evaluate post-pillar stability with respect to mine excavation height at varying mining depth. First model simulates hydraulic filling material, as seen in Figure 3.14 and given strength properties in Table 3.15 and second model simulates cemented rock filling material, as seen in Figure 3.15 and given strength properties in Table 3.16.

Table 3.15. Mechanical properties of hydraulic filling (Naung et.al. 2018; Abdellah, 2015)

E(MPa)	σ_c(MPa)	σ_t(MPa)	c(MPa)	ϕ (°)	K(GPa)	G(GPa)
1.4	1.6	0.01	1.2	34.5	1.16	0.53

Due to lack of experimental studies on mechanical properties of backfilling material (e.g. strength and deformation properties) for TUM, the backfilling material properties were adapted from literature as input parameters for numerical simulation. Mechanical properties of the backfilling material were approximated considering similar case studies which thought to be similar to the case study at TUM.

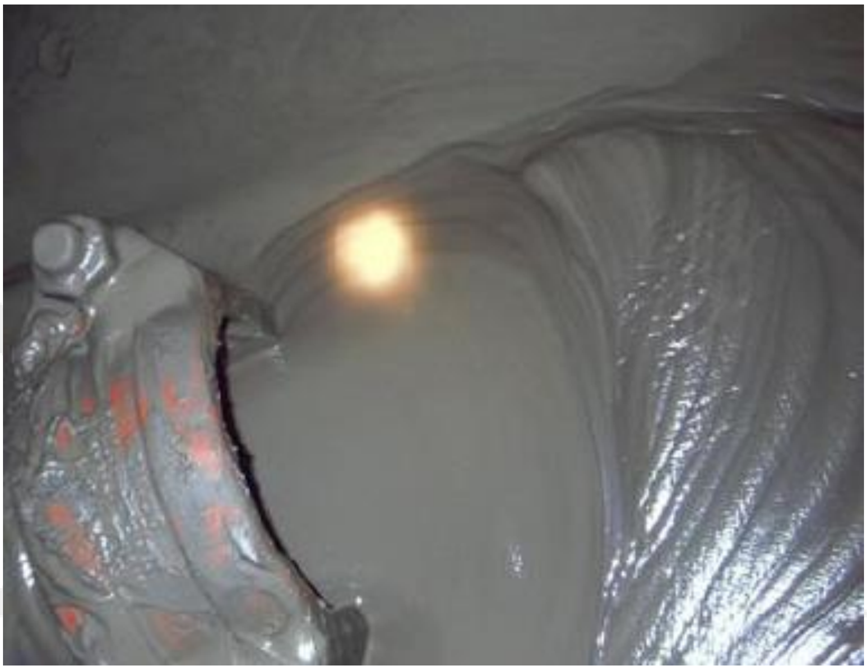

Figure 3.14. Hydraulic fill – Model 1 (O'Toole et al., 2011)

Backfilling materials (e.g. hydraulic filling, paste filling, cemented rock filling) help in reducing ore dilution and enabling maximum ore recovery. Moreover, backfilling materials are capable of bearing active pressures, providing not only ground support but also improves wall rock stability and provide confinement to post-pillars (Emad, 2013).

Table 3.16. Mechanical properties of cemented rock filling (Abdellah et al., 2012; Yang et al., 2015; Emad 2017; Deng 2017; Naung et al., 2018; Zhou et al., 2019)

Case No.	E (GPa)	ν	σ_c (MPa)	σ_t (MPa)	c (MPa)	ϕ (°)
1.	0.1	0.3	3	0.01	1	30
2.	-	-	3	0.21	0.59	28
3.	2.50	0.35	-	0.03	1.10	37
4.	2.85	0.34	6.5	0.7	1.4	25.4
5.	1.13	0.26	8.50	1.01	1.16	48
6.	1	0.3	3.5	0.5	0.65	35
Average	1.5	0.31	4.9	0.41	0.98	33.9

The bulk modulus (K) and shear modulus (G) were calculated from the deformation modulus and Poisson's ratio of backfill material using equations (50) and (51).

$$K = \frac{E}{3(1-2\nu)} \qquad (3.50)$$

$$G = \frac{E}{2(1+\nu)} \qquad (3.51)$$

After calculations, K = 1.31 (GPa) and G = 0.57 (GPa)

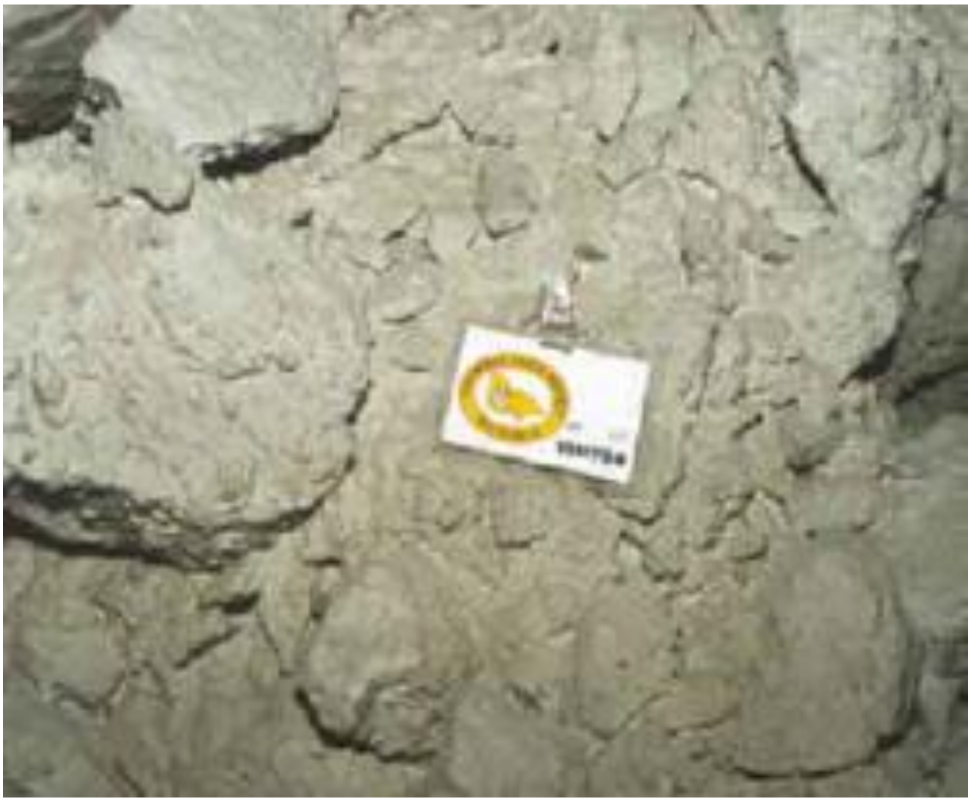

Figure 3.15. Cured cemented rock fill– Model 2 (Dorricott and Grice, 2002)

The domain outline describing the problem is given in Figure 3.16 using FLAC^{3D}; only half of the model in y-direction is given due to the symmetry of the stope geometry and other conditions. Also, a system of reference axes was selected with the orientation of the stope excavation and the origin at the intersection of the stope axis with the front face of the domain problem.

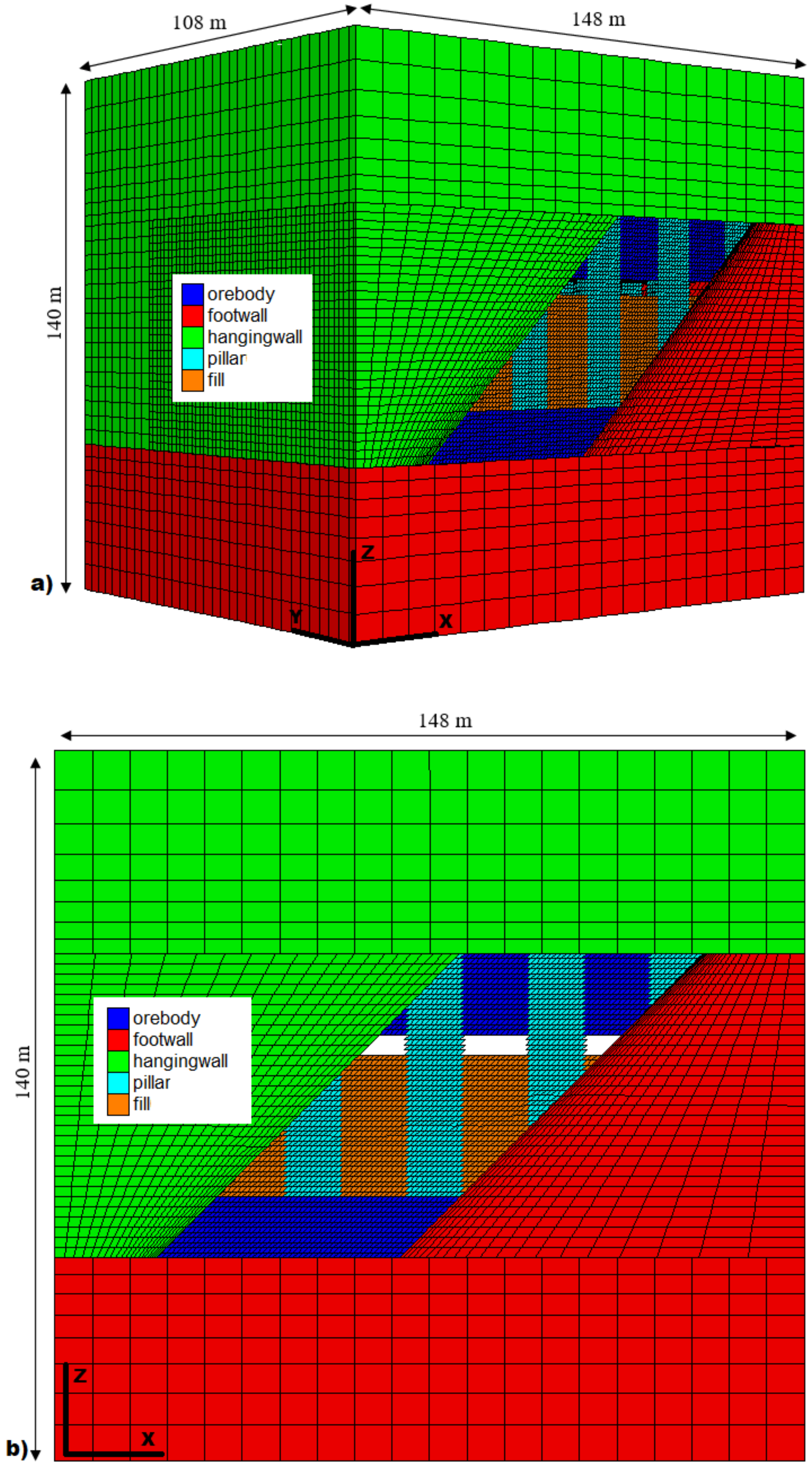
108 m
148 m
140 m
orebody
footwall
hangingwall
pillar
fill
a)
Z
Y
X
148 m
140 m
orebody
footwall
hangingwall
pillar
fill
b)
Z
X

Figure 3.16. Numerical modeling of central ore body at TUM. a) represent half of the model in y-direction, b) represent front view model in y-direction

Hence, to maintain stope stable optimum mine excavation height and post-pillar dimensions must be determined based on expanded failure zone and maximum principal stress distributed around the mined-out stopes and in post-pillars. The lithology within the model is relatively simple, hanging wall is volcanic breccia, ore body is sulfide mineralization and footwall is limestone. The numerical model is 148 m in the x-direction, 216 m in y-direction and 140 m in the z-direction with a total of nearly 371520 numbers of zones and 394192 grid-points. All brick elements follow ideal elasto-plastic constitutive model, where the Mohr-Coulomb yield criterion is accepted.

Mining sequences and modeling stages are presented in Table 3.17. The excavation and backfilling steps have been considered in the numerical analysis. The development of failure zone in post-pillars and around mined-out stope (e.g. hanging wall and/or footwall) are obtained by simulating the different excavation and filling stages.

Table 3.17. Mining stages and sequences carried out in numerical modeling

Depth (m)	Stage height (m)	Mining Stage	Mining sequence	FLAC model
453 573 693 813 933	4	First stage	Excavation 1 Fill 1	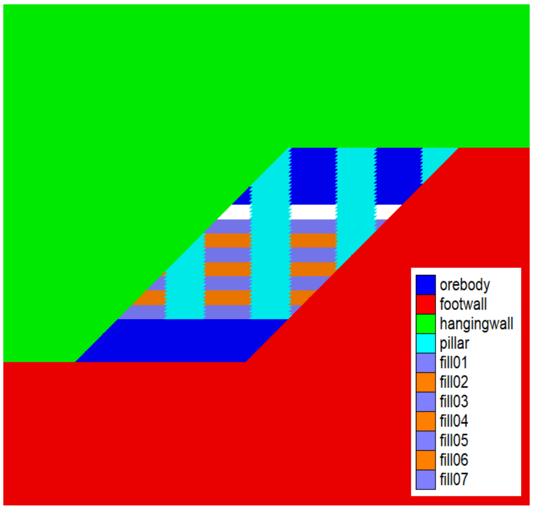 orebody footwall hangingwall pillar fill01 fill02 fill03 fill04 fill05 fill06 fill07
	4	Second stage	Excavation 2 Fill 2	
	4	Third stage	Excavation 3 Fill 3	
	4	Forth stage	Excavation 4 Fill 4	
	4	Fifth stage	Excavation 5 Fill 5	
	4	Sixth stage	Excavation 6 Fill 6	
	4	Seventh stage	Excavation 7 Fill 7	
	4	Eighth stage	Excavation 8 -	
Note:	Mining stope: 72 m in length, 48 m in width and 4 m in height. Post-pillars: square pillars of 13 m x 13 m cross section with 10 m x 10 m spacing. square pillars of 12 m x 12 m cross section with 12 m x 12 m spacing. square pillars of 10 m x 10 m cross section with 14 m x 14 m spacing. square pillars of 7 m x 7 m cross section with 15 m x 15 m spacing.			

3.6. Numerical Analysis of Cut-and-Fill Stoping Method

In numerical modeling, one of the utmost important concerns is the accurate assessment of the input parameters. Hence, the predicted results by numerical modeling are widely depending upon the question of how well the input parameters are approximated.

3.6.1. Post-pillar design for overhand cut-and-fill stoping method

The general geometry of the stope to be modeled in FLAC^{3D} is given in Figure 3.10 with all design parameters. Stope design parameters are discussed in Section 3.4.1.

3.6.2. Rock mass properties

Geotechnical properties of the rock mass used in the numerical modeling are presented in Table 3.10. Rock mass properties were calculated based on rock mass classification systems for modeling purposes and are summarized in Table 3.5. Table 3.5 shows that RMR ranges from medium rock mass (57.4) to good rock mass (72.2).

Then, backfilling properties were adapted from literature and are given in Table 3.15 for hydraulic filling and Table 3.16 for cemented rock filling. The Mohr-Coulomb failure criterion with is used for the rock masses and a backfilling material in the numerical modeling is given in equation (3.52) and (3.53), as following (Li et al., 2013):

$$f_s = \sigma_1' - \sigma_3' \frac{1+\sin\varphi_m}{1-\sin\varphi_m} - 2c_m\sqrt{\frac{1+\sin\varphi_m}{1-\sin\varphi_m}} \quad (3.52)$$

$$f_t = \sigma_3' - \sigma_{tm} \quad (3.53)$$

Where; σ_1' and σ_3' represent the maximum and minimum principal stress, c_m and φ_m represent cohesion and internal friction angle. If $f_s > 0$ a shear failure will occur, whereas, tensile failures occur if tensions exceed tensile strength of the material.

3.6.3. In situ stress state

In numerical modeling analysis, initial stresses are strongly required to be estimated in order to simulate deep underground stopes below the ground surface. Initial stresses such as vertical in situ stress state (p_v) are calculated analytically from equation (3.54) and (3.55) varying with depth.

$$p_v = \gamma \times z \tag{3.54}$$

$$p_h = k \times p_v \tag{3.55}$$

Results of vertical and horizontal in situ stress state are tabulated in Table 3.18. The ratio of horizontal stress (p_x) to vertical stress (p_v) was adopted $(k = 1)$ due to the deep underground stopes and the hydrostatic stress conditions. Unfortunately, there is no in situ stress measurement in the mine site.

Table 3.18. In situ stress state for numerical modeling

In situ stress state	Mining depth		
	693 m	813 m	933 m
$p_v = p_h$	18.7 MPa	21.9 MPa	25.1MPa

3.6.4. Mesh and boundary conditions

The FLAC^{3D} model is constructed using brick-shaped mesh. The finer mesh is used within ore body brick-shaped mesh to get more accurate results. The displacement boundary conditions of the model consist of (1) fixed in x-direction displacement at the right and left boundaries, (2) fixed in y-direction displacement at the back and front of the boundaries, (3) fixed z-direction displacement at the bottom and at the top of the boundary.

After defining the constitutive relation and properties of rock masses, assigning boundary conditions and initial state, then the model was run until the equilibrium stage has been achieved.

4. RESULTS AND DISCUSSION

In this chapter, blast vibration measurements, rock mass damage analysis and control based on rock mass damage threshold levels by extrapolating the far-field PPV predictor equation closer to the blast source and maximum charge per delay will be discussed. Further, numerical analysis results of post-pillar design for overhand cut-and-fill stoping method and new assessment index i.e. Pillar Yield Ratio (PYR) together with new Pillar Stability Graph (PSG)will be introduced.

4.1. Assessment of Rock Mass Damage due to Blasting

Rock mass damage induced by blasting causes safety threats and production losses. The main objective during ore exploitation process is to achieve the desired extraction profile of the ore body as safely as possible, leaving the rest of the ore body with minimal damage. Rock mass damage due to blasting could result in rock failures and unstable ground conditions. Knowing how far the fractures are generated by a production blast will go into the unexcavated ore body is very important for blast engineers to design a safe recovery process. In order to avoid strong tensile and some eventual radial cracking to the rest of the rock mass, the quantity of explosives detonated per delay must be decreased in order to achieve the desired extraction profile.

In this section, an attempt has been made to describe the ground vibration threshold levels for rock mass damage in a deep underground production stope. Rock mass damage due to blasting has been correlated with the possible threshold PPV levels. Extrapolating far-field PPV predictor equation, PPV threshold levels for different rock mass damage were proposed. Further, the goal here was to fix the maximum permissible charge per delay that can be detonated maintaining ground vibration in range of ($50 \text{ mm/s} \leq \text{PPV} < 250 \text{ mm/s}$). The blast pattern design and maximum charge per delay have been completed maintaining the PPV values below the 250 mm/s level.

4.1.1 Blast vibration measurements and predictor equation

Triaxial geophones were installed near and within the stope boundary varying distance from the blasting point to measure PPV values. These instruments are capable of measuring ground velocities up to 250mm/s between the 2Hz to 250Hz range. The seismic field data, consisting of the measurement of peak particle velocity over a period of time was recorded on an Instantel^{TM} Micromate®. Figure 4.1 present the Micromate®, with triaxial geophone used to monitor blast-produced seismic vibrations.

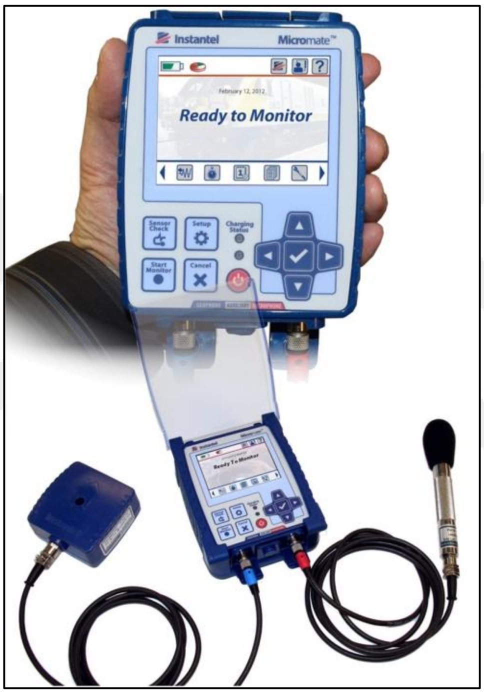

Figure 4.1. Micromate® and triaxial geophone

The general specifications of the geophone utilized were obtained from the product instruction sheet as given in Table 4.1.

Table 4.1. General specification of triaxial geophone(www.instantel.com)

Amplitude range	Up to 254 (mm/s)
Frequency range	2 to 250Hz
Response standard	ISEE Seismograph specification or DIN 45669-1
Resolution	0.00788 (mm/s)
Transducer density	2.2 g/cc
Seismic trigger	0.13 to 254 mm/s
Record time	1 to 90 seconds

Blast vibration monitoring and measurement were conducted in order to establish the ground vibration predictor equation. The blast vibrations have been monitored at the floor of the production stope using triaxial geophones, as seen in Figure 4.1. Thus, for each round of the blast, the PPV values were measured for varying radial distance (D) and maximum charge per delay (W). In Table 4.2, monitored data for each blast round radial distance, charge weight per delay, scaled distance and PPV values are presented. Scaled distance was calculated using equation (2.1).

Table 4.2. Blast vibration monitoring details at Trepça underground mine

No.	**Distance**	**Charge weight per delay**	**Scaled Distance**	**Peak Particle Velocity**
	D(m)	**W (kg)**	**SD (m/kg1/2)**	**PPV (mm/s)**
1	17.8	9.8	5.69	84.83
2	14.5	12.2	4.14	91.45
3	16	12.2	4.57	80.74
4	12.8	11.2	3.82	102.9
5	27.6	11.6	8.1	59.48
6	33.5	9.8	10.70	46.15
7	24	11.2	7.17	52.13
8	65	12.6	18.3	18.64
9	15.7	13.3	4.3	100.5
10	31	12.6	8.7	51.77
11	53.8	12.6	15.2	24.27
12	51.3	17.5	12.3	32.55
13	24.8	13.1	6.8	60.36
14	22.8	15.9	5.7	75.93
15	24	11.2	7.2	52.13

Blast vibration measurements have been assessed to accomplish a safe blast design including delay sequence, drill and charge pattern. So, maximum charge per delay was suggested for safe exploitation process at TUM. It has been indicated that the SD formula, given in equation (2.1) shows a reasonable correlation coefficient ($R^2 = 0.95$). The best fit blast vibration predictor is shown in Figure 4.2.

$$PPV = 440.72\left(\frac{D}{\sqrt{W}}\right)^{-1.036} \tag{4.1}$$

Where;

D – is the distance (m)

W – is the maximum charge per delay (kg)

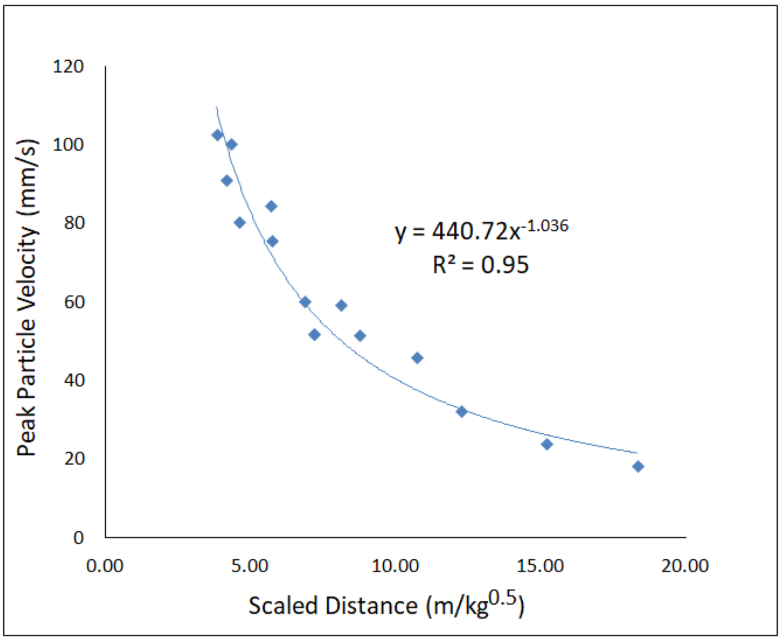

Figure 4.2. Blast vibration predictor for blast at Trepça underground mine

Figure 4.2 shows the PPV results for different numbers of blasted rounds recorded on geophone installed at varying distances within the stopes. It is clearly seen that the PPV values decrease with the distance to the source of blast. The highest peak particle value recorded at mine site was 102.9 mm/s, whereas, the lowest peak particle value recorded was 18.64 mm/s. The PPV vs. SD power law best-fit curve is estimated from 15 blast rounds. From the graph shown in Figure 4.2 it is understood that the higher PPV values occur in the vicinity of the blasting area. Furthermore, in order to achieve at a conclusion on what possible scenarios there might be a geological rock mass damaged or completely detached from the back of the stope and/or hanging wall and footwall, a further research have been undertaken extrapolating PPV predictor equation, as described in Section 4.1.2.

4.1.2 Extrapolation of the far-field PPV predictor equation

PPV is the most well-known, widely used, and is considered as the most acceptable rock mass damage criteria, predicting the rock mass damage based on threshold limits proposed by different researchers. In this research, an attempt has been made to evaluate the rock mass damage adapting the rock damage threshold levels by extrapolating the far-field PPV predicator equation closer to the blast source. Hence, the extrapolated PPV values for the rock mass damage threshold levels of PPV are shown in Figure 4.3.

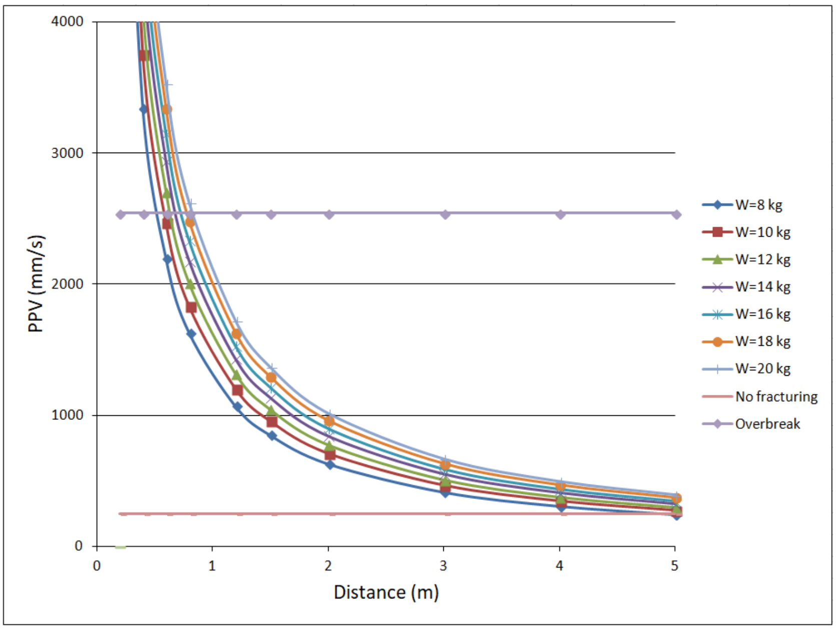

Figure 4.3. Extrapolated PPV values with varying distances

Figure 4.3 shows that PPV threshold limit for overbreak/rock mass damage is above 2540 mm/s for the rock type and underground production stope. The overbreak predicted at this PPV level 2800 mm/s, rock damage is observed to be 0.42 m when using 8 kg and 0.63 m when using 20 kg of explosive quantity per delay. In Figure 4.4 an overbreak case due to rock blasting is shown at TUM at a depth of 813 m below ground surface. Fortunately, no miners were present at that time.

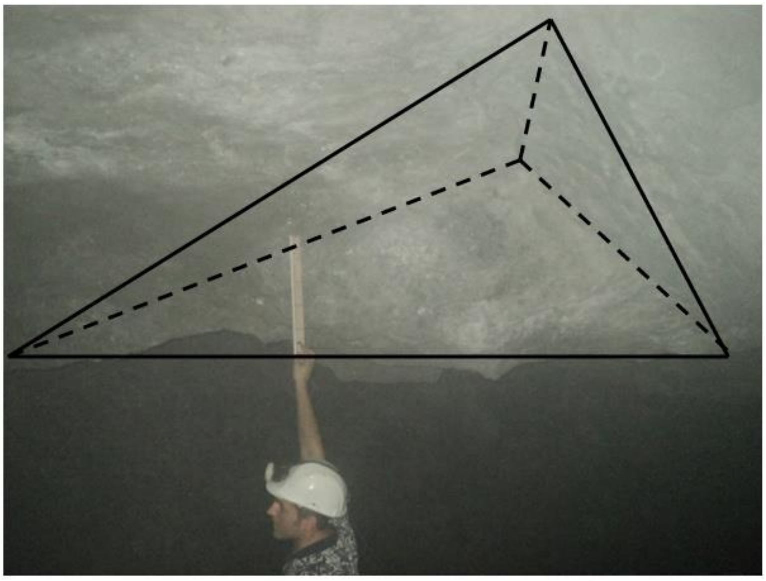

Figure 4.4. A few cubic meters of rock fallen of block from the roof of the stope due to rock blasting at TUM

4.1.3 The assessment of maximum charge per delay

The safe PPV threshold levels for rock mass damage were adapted from the literature presented in Table 2.2. Using the predictor equation, the maximum charge per delay has been fixed for an allowable vibration level of 50 mm/s, 150 mm/s, and 250 mm/s, as shown in Table 4.3.

Table 4.3. Maximum allowable charge per delay with distance

Distance (m)	Maximum charge per delay (kg)		
	PPV = 50 mm/s	PPV = 150 mm/s	PPV = 250 mm/s
4	0.91	2.00	5.36
6	2.05	4.49	12.05
8	3.65	7.99	21.42
10	5.71	12.48	33.47
12	8.22	17.98	48.20
14	11.19	24.47	65.60

In this research, different rock mass damage assessment techniques have been reviewed. Based on the ground vibration predictor equation the safe maximum allowable charge per delay has been suggested. Also, extrapolation of the far-field PPV predictor equation was performed assessing the rock mass damage threshold levels.

4.2. Post-Pillar Performance Assessment Index

In the following, new assessment index i.e. Pillar Yield Ratio (PYR) is described, which is used as a basis for the interpretation of numerical results applied to the assessment of geotechnical stability of the modeled post-pillars for overhand cut-and-fill stoping method.

4.2.1. Development of failure zones

The failure criterion is the most common used in numerical modeling stage when elasto-plastic solution is used. According to Zhang and Mitri, (2008) failure state is reached when the stress state reaches the surface of the failure function, when the rock is loaded beyond its elastic limit. Hence, the failure state is used to evaluate the stability of post-pillars performance. In this study, the Mohr-Coulomb yield criterion is accepted and elasto-plastic behavior of the rock mass is employed. Moreover, extent of failure zones will be considered a measure for post-pillar rating performance determining a border line between stable, potentially unstable, and failure state.

4.2.2. Pillar Yield Ratio (PYR)

The Pillar Yield Ratio (PYR) has been developed to compare of potential instabilities of post-pillars under different mining conditions (e.g. dimension of pillars, mine excavation height, mining depth). In this assessment index, the percentage of yield domain area of the pillar is calculated according to the following equations:

$$(PYR)_{CC} = \frac{\mathrm{A_Y}}{\mathrm{w_p \times w_p}} = \frac{\mathrm{A_Y}}{\mathrm{A_{pCC}}} \times 100\% \quad (4.2)$$

$$(PYR)_{AA} = \frac{\mathrm{A_Y}}{\mathrm{w_p \times h_p}} = \frac{\mathrm{A_Y}}{\mathrm{A_{pAA}}} \times 100\% \quad (4.3)$$

$$(PYR)_{BB} = \frac{\mathrm{A_Y}}{\mathrm{w_p \times h_p}} = \frac{\mathrm{A_Y}}{\mathrm{A_{pBB}}} \times 100\% \quad (4.4)$$

Where;

(PYR) - is the Pillar Yield Ratio,
(A_Y) - is the total yield domain area of the pillar,
(A_{pCC}) - is the total domain area of the pillar in horizontal cross section (i.e. plan view),
(A_{pAA}) - is the total domain area of the pillar in vertical cross section (i.e. side view),
(A_{pBB}) - is the total domain area of the pillar in vertical cross section (i.e. front view).

Both shear and tension failure modes (Figure 4.5) are considered during calculation procedure using equations (4.2), (4.3) and (4.4). The yield ratio in percentage (%) is obtained based on cumulative number of yield domain area of the pillar (A_Y) to the total domain area of the pillar (A_P). If the yield domain area of the pillar is ‘100’ this indicate total failure state and when the yield domain of the pillar is ‘0’ this indicate none failure state. Further, yielding will be considered as a rule for post-pillar instability performance, as presented in Table 4.4. A rule of thumb being used in this assessment index is taking into account the highest PYR values of the yield domain area after comparing three different cross section views of post-pillar, as shown in Figure 4.5.

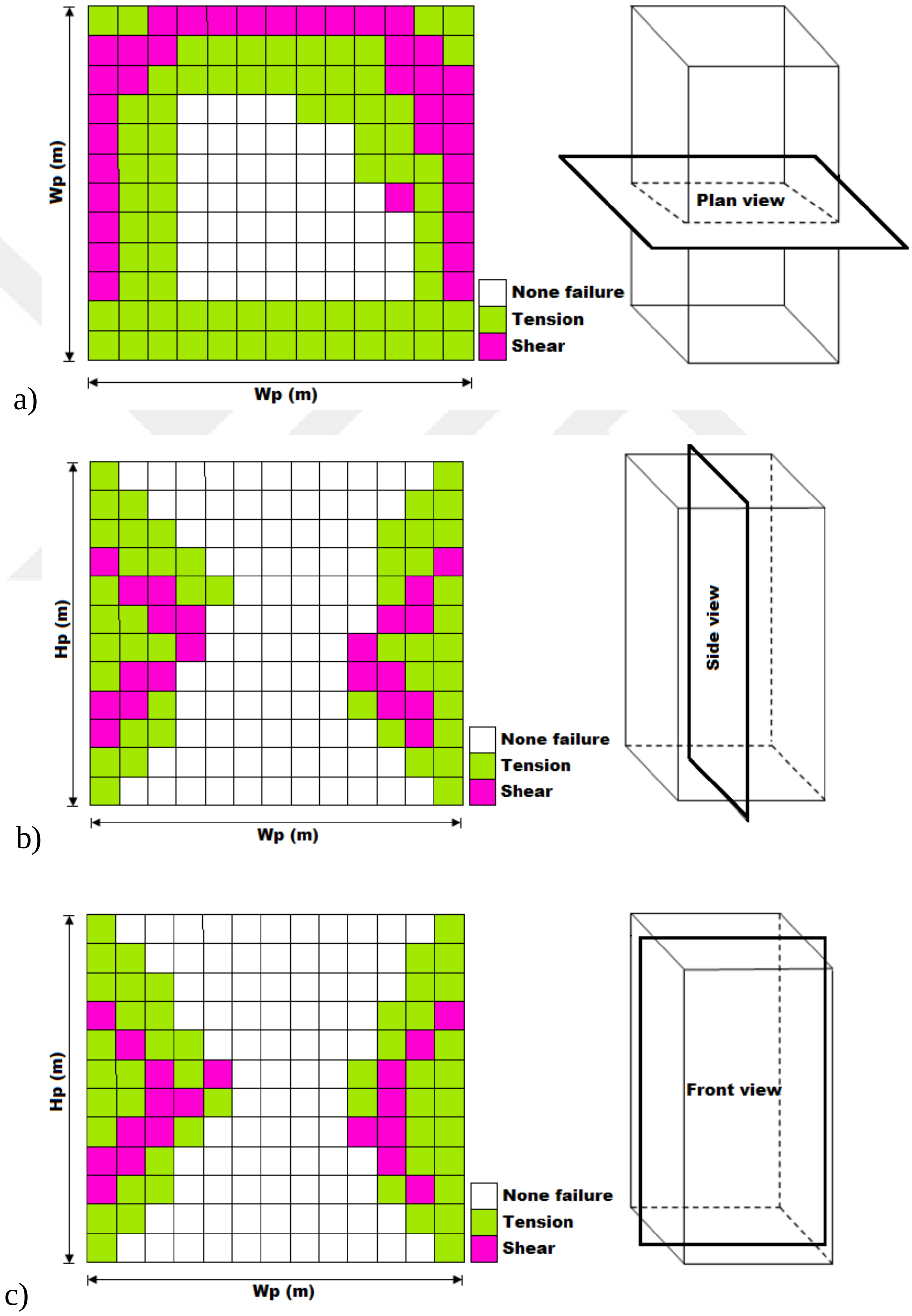
Wp (m)
Wp (m)
None failure
Tension
Shear
Plan view
a)
Hp (m)
Wp (m)
None failure
Tension
Shear
Side view
b)
Hp (m)
Wp (m)
None failure
Tension
Shear
Front view
c)

Figure 4.5. Post-pillar model cross-section view. a) Post-pillar plan view – CC, b) Post-pillar side view – BB, c) Post-pillar front view – AA

During numerical analysis results, it has been felt the need to develop a classification index to define the post-pillar failure state more precisely, without judging only the visual extent of the failure zones in a pillar or describing in words as failed or partially failed. Herein, the objective of PYR classification index is to determine a border line between stable, potentially unstable, and failed pillars, as given in Table 4.4.

Table 4.4. Pillar Yield Ratio (PYR) classification index

Pillar Yield Ratio Description	Rating (%)
Stable state	$0 \leq PYR < 35$
Potentially unstable state	$35 \leq PYR < 60$
Failure state	$60 \leq PYR < 100$

Furthermore, a new Pillar Stability Graph (PSG) was developed for Trepça Underground Mine (TUM) following the principle of PYR classification index. PSG is developed mainly based on Lunder's pillar stability graph (Lunder, 1994). The Pillar Stability Graph (PSG) is originally a site-specific database for the Trepça Underground Mine (TUM) that investigates the minimum allowable pillar dimensions to be left in stope, as shown in Figure 4.6. In this section, a case study tabulated in Table 4.5 is simulated to determine post-pillar stability state based on Underground Pillar Stability Graph (UPSG) developed by Lunder (1994) and compared with new developed Pillar Stability Graph (PSG), as seen in Figure 4.6.

Table 4.5. Stoping design parameters

Case study design parameters	Values
Depth below ground surface (m)	933
Uniaxial compressive strength of intact rock i.e. ore body (MPa)	78
Pillar width (m)	12
Pillar length (m)	12
Mine excavation height (m)	4

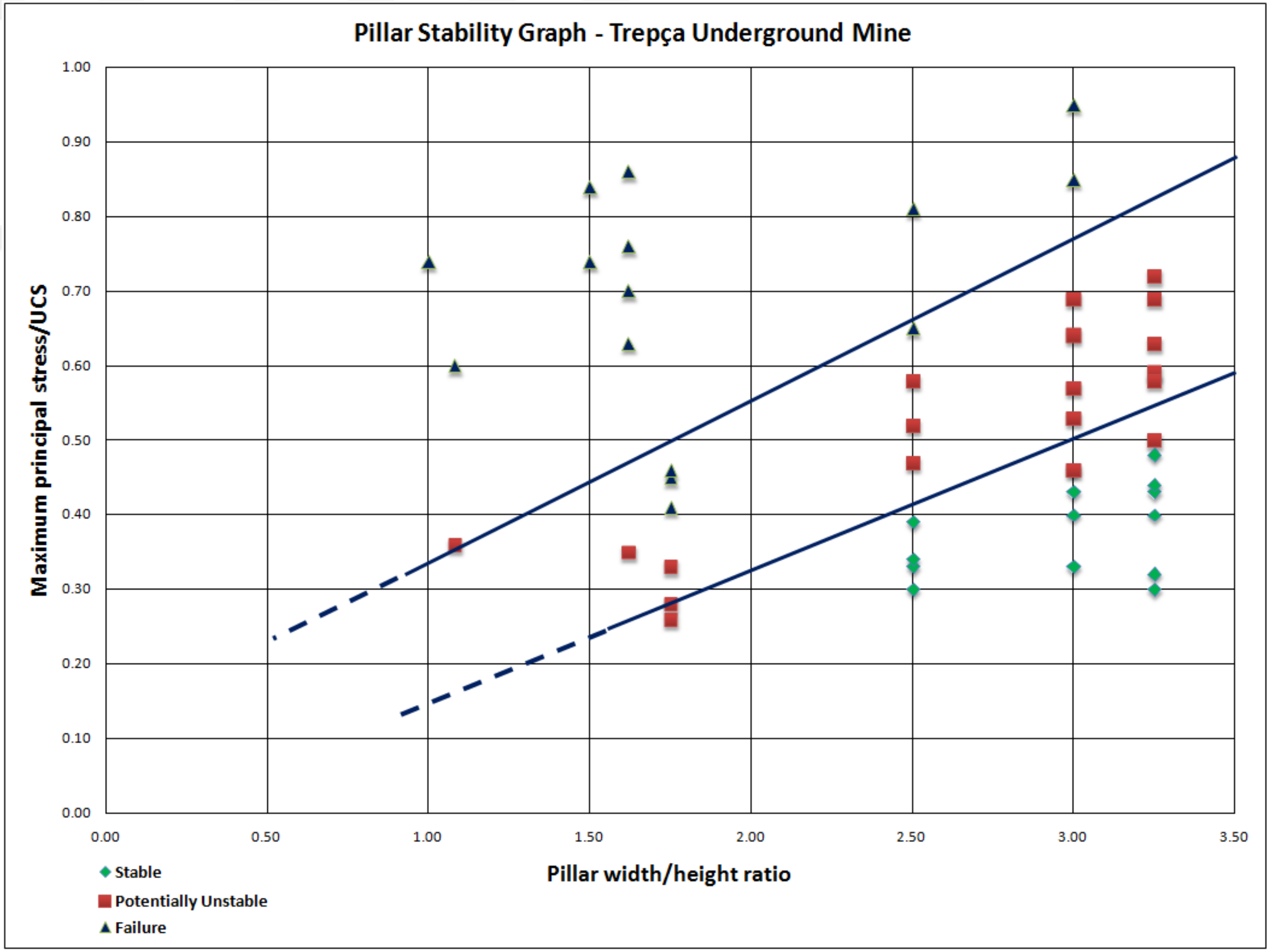

Figure 4.6. Pillar Stability Graph (PSG) for Trepça Underground Mine (TUM)

Based on numerical analysis results, the maximum principal stress in pillar is determined to be $(\sigma_{max} = 37.9 \text{ MPa})$, whereas, the pillar width to height ratio is adapted to be $\left(w_p/h_p = 3.0\right)$. Hence, knowing the uniaxial compressive strength $(\sigma_{ci} = 78 \text{ MPa})$, it is very easy to assess the stability of post-pillars based on Lunder's graph given in Figure 4.7 and compare the results to recently developed PSG graph given in Figure 4.6.

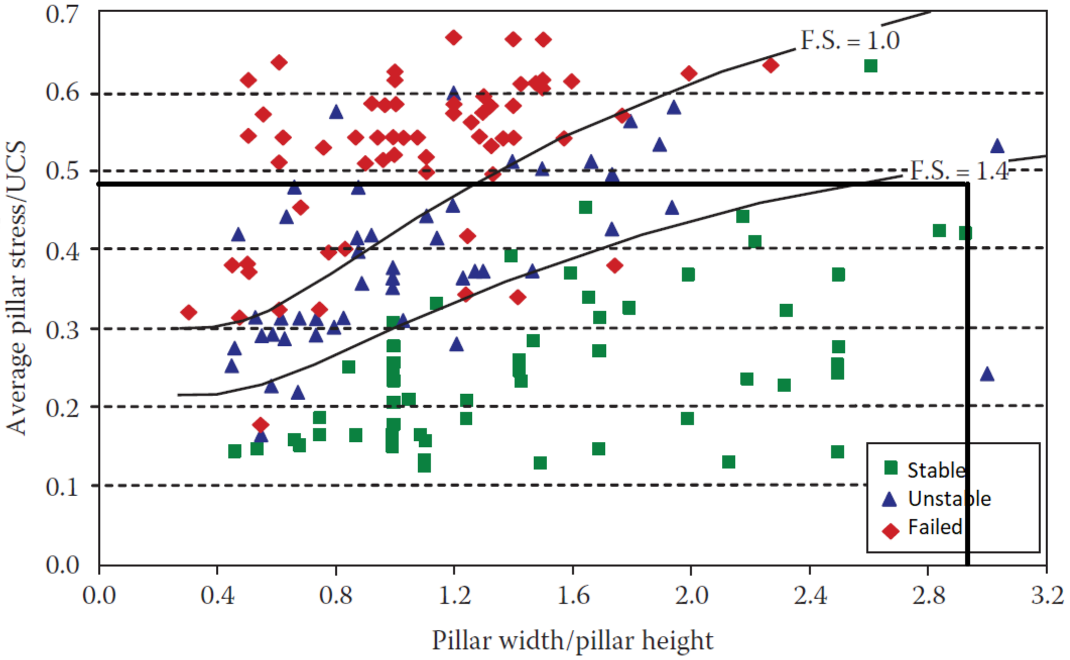

Figure 4.7. Case study post-pillar assessment based on maximum principal stress obtained from numerical analysis FLAC^{3D}

4.3. Numerical Analysis Results

In this Section, numerical analysis results are divided into two parts: Post-pillar design for overhand cut-and-fill stoping method using Hydraulic Filling (HF) material and Cemented Rock Fill (CRF) material. Numerical modeling is performed using FLAC^{3D} software (Itasca, 2005) to represent e typical geometry of the central ore body of Trepça Underground Mine (TUM), as seen in Figure 4.8. Only the region around the ore body is discretized to be a dense mesh grid. Three different geological rock units representing hanging wall i.e. volcanic breccia, ore body i.e. sulfide mineralization, and footwall i.e. limestone are simulated. The geometry of the ore body is discussed in Section 3.5.1. This analysis is based on the Mohr-Coulomb failure criterion and material behavior for the rock mass assumes to be elastic-perfectly-plastic material behavior.

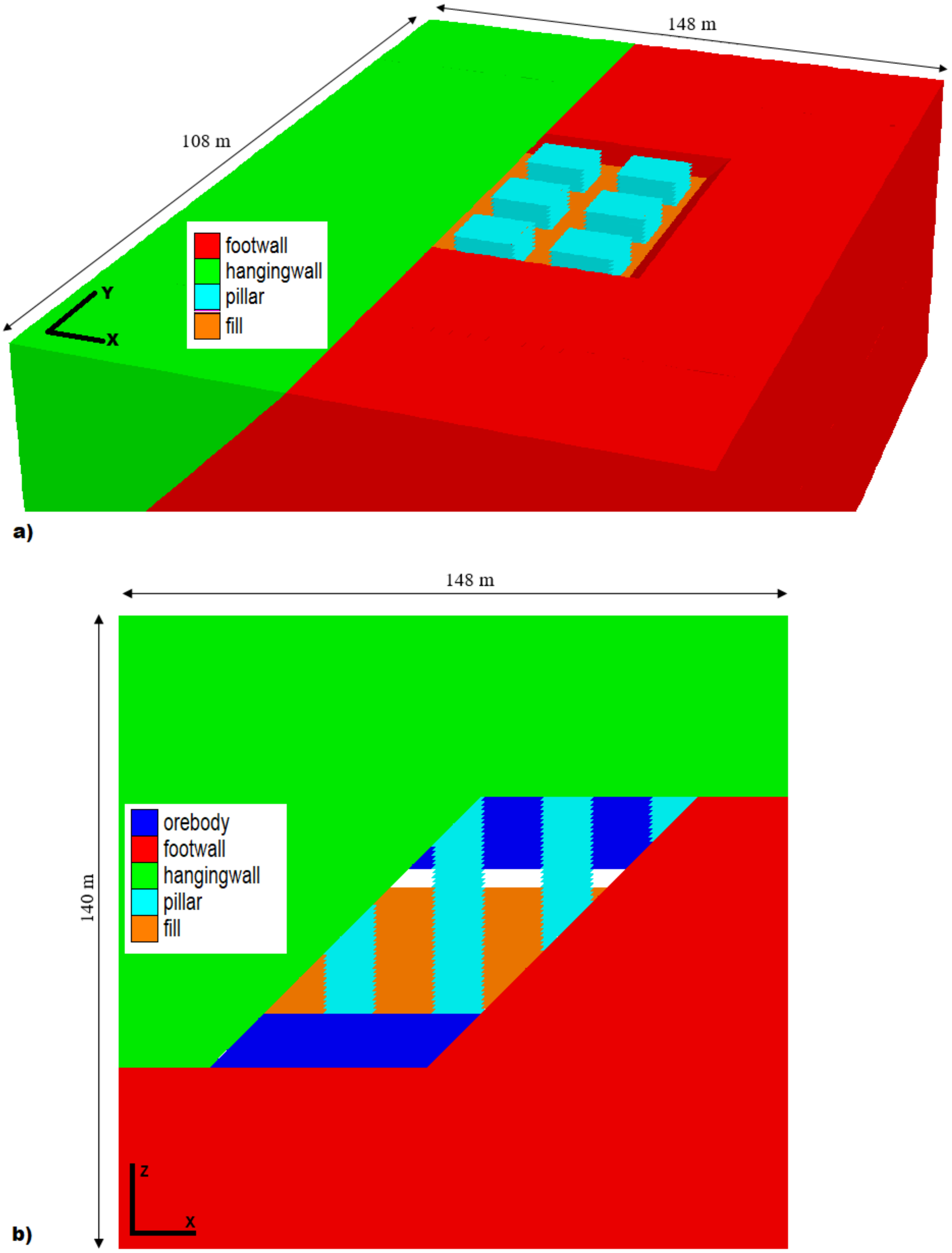
148 m
108 m
footwall
hangingwall
pillar
fill
Y
X
a)
148 m
140 m
orebody
footwall
hangingwall
pillar
fill
Z
X
b)

Figure 4.8. FLAC^{3D} numerical model setup of post-pillar and overhand cut-and-fill stoping method. a) three-dimensional perspective view of the stope and post-pillars with delayed backfill, b) two-dimensional cross section view of the modeled stope and post-pillars with delayed backfill

Further, eight stops are excavated advancing upwards with delayed backfill. The average values of all geotechnical rock mass and material properties are used in both models. Herein, the objective is to investigate the confinement effect of backfilling materials (e.g. hydraulic and cemented rock filling) on post-pillars with respect to mine excavation height and depth. In numerical modeling process, mining stages are used to simulate the mining sequences i.e. mine excavation with delayed backfill.

4.3.1. Stability assessment of post-pillars at different mine excavation height using hydraulic fill material

In this section, numerical simulations have been performed to examine the effect of mine excavation height on the post-pillars stability. In the numerical modeling process, modeling mining sequences are used to simulate the mine excavation stage and delayed backfill. Numerical modeling results for extent of failure zone are shown in Figure 4.9. Left picture in Figure 4.9 indicates the front view of the central ore body, whereas, the right picture indicates the plan view.

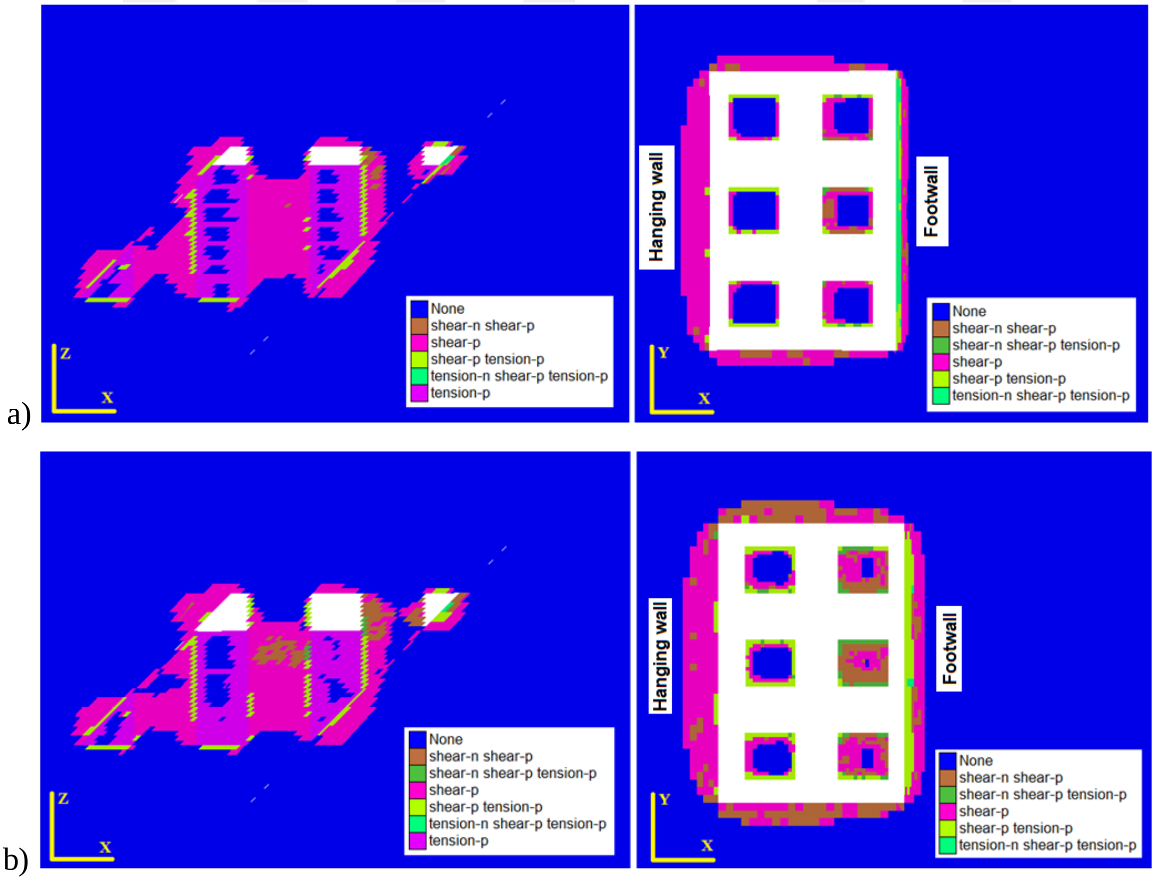
a)
None
shear-n shear-p
shear-p
shear-p tension-p
tension-n shear-p tension-p
tension-p
Z
X
Hanging wall
Footwall
None
shear-n shear-p
shear-n shear-p tension-p
shear-p
shear-p tension-p
tension-n shear-p tension-p
Y
X
b)
None
shear-n shear-p
shear-n shear-p tension-p
shear-p
shear-p tension-p
tension-n shear-p tension-p
tension-p
Z
X
Hanging wall
Footwall
None
shear-n shear-p
shear-n shear-p tension-p
shear-p
shear-p tension-p
tension-n shear-p tension-p
Y
X

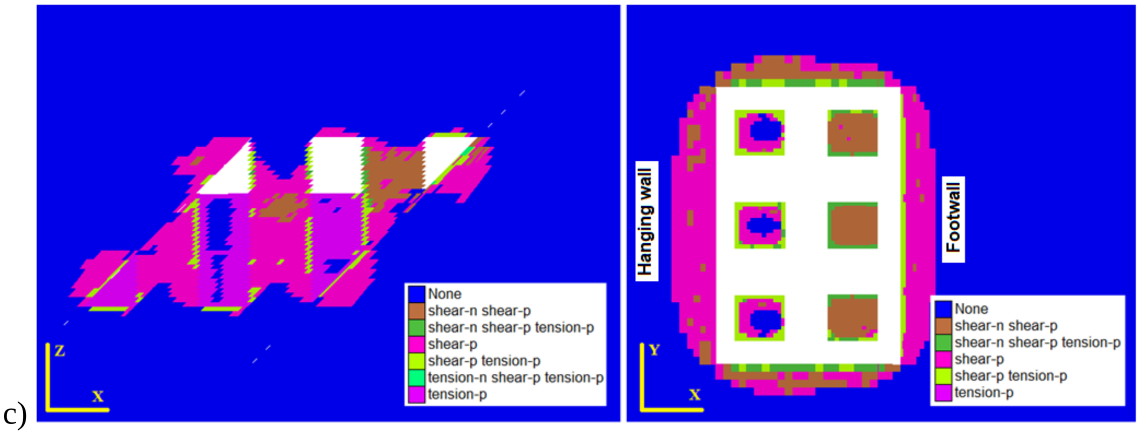
c)
Z
X
None
shear-n shear-p
shear-n shear-p tension-p
shear-p
shear-p tension-p
tension-n shear-p tension-p
tension-p
Hanging wall
Footwall
Y
X
None
shear-n shear-p
shear-n shear-p tension-p
shear-p
shear-p tension-p
tension-p

Figure 4.9. Extent of failure zones with modeling mine excavation height and delayed backfill (e.g. hydraulic fill material). a) mine excavation height is 4 m, b) mine excavation height is 8 m, and c) mine excavation height is 12 m

Figure 4.9 illustrate the extent of failure zone in post-pillars and around excavated stope due to the effect of mine excavation height. It can be clearly seen that the failure zone extends in post-pillars as mine excavation height increases.

The highest value of the failure zone in post-pillars located at the footwall side of the stope is 100, as seen in Figure 4.9c, since the mine excavation height reaches 12 m. Whereas, the lowest value of the failure zone in post-pillars located at the hanging wall side of the stope is 30, as seen in Figure 4.9a, since the mine excavation height reaches 4 m. For post-pillars with dimensions of 12 m × 12 m, the allowable mine excavation height for such mining conditions presented in Table 4.6 is 4 m.

Table 4.6. Extent of failure zones in post-pillars at different mine excavation heights using hydraulic fill material

Mining Depth (m)	Post-pillar dimension (m)	Mine excavation height (m)	Development of failure zones (%)					
			Hanging wall			Footwall		
			HW1	HW2	HW3	FW1	FW2	FW3
693	12 × 12	4	31	30	31	51	59	51
		8	54	53	55	90	91	90
		12	74	79	74	100	100	100

The extent of failure zone for each post-pillar located at the hanging wall and footwall side is tabulated in Table 4.6. Figure 4.10 shows the mine excavation height with respect to the extent of failure zones in post-pillars.

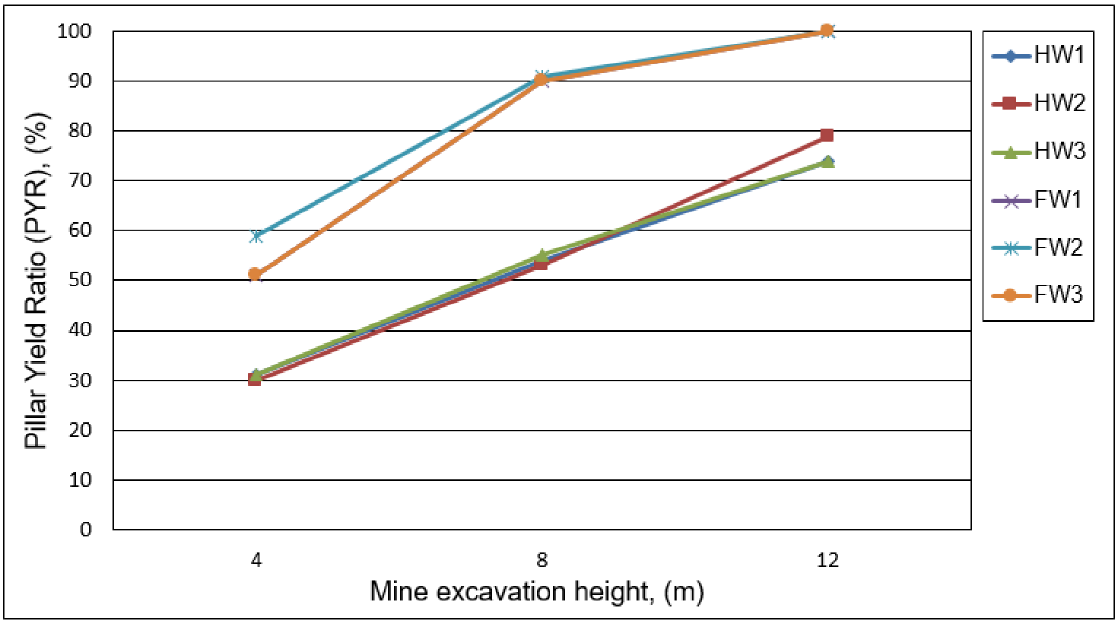

Figure 4.10. Mine excavation height vs. extent of failure zones in post-pillars using hydraulic fill material

4.3.2. Stability assessment of post-pillars at different mine excavation height using cemented rock fill material

Numerical modeling results for extent of failure zones are shown in Figure 4.11. In Figure 4.11, left picture indicates the front view of the central ore body, whereas, the right picture indicates the plan view.

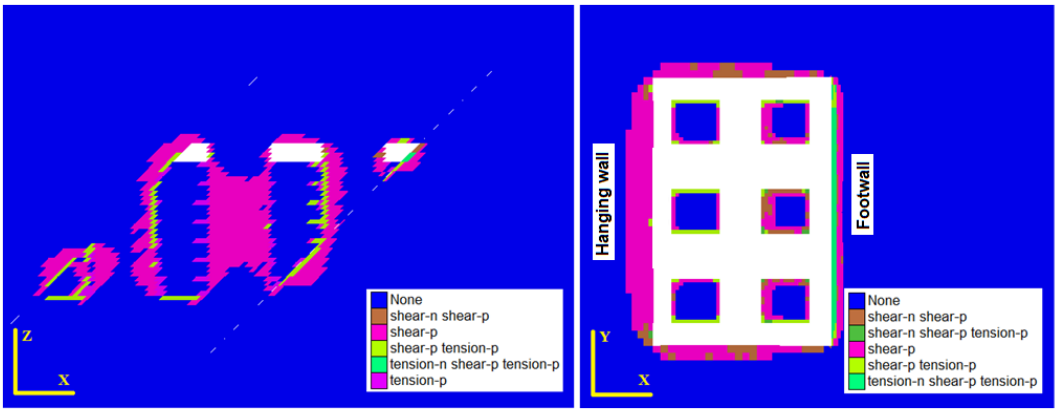
Z
X
None
shear-n shear-p
shear-p
shear-p tension-p
tension-n shear-p tension-p
tension-p
Hanging wall
Footwall
Y
X
None
shear-n shear-p
shear-n shear-p tension-p
shear-p
shear-p tension-p
tension-n shear-p tension-p

a)

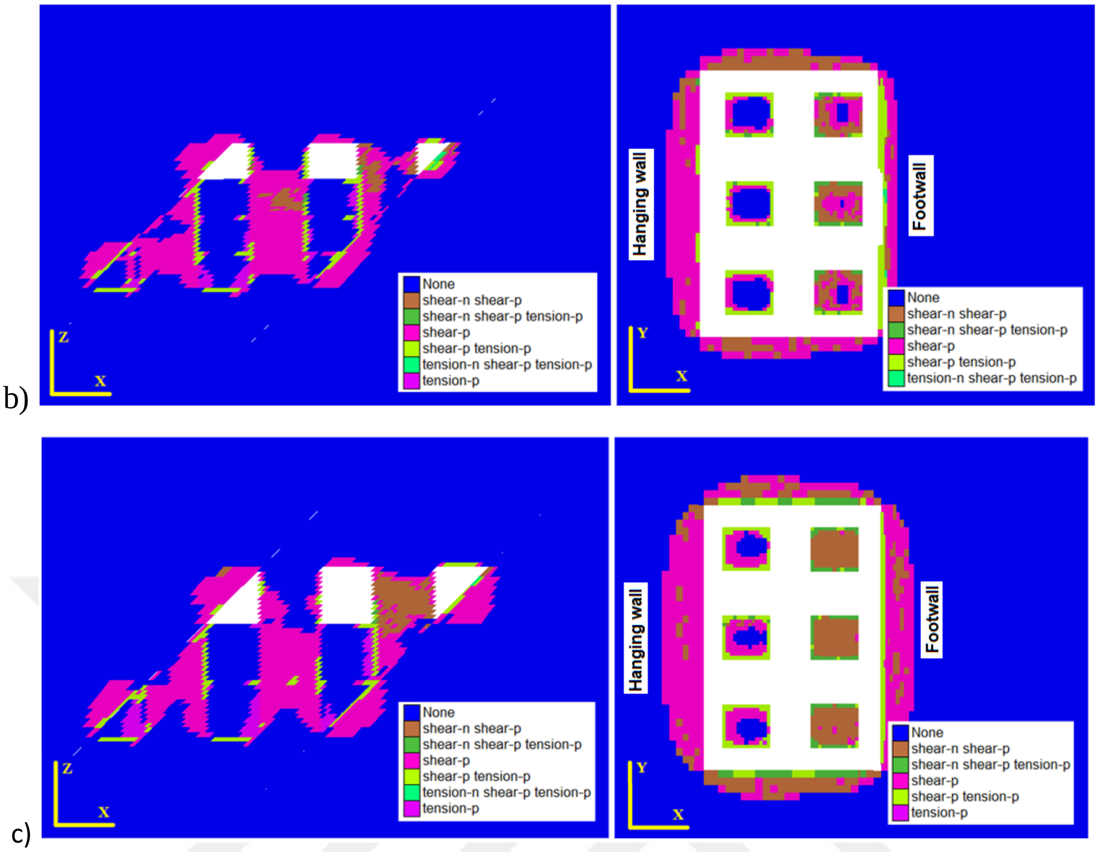
b)
Z
X
None
shear-n shear-p
shear-n shear-p tension-p
shear-p
shear-p tension-p
tension-n shear-p tension-p
tension-p
Hanging wall
Footwall
Y
X
None
shear-n shear-p
shear-n shear-p tension-p
shear-p
shear-p tension-p
tension-n shear-p tension-p
c)
Z
X
None
shear-n shear-p
shear-n shear-p tension-p
shear-p
shear-p tension-p
tension-n shear-p tension-p
tension-p
Hanging wall
Footwall
Y
X
None
shear-n shear-p
shear-n shear-p tension-p
shear-p
shear-p tension-p
tension-p

Figure 4.11. Extent of failure zones with modeling mine excavation height and delayed backfill (e.g. cemented rock fill material). a) mine excavation height is 4 m, b) mine excavation height is 8 m, and c) mine excavation height is 12 m

Figure 4.11 illustrate the extent of failure zone in post-pillars and around excavated stope due to the effect of mine excavation height. As in first case when the hydraulic filling material was used, even in this case when cemented rock fill material is being used the results are similar meaning that backfilling material does not really play a significant role as support system. It can be clearly seen that the failure zone extends in post-pillars as mine excavation height increases. The highest value of the failure zone in post-pillars located at the footwall side of the stope is 100, as seen in Figure 4.11c, since the mine excavation height reaches 12 m. Whereas, the lowest value of the failure zone in post-pillars located at the hanging wall side of the stope is 31, as seen in Figure 4.11a, since the mine excavation height reaches 4 m. For post-pillars with dimensions of 12 m × 12 m, the allowable mine excavation height for such mining conditions presented in Table 4.7 is 4 m.

The extent of failure zone for each post-pillar located at the hanging wall and footwall side is tabulated in Table 4.7.

Table 4.7. Extent of failure zones in post-pillars at different mine excavation height using cemented rock fill material

Mining Depth (m)	Post-pillar dimension (m)	Mine excavation height (m)	Development of failure zones (%)					
			Hanging wall			Footwall		
			HW1	HW2	HW3	FW1	FW2	FW3
693	12 × 12	4	32	31	32	51	59	51
		8	56	57	56	90	98	90
		12	74	77	74	100	100	100

Figure 4.12 shows the mine excavation height with respect to the extent of failure zones in post-pillars. It can be seen from Figure 4.12 and Table 4.7 that the PYR values are gradually increasing as mine excavation height increases. Interpretation of the numerical results after mine excavation height reaches 12m, indicates that the post-pillars are totally failed based on PYR classification index, as presented in Table 4.4.

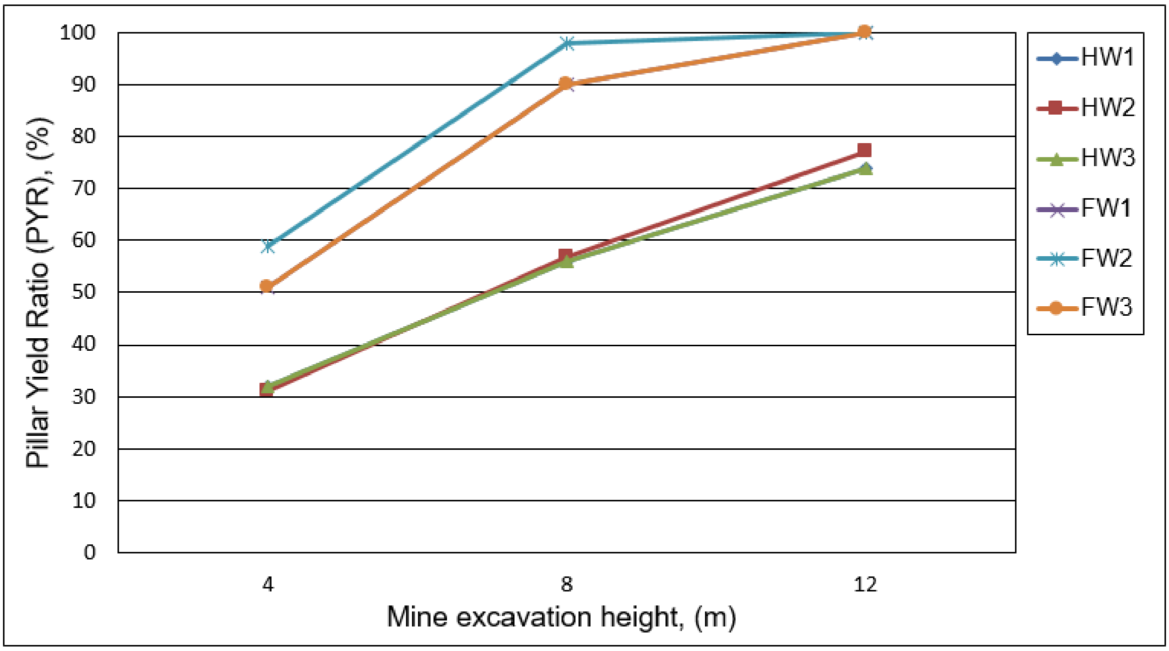

Figure 4.12. Mine excavation height vs. extent of failure zones in post-pillars using cemented rock fill material

4.3.3. Stability assessment of post-pillars at different mine excavation depth using hydraulic filling material

In this section, numerical simulations have been performed to examine the effect of mine excavation depth on the post-pillars stability. Numerical modeling results for extent of failure zone are shown in Figure 4.13. Figure 4.13 illustrate the extent of failure zone in post-pillars and around excavated stope due to the effect of mine excavation height. It can be clearly seen that the failure zone extends in post-pillars as mine excavation height increases. The highest value of the failure zone in post-pillars located at the footwall side of the stope is 55, as seen in Figure 4.13e, since the mine excavation depth reaches 933 m.

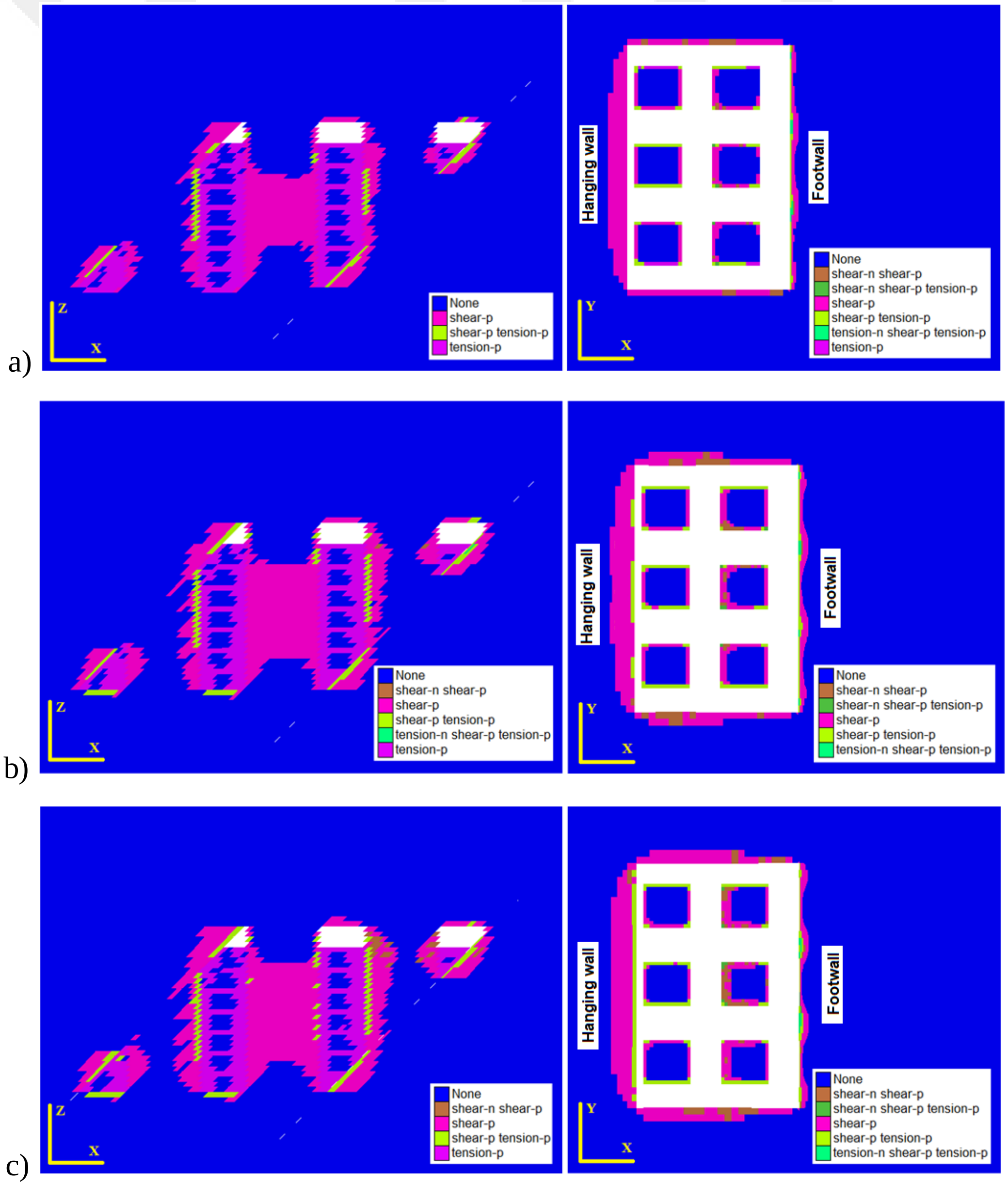
a)
Z
X
None
shear-p
shear-p tension-p
tension-p
Hanging wall
Footwall
Y
X
None
shear-n shear-p
shear-n shear-p tension-p
shear-p
shear-p tension-p
tension-n shear-p tension-p
tension-p
b)
Z
X
None
shear-n shear-p
shear-p
shear-p tension-p
tension-n shear-p tension-p
tension-p
Hanging wall
Footwall
Y
X
None
shear-n shear-p
shear-n shear-p tension-p
shear-p
shear-p tension-p
tension-n shear-p tension-p
c)
Z
X
None
shear-n shear-p
shear-p
shear-p tension-p
tension-p
Hanging wall
Footwall
Y
X
None
shear-n shear-p
shear-n shear-p tension-p
shear-p
shear-p tension-p
tension-n shear-p tension-p

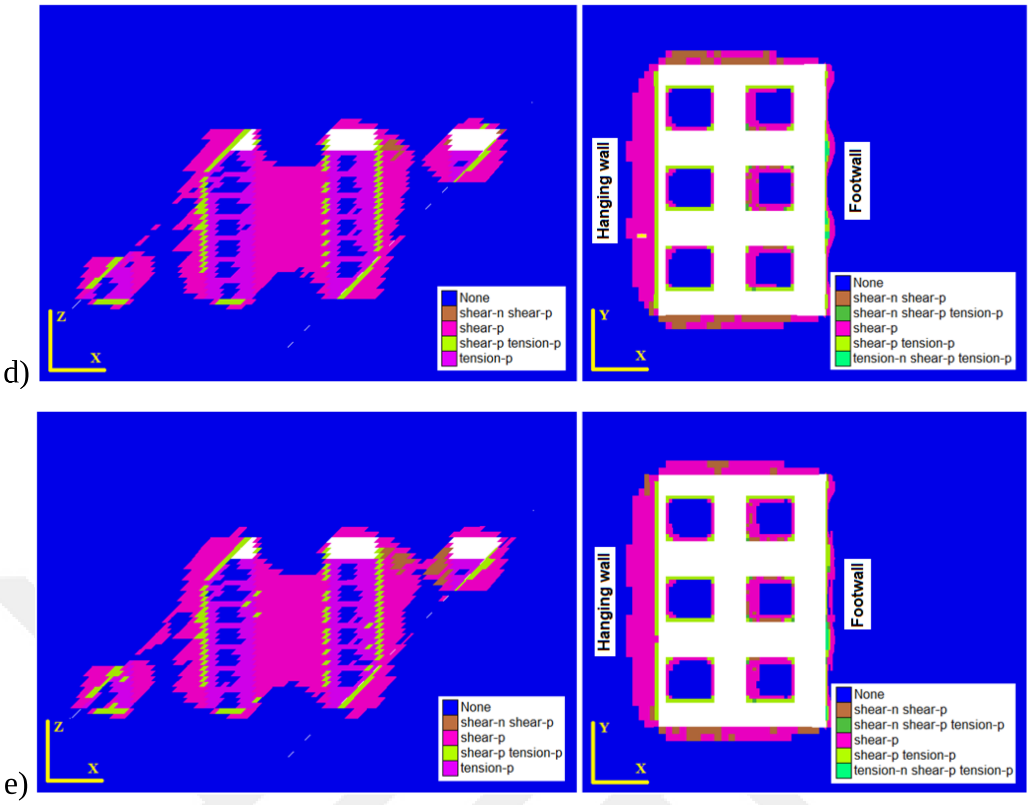
d)
e)
Z
X
Y
Hanging wall
Footwall
None
shear-n shear-p
shear-p
shear-p tension-p
tension-p
shear-n shear-p tension-p
tension-n shear-p tension-p

Figure 4.13. Extent of failure zones in post-pillars with modeling mine excavation depths and delayed backfill (e.g. hydraulic fill material). a) mine excavation depth is 453 m, b) mine excavation depth is 573 m, c) mine excavation depth is 693 m, d) mine excavation depth is 813 m, e) mine excavation depth is 933 m

Whereas, the lowest value of the failure zone in post-pillars located at the hanging wall side of the stope is 26, as seen in Figure 4.13a, since the mine excavation depth reaches 453 m. The extent of failure zones for each post-pillar located at the hanging wall and footwall side is tabulated in Table 4.8.

Table 4.8. Extent of failure zones in post-pillars at different mine excavation depth using hydraulic fill material

Mine excavation height (m)	Post-pillar dimension (m)	Mining depth (m)	Development of failure zones (%)					
			Hanging wall			Footwall		
			HW1	HW2	HW3	FW1	FW2	FW3
4	13 × 13	453	27	27	27	26	31	26
		573	28	28	28	36	39	36
		693	29	28	29	45	47	44
		813	30	31	30	49	55	49
		933	31	30	32	54	55	52

Figure 4.14 shows the mine excavation depth with respect to the extent of failure zones in post-pillars.

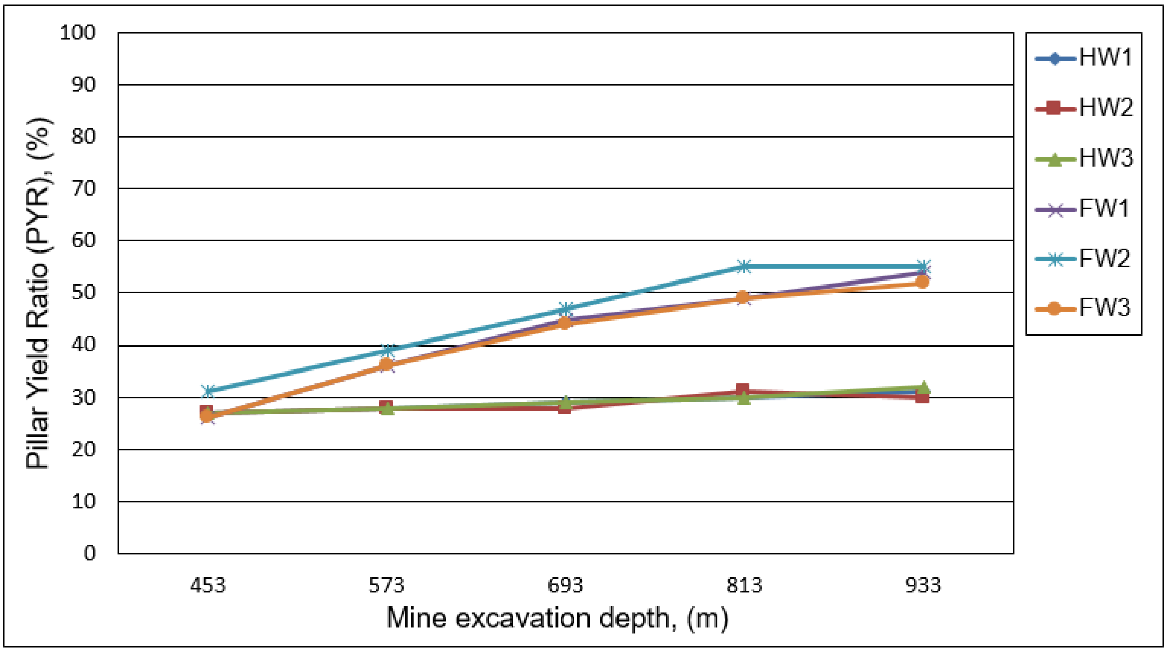

Figure 4.14. Mine excavation depth vs. extent of failure zones in post-pillars using hydraulic fill material

4.3.4. Stability assessment of post-pillars at different mine excavation depth using cemented rock fill material

Numerical modeling results for extent of failure zones are shown in Figure 4.15. Figure 4.15 illustrate the extent of failure zone in post-pillars and around excavated stope due to the effect of mine excavation depth.

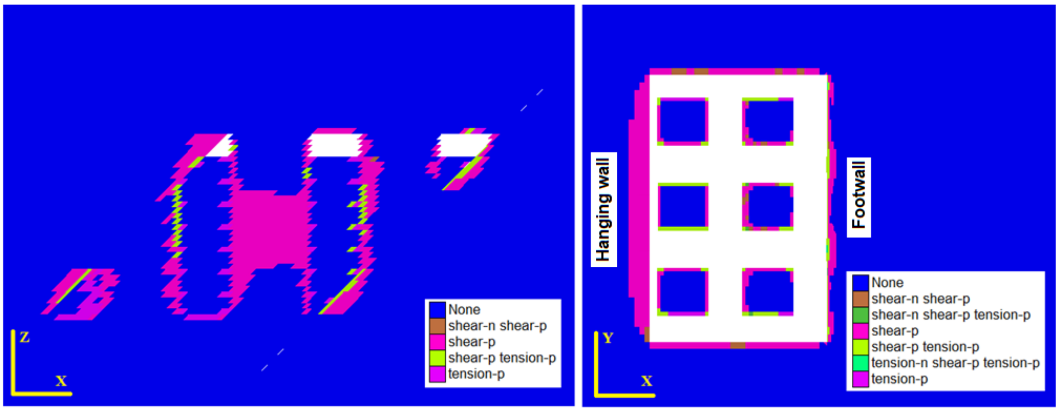
None
shear-n shear-p
shear-p
shear-p tension-p
tension-p
Z
X
Hanging wall
Footwall
None
shear-n shear-p
shear-n shear-p tension-p
shear-p
shear-p tension-p
tension-n shear-p tension-p
tension-p
Y
X

a)

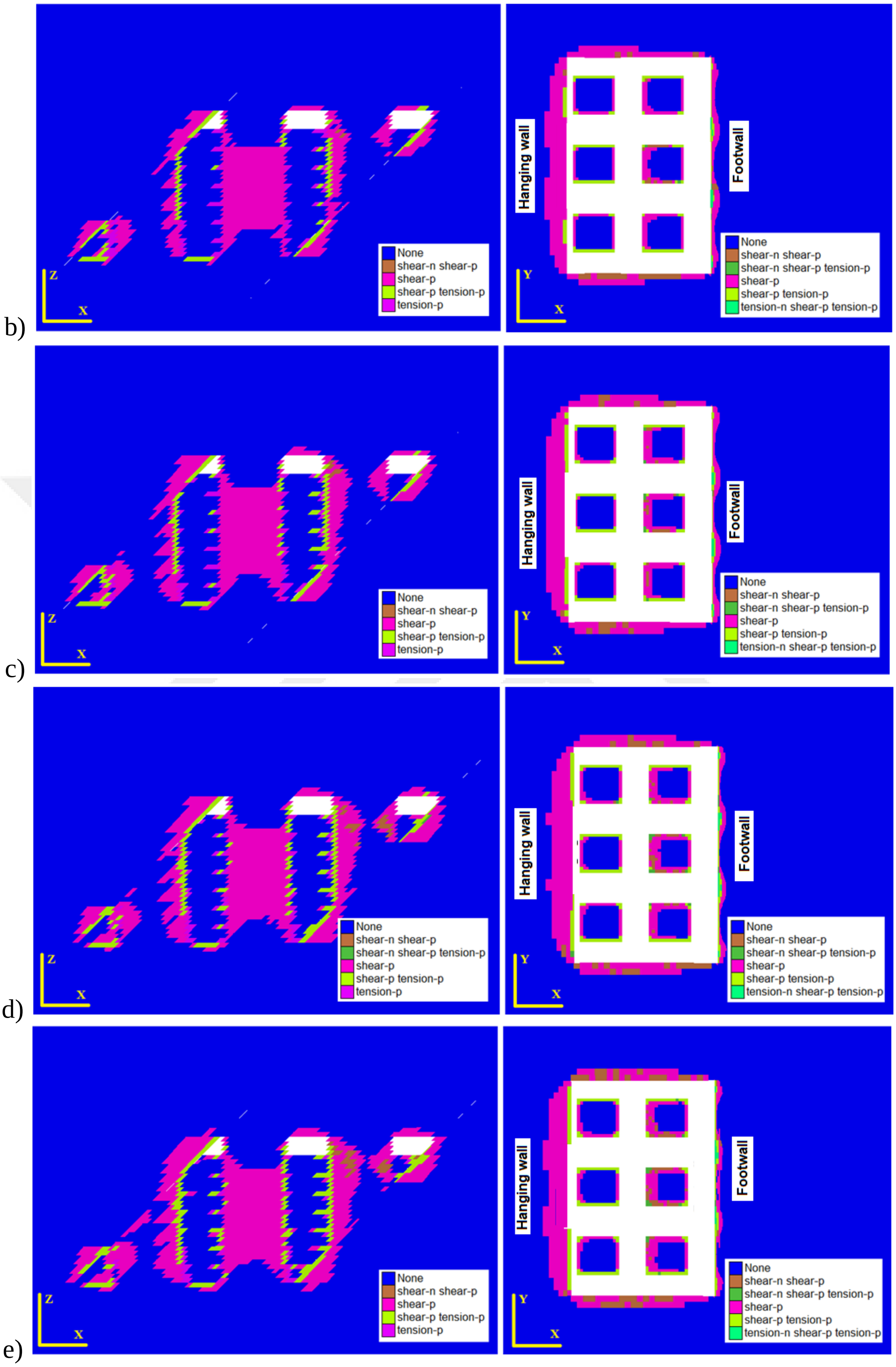
b)
Z
X
None
shear-n shear-p
shear-p
shear-p tension-p
tension-p
Hanging wall
Footwall
Y
X
None
shear-n shear-p
shear-n shear-p tension-p
shear-p
shear-p tension-p
tension-n shear-p tension-p
c)
Z
X
None
shear-n shear-p
shear-p
shear-p tension-p
tension-p
Hanging wall
Footwall
Y
X
None
shear-n shear-p
shear-n shear-p tension-p
shear-p
shear-p tension-p
tension-n shear-p tension-p
d)
Z
X
None
shear-n shear-p
shear-n shear-p tension-p
shear-p
shear-p tension-p
tension-p
Hanging wall
Footwall
Y
X
None
shear-n shear-p
shear-n shear-p tension-p
shear-p
shear-p tension-p
tension-n shear-p tension-p
e)
Z
X
None
shear-n shear-p
shear-p
shear-p tension-p
tension-p
Hanging wall
Footwall
Y
X
None
shear-n shear-p
shear-n shear-p tension-p
shear-p
shear-p tension-p
tension-n shear-p tension-p

Figure 4.15. Extent of failure zones in post-pillars with modeling mine excavation depth and delayed backfill (e.g. cemented rock fill material). a) mine excavation depth is 453 m, b) mine excavation depth is 573 m, c) mine excavation depth is 693 m, d) mine excavation depth is 813 m, e) mine excavation depth is 933 m

It can be seen that the failure zone extends in post-pillars as mine excavation depth increases. The highest value of the failure zone in post-pillars located at the footwall side of the stope is 55, as seen in Figure 4.15e, since the mine excavation depth reaches 933 m. Whereas, the lowest value of the failure zone in post-pillars located at the hanging wall side of the stope is 27, as seen in Figure 4.15a, since the mine excavation depth reaches 453 m. The extent of failure zones for each post-pillar located at the hanging wall and footwall side is tabulated in Table 4.9.

Table 4.9. Extent of failure zones in post-pillars at different mine excavation depth using cemented rock fill material

Mine excavation height (m)	Post-pillar dimension (m)	Mining depth (m)	Development of failure zones (%)					
			Hanging wall			Footwall		
			HW1	HW2	HW3	FW1	FW2	FW3
4	13 × 13	453	28	27	28	27	32	27
		573	27	29	28	36	41	36
		693	29	29	29	45	48	45
		813	30	31	30	49	55	48
		933	32	32	32	53	55	52

Figure 4.16 shows the mine excavation depth with respect to the extent of failure zones in post-pillars.

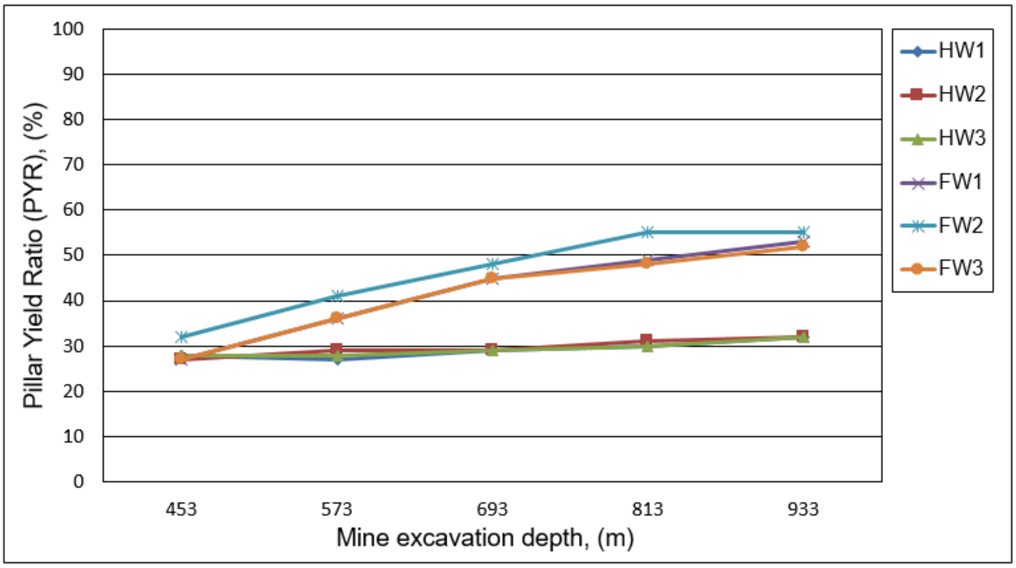

Figure 4.16. Mine excavation depth vs. extent of failure zones in post-pillars using cemented rock fill material

From Section 4.3 it can be concluded that increasing mine excavation height when extraction process is being carried out at a certain depth, post-pillars are indicated to lose bearing capacity, as seen in Figure 4.9. Hence, the allowable mine excavation height should be kept 4 meters and seems to be much more stable when the ratio of post-pillar width to height ratio is more than 2.5. Post-pillars left on the footwall side seems to be potentially unstable due to the fact that are located almost in the center of the mined-out stope and are meant to support the whole back of the stope. From Figure 4.13 and Figure 4.15 it was observed that the extent of failure zones increases gradually with the increase of mine excavation depth despite the fact that in Figure 4.15 there is applied cemented rock fill material having higher strength properties compared to hydraulic filling material. Failure zone has also extended in sidewalls (e.g. hanging wall and/or footwall). Post-pillars are designed to gradually yield below the lower levels.

5. CONCLUSION AND RECOMMENDATIONS

In this thesis, stability of deep underground excavations (e.g. stopes) and post-pillars have been investigated under static loading conditions, the effects of post-pillar width to height ratio (W_p/h_p) with respect to mine excavation height and mine excavation depth were analyzed. This research has attempt to determine the most optimal mine excavation height and minimum size of post-pillars under hydrostatic in situ stress conditions using FLAC^{3D} numerical modeling technique.

The main findings of this research based on numerical analysis under static loading conditions are discussed as below;

- Different rock mass damage assessment techniques have been reviewed. Based on the ground vibration predictor equation, the safe maximum allowable charge per delay has been suggested. Also, extrapolation of the far-field PPV predictor equation was performed assessing the rock mass damage threshold levels.The overbreak predicted at the PPV level of 2800 mm/s, rock damage is observed to be 0.42 m when using 8 kg and 0.63 m when using 20 kg of explosive quantity per delay. In Figure 4.4 an overbreak case due to rock blasting is shown at TUM at a depth of 813 m below ground surface.

- Mine excavation height has been investigated between 4m and 12m in 4-meter intervals with respect to mining depth. From the numerical analysis results it is carefully observed and found out that exceeding of mine excavation height more than 4m, deep underground production stopes can suffer from serious ground problems where failure zone and maximum principal stresses occur in the hanging wall and footwall as the main ore body has low dip angle(45°). In very deep underground production levels, mine excavation height is suggested to be as maximum mine excavation height as 3m and post-pillar dimension should be at least $(w_p/h_p \geq 2.5)$ and installing of cable bolting to support hanging wall and footwall is unquestionable due to progressive extent of failure zone.

- Stability assessment of post-pillars is accomplished based on new developed assessment index i.e. Pillar Yield Ratio (PYR). PYR classification index enables post-pillar to be divided into three main classes such as stable, potentially unstable and total failure. Furthermore, based on PYR classification index and Underground Pillar Stability Graph (UPSG) developed by (Lunder, 1994), new Pillar Stability Graph (PSG) has been developed and shows a good match-out of the results.

5.1. Recommendations for Future Work

This thesis presents the numerical analysis results assessing stope and post-pillar stability assessment under static loading conditions through three-dimensional numerical modeling. However, the following recommendations for future research are given as follows;

- Study the support design of deep underground mine excavations (e.g. stopes) with respect to mine excavation height varying mine excavation depth at Trepça Underground Mine (TUM)

- Study the mechanical properties of rock and backfilling materials applied in deep production levels at TUM in order to improve stope stability performance and provide good confinement to post-pillars

- Study the blast-induced damaged zone around underground excavations (e.g. galleries and drifts) and predict the overbreak considering rock parameters, drilling parameters (e.g. drill pattern and machine used), characteristic of explosives, the initiation process, and drilling accuracy. Also, investigate rock support performance depending mainly on the competence of the damaged zone

5.2. Statement of Contributions

This research has attempt for the first time to adapt three-dimensional numerical modeling developing a new assessment index i.e. Pillar Yield Ratio (PYR). This new developed index falls to classification rating tools which are used to compare and classify of potential instabilities of the post-pillars. This assessment index enables pillars to be classified into three main classes as stable, potentially unstable, and total failure. The proposed assessment index takes into account the extent of failure zones based on elasto-plastic solution. Further, a Pillar Stability Graph (PSG) was developed based on PYR classification index considering the pillar width to height ratio and maximum principal stress to uniaxial compressive strength of intact rock ratio.

REFERENCES

Abdellah, W., Mitri, H.S., Thibodeau, D., Moreau-Verlan, L., 2012, Stochastic evaluation of haulage drift unsatisfactory performance using random Monte-Carlo simulation, International Journal of Mining and Mineral Engineering, 4(1), pp. 63-87

Abdellah, W., 2015, Parametric stability analysis of room and pillar method in deep coal mines, Journal of engineering science-Assiut University, 43(2), pp. 1440-1451

Aksoy, C.O., Genis, M., 2010, A review of the numerical modeling procedure in mining, International Journal of Mining and Mineral Processing, ISP, New Delhi, India, 1(1), pp. 33-43

Alpay, S., Yavuz, M., 2009, Underground mining method selection by decision making tools, Tunneling and Underground Space Technology, 24 (2), 173-184

Atlas Copco, 2007, Mining methods in underground mining, pp. 33-41

Aydan, O., Ulusay, R., Kawamoto, T., 1997, Assessment of rock mass strength for underground excavations, In: Proceedings of the 36th US rock mechanics symposium, pp.777-786

Aydan, O., Dalgic, S., 1998, Prediction of deformation behavior of 3 ;anes Bolu tunnels through squeezing rocks of North Anotolian fault zone (NAFZ), In: Proceedings of the regional symposium on sedimentary rock engineering, Taipei, pp. 228-233

Aydan, O., Kawamoto, T., 2000, Assessing mechanical properties of rock masses through RMR rock classification system, GeoEng2000, Melbourne, Australia

Aydan, O., Genis, M., Tokashiki, N., 2012, Some considerations on yield (failure) criteria in rcok mechanics, In: 46th US rock mechanics/geomechanics symposium, Chicago, USA, ARMA 12, 640p

Bauer, A., Calder, P.N., 1970, Open pit and blasting, Seminar Mining Engineering, Department publication, Queen's University, Kingston, Ontario, 3p.

Barton, N., Lien, R., Lunde, J., 1974, Engineering classification of rock masses for the design of tunnel support, Rock Mechanics, 6 (4), pp. 189-236

Barton, N., 1995, The influence of joint properties in modeling jointed rock masses, Keynote Lecture, 8th ISRM Congress, Balkema, Rotterdam, Tokyo, vol 3, pp.1023-1032

Barton, N., 2002, Some new Q value correlations to assist in site characterization and tunnel design, International Journal of Rock Mechanics and Mining Science, 39, pp. 185-216

REFERENCES (continued)

Basarir, H., Ozsan, A., Karakus, M., 2005, Analysis of support requirements for a shallow diversion tunnel at Guledar dam site, Turkey, Engineering Geology, 81(2), pp. 131-145

Basarir, H., Genis, M., Ozarslan, A., 2010, The Analysis of radial displacements occurring near the face of a circular opening in weak rock mass, International Journal of Rock Mechanics and Mining Sciences, 81, pp.771-783

Bellman, R.E., Zadeh, L.A., 1970, Decision making in a fuzzy environment, Management science, 17, 141-164

Bhasin, R., Grimstad, E., 1996, The use of stress-strength relationships in the assessment of tunnel stability, Tunneling and Underground Space Technology, 11(1), oo. 93-98

Bieniawski, Z.T., 1976, Rock mass classifications in rock engineering, In: Proceedings Symposium on Exploration for Rock Engineering, Johannesburg, South Africa, pp. 97-106

Bieniawski, Z.R., 1978, Determining rock mass deformability: experience from case histories, International Journal of Rock Mechanics and Mining Science & Geomechanics, 15, pp. 237-247

Bieniawski, Z.T., 1989, Engineering rock mass classification, John Wiley & Sons, New York, 237p.

Boshkov, S.H., Wright, F.D., 1973, Basic and parametric criteria in the selection, Design and Development of underground mining systems, SME Mining Engineering Handbook, SME-AIME, New York

Bullock, R.L., 2011, Comparison of underground mining methods, In: P. Darling, ed. SME Mining Engineering Handbook, USA, Society for Mining, Metallurgy and Exploration, Inc., pp. 385-403

Brady, B.H.G., Brown, E.T., 1985, Rock mechanics for underground mining, 1st edn, Allen & Unwin, London, 628p

Brady, T., Martin, L., Pakalnis, R., 2003, Empirical approaches for weak rock masses, 98th Annual AGM-CIM Conference, Montreal, QC.

Brady, B.H.G., Brown, E.T., 2007, Rock mechanics for underground mining, Xst edn, Allen & Unwin, London, 628p

REFERENCES (continued)

Caceres, C., 2011, Quantifying the effect of rock mass quality on peak particle velocity for underground drift development, PhD Thesis, University of British Coulombia, pp.44-53, pp. 74-83

Carter, P.G., 2011, Selection process for hard-rock mining, In: P.Darling, edit, SMS Mining Engineering Handbook, USA: Society for Mining, Metallurgy and Exploration, Inc., pp. 357-376

Cepuritis, M.P., 2010, An integrated approach to span design in open stope mining, PhD thesis, Curtin University of Technology, Western Australian School of Mines, Australia, pp. 11-18

Chen, C., Klein, C.M., 1997, An efficient approach to solving fuzzy MADM problems, Fuzzy Set Systems, 88, 51-67

Chen, G., Jia, Z., Ke, J., 1997, Probabilistic analysis of underground excavation stability, International journal of Rock mechanics and Mining science, 34, pp. 3-4

Deng, J., 2017, Reliability analysis and design of backfill in a cut-and-fill mining method, PASTE, Beijing, China, pp. 268-276

Dimitrijevic, M.D., 1995, The Kopaonik block – its position in the Vardar zone, In: Proceedings, Geology and Metallogeny of the Kopaonik Mountain Symposium, pp.33-40

Dowding, C.H., 1985, Blast vibration monitoring and control, Prentice-Hall, Inc, Englewood Cliffs, NJ, USA, 289p.

Dorricott, M.G., Grice, A.G., 2002, Backfill – The Environmentally Friendly Tailings Disposal System, In: Proceedings Green Processing, The Australasian Institute of Mining and Metallurgy, Melbourne, pp. 265-270.

EduMine, 2019, Mining method Selection-Online tool, http://www.edumine.com/xtoolkit/xmethod/miningmethodgraphic.htm

Emad, M.Z., 2013, Dynamic performance of cemented rock fill under Blast-induced vibrations, PhD Thesis, McGrill University, pp. 2-9

Emad, M.Z., 2017, Numerical modeling approach for mine backfill, Indian Academy of Science, 42 (9), pp. 1595-1604

Feng, X.T., Hudson, J.A., 2010, Specifying the information required for rock mechanics modeling and rock engineering design, International Journal of Rock Mechanics and Mining Science, 47, pp. 179-794

REFERENCES (continued)

Forgan, 1936, Trepca Mines Limited II: Essential geological features of the Stan Trg lead-zinc ore body, Mining and Metallurgy, pp. 481-484

Forgan, C.B., 1950, Ore deposits at the Stantrg lead-zinc mine. K. C. Dunham editor, 18th International Geological Congress, London, Part VII, Symposium of Section F, pp. 290-307

Galera, J.M., Alvarez, M., Bieniawski, Z.T., 2005, Evaluation of the deformation modulus of rock masses: comparison of pressuremeter and dilatometer tests with RMR prediction, In: Proceedings of the ISP5-PRESSIO International symposium, Madrid, Spain, pp.1-25

Genis, M., Colak, B., 2015, Stability assessment of the Gokgol Karstic Cave (Zonguldak, Turkey) by analytical and numerical methods, Rock Mechanics and Rock Engineering 48, pp.2383-2403

Genis, M., Basarir, H., Ozarslan, A., Bilir, E., Balaban, E., 2007, Engineering geological appraisal of the rock masses and preliminary support design, Dorukhan Tunnel, Zonguldak, Turkey, Engineering Geology, 92, pp. 14-26

Gokceoglu, C., Sonmez, H., Kayabasi, A., 2003, Predicting the deformation moduli of rock masses, International Journal of Rock Mechanics & Mining Sciences, 40, pp. 701-710

Grimstad, E., Barton, N., 1993, Updating of the Q-system for NMT. In: Proceeding on international symposium on sprayed concrete, Fagernes, Norway, Norwegian Concrete Association, Oslo, Norway, 20p.

Hamrin, H., 2001, Underground mining methods and applications, Society for Mining, Metallurgy, and Exploration, pp. 3-28.

Hartman, H.L., 1987, Introductory mining engineering, 1st ed, New York, Wiley

Hartman, H.L., Mutmansky, J.M., 2002, Introductory Mining Engineering, John Wiley, New Jersey

Heidarzadeh, S., Saeidi, A., Rouleau, A., 2019, Evaluation of the effect of geometrical parameters on stope probability of failure in the open stoping method using numerical modeling, International Journal of Mining Science and Technology, 29: pp. 399-408

Hetemi, M., 2013, Contribution to the optimal modeling of mine field opening from level XI to level XIII in Stan Trg mine, PhD Thesis (in Albanian), University of Prishtina, pp. 56-60

REFERENCES (continued)

Himanshu, V.K., Kushwaha, A., 2015, Numerical modeling based design of stoping parameters, The Indian mining and Engineering Journal, 54(8), pp. 8-14

Hoek, E., Brown, E.T., 1980, Empirical strength criterion for rock masses, Journal of Geotechnical and Geoenvironment Engineering, 106(9), pp.1013-35

Hoek, E., Grabinsky, M.V., Diederichs, S.M., 1991, Numerical modeling for underground excavation design, The Institution of Mining and Metallurgy Engineering, pp. A22-A30

Hoek, E., Kaiser, P.K., Bawden, W.F., 1995, Support of underground excavations in hard rock, Rotterdam, Balkema, Brook-field, 213p

Hoek, E., Brown, E.T., 1998, Practical estimates of rock mass strength, International Journal of Rock Mechanics and Mining Science, 34(8), pp.1165-86

Hoek, E., Carranza-Torres, C., Corkum, B., 2002, Hoek-Brown failure criterion -2002 edition, In: Proceedings of NARMS-Tac, University of Toronto, Toronto, pp.267-73

Hoek, E., 2004, Personal communication, Rocscience, In Zhang, L., 2016, Determination and application of rock quality designation (RQD), Journal of Rock Mechanics and Geotechnical Engineering, 8, pp. 389-397

Hoek, E., Diederichs, M.S., 2006, Empirical estimation of rock mass modulus, International Journal of Rock Mechanics and Mining Science, 43(2), pp.203-15

Hoek, E., 2007, Rock mass properties, In Practical Rock Engineering, Available online at http://www.rockscience.com/hoek/corner/11_Rock_mass_properties.pdf

Holmberg, R,. Persson, P.A., 1979, Swedish Approach to Contour Blasting, In: proceedings of Fourth International Conference on Explosive and Blasting Techniques, pp. 113-127

Hudson, J.A., Feng, X.T., 2007, Updated flowcharts for rock mechanics modeling and rock engineering design, International Journal of Rock Mechanics and Mining Science, 44 (2), pp. 174-195

Hughes, P.B., Milne, D., Pakalnis, R.C., Samaniego, A., 2017, Empirical design methods in underground mining from: Rock Mechanics and Engineering, vol. 3, Analysis, Modeling & Design, CRC Press, pp. 401-424

REFERENCES (continued)

Hustrulid, W.A., Bullock, R.L., 2001, Underground mining methods: Engineering fundamentals and international case studies, Society for mining metallurgy and exploration, pp.35-45

Hyseni, S., Large, D., 2003, The Trepça lead-zinc mineral belt, Kosovo-Geological overview and interpretation, 7th Biennial SGA Meeting on mineral exploration and sustainable development poster, Athens-Greece, 120, pp.1-2

Hyseni, S., Durmishaj, B., Fetahaj, B., Shala, F., Berisha, A., Lage, D., 2010, Trepça ore belt and Stan Trg mine – Geologica overview and interpretation, Kosovo (SE Europe), Geologija, Ljubljana, 53(1), pp. 87-92

Itasca, 2005, FLAC3D-Fast lagrangian analysis of continua-user manual, ver. 2.21, Minneapolis, Itasca Consulting Group

Kabongo, K.K., Bron, K.L., 1999, Effect of dynamic loading and tunnel support in deep level mines, In: Proceedings of EXPLO'99, Kalgoorlie, WA, pp. 81-89

Kabwe, E., 2017, Optimal mining method selection for Nchanga's upper ore body using analytical hierarchy process and Yager's method, Mining Technology, 126(3), pp. 151-162

Kalamaras, G.S., Bieniawski, Z.T., 1995, A rock strength concept for coal seams incorporating the effect of time, In: Proceedings of the 8th ISRM congress, Tokyo, Japan, vol 1, pp. 295-302

Khawar, M., (2013), Development of correlation between rock classification system and modulus of deformation, University of Engineering and Technology, Lahore, Pakistan

Kulatilake, P.H.S.W., Qiong, W., Zhengxing, Y., Fuxing, J., 2013, Investigation of stability of a tunnel in a deep coal mine in China, International Journal of Mining Science and Technology, 23, pp. 579-589

Kumar, P., Pakalnis, R., Roque, P., Corey, G., 2002, Development of empirical a numerical design technique in burst prone ground at Goldcorp Red Lake Mine, presented at AGM-CIM, Voncouver, 8p.

Langefors, U., Kihlstrom, B., 1973, The Modern Techniques of Rock blasting, John Wiley and Sons, New York p473

Lang, B., 1994, Span design for entry-type excavations, Master of Science thesis, University of British Colombia, pp.180-190

REFERENCES (continued)

Laubscher, D.H., 1981, Selection of mass underground mining methods, Design and operation of caving and sublevel stoping mines, SME-AIME, New York

Laubscher, D.H., Page, C.H., 1990, The design of rock support in high stress or weak rock environments, Ottawa, ON, CIM

Li, Ch., Li, H., Li, Y., Cheng, Y., Wang, G., Chen, Y., 2011, Stability analysis of long anchors cables reinforcement for stope roof in upward horizontal cut and fill stoping method, International Conference on Electric Technology and Civil Engineering (ICETCE), IEEE, pp.702-706

Li, X., Li, D., Liu, Zh., Zhao, G., Wang, Q., 2013, Determination of the minimum thickness of crown pillar for safe exploitation of a subsea gold mine based on numerical modeling, International Journal of Rock Mechanics and Mining Science, 57, pp. 42-56

Li, X., Gong, F., Tao, M., Dong, L., Du, K., Ma, Ch., Zhou, Z., Yin, T., 2017, Failure mechanism and coupled static-dynamic loading theory in deep hard rock mining: A review, Journal of Rock Mechanics and Geotechnical Engineering, 9, pp. 767-782

Lunder, P., 1994, Hard rock pillar strength estimation: an applied empirical approach, M.A.Sc Thesis, University of British Columbia, 166p.

McKenize, C., Holley, K.., 2004, A study of Damage Profiles behing Blasts, In: Proceedings of the 30th Annual Conference on Explosive and Blasting Technique, New Orleans, Lousiana, pp. 203-214

Maliqi, G., 2001, Geological and structural of the Trepça ore deposit, PhD Thesis (in Albanian), Polytechnic University of Tirana, Prishtina, 137p.

Martin, C.D., Kaiser, P.K., Christiansson, R., 2003, Stree, instability and design of underground excavations, International Journal of Rock Mechanics and Mining Science, 40, pp. 1024-1047

Meyer, T., Duun., P.G., 1995, Fragmentation and Rockmass Damage Assessment Sunburst Excavator and Drill and Blast, In: Proceedings of North American Rock Mechanics Symposium, pp. 609-616

Miller-Tait, L., Pakalnis, R., Poulin, R., 1995, UBC Mining method selection, Calgary, 4th International Symposium on Mine Planning and Equipment Selection.

REFERENCES (continued)

Murphy, S.K., 2012, Linear elastic numerical modelling for failure prediction-an assessment, The Journal of the Southern African Institute of Mining and Metallurgy, 112, pp. 737-748

Morrison, R.G.K., 1976, AW Philosophy of Ground Control, McGrill University, Montreal, Canada

Nateghi, R., 2012, Evaluation of blast induced ground vibration for minimizing negative effects on surrounding structures, Soil Dynamics and Earthquake Engineering, 43, pp. 133-138

Naung, N., Sasaoka, T., Shimada, H., Hamanaka, A., 2018, Stability assessment of open stope under overlaying mined-out regions at Modi Taung gold mine, Myanmar, International Journal of Geosciences, 9, pp.547-571

Nicholas, D.E., 1981, Method selection, In: D. Stewart, ed. A Numerical approach, design and operation of caving and sublevel stoping mine, New York, SME-AIME, pp. 39-53

Nicholson, G.A., Bieniawski, Z.T., 1990, A nonlinear deformation modulus based on rock mass classification, International Journal of Mining and Geological Engineering, 8, pp.181-202

Ortlepp, W.D., Stacey, T.R., 1994, Rockburst Mechanisms in Tunnels and Shafts, Tunneling and Underground Space Technology, 9(1), pp.59-65

Oriard, L.L., 1982, Blasting Effectx and Their Control, SME of AIME, Littelton, Colorado, pp. 1590-1603

O'Toole, D., et al., 2011, Backfill – Queens Mine Design Wiki.

Pakalnis, R., 2014, Empirical design methods - update (2014), Presented at 1st International Conference on Applied Empirical Design methods in Mining-Lima, Peru

Pakalnis, R., 2015, Empirical design methods in practice, in Y Potvin (ed.), Proceedings of the International Seminar on Design Methods in Underground Mining, Australian Centre for Geomechanics, Perth, pp. 37-56.

REFERENCES (continued)

Palinkas, S.S., Palinkas, L.A., Renac, Ch., Spnagenberg, J.E., Lueders, V., Molnar, F., Maliqi, G., 2013, Metallogenic model of the Trepça Pb-Zn-Ag skarn deposit, Kosovo: evidence from fluid inclusions, rare earch elements, and stable isotope data, Economic Geology, 108(1), pp.153-162

Palmstrom, A., 2009, Combining the RMR, Q, and RMi classification systems, www.rockmass.net, 25p.

Peskens, T.W., 2013, Underground mining method selection and preliminary techno-economic mine design for the Wombat orebody, Kylylahti deposit, Finland (PhD Thesis), Delft University of Technology, Netherlands

Potvin, Y., Dight, P.M., Wesseloo, J., 2012, Some pitfalls and misuses of rock mass classification systems for mine design, The Journal of The Southern African Instıtute of Mining and Metallurgy, 112, pp. 697-702

Rajmeny, P.K., Joshi, A., Agrawal, A., 1995, Assessment of rock damage during 145 tonne blast at Mochia, In: Proceedings of EXPLO'95 Conference, Brisbane, pp. 375-382

Ramamurthy, T., 1986, Stability of rock masses, Indian Geotechnical Journal, 16(1), pp.1-74

Ramamurthy, T., 2004, A geo-engineering classification for rocks and rock masses, International Journal of Rock Mechanics and Mining Science, 41, pp.89-101

Read, S.A.L., Richards, L.R., Perrin, N.D., 1999, Applicability of the Hoek-Brown failure criterion to New Zealand greywacke rocks, In: Proceedings of the 9th international symposium on rock mechanics, Paris, pp.655-60

Resende, R., Lamas, L., Lemos, J., Calçada, R., 2014, Stress wave propagation test and numerical modeling of an underground complex, International Journal of Rock Mechanics and Mining Science, 72, pp. 26-36

Rustan, A., Naarttijarvi, T., Ludvig, B., 1985, Controlled Blasting in hard intense Jointed Rock in Tunnels, CIM Bulletin, December, 76(884), pp. 63-68

Saaty, T.L., 1980, The analytic hierarchy process, McGraw-Hill, Pittsburgh

Saaty, T.L., 2000, Fundamentals of decision making and priority theory with the analytic hierarchy process, RWS, Pittsburgh

Saaty, T.L., Ozdemir, M.S., 2003, Why the magic number seven plus or minus two, Mathematical and computer modelling, 38, pp. 233-244

REFERENCES (continued)

Schumacher, F., 1950, Die lagerstatte der Trepca und ihre Umgebung, Izdavacko preduzece saveta za energetiku i ekstraktivnu industriju vlade FNRJ, Beograd

Serafim, J.L., Pereira, J.P., 1983, Considerations of geomechanics classification of Bieniawski, In: Proceedings of the International Symposium on engineering geology and underground construction, Rotterdam, Balkema, pp.1133-42

Sharma, K.G., 2009, Numerical analysis of underground structures, Indian Geotechnical Journal, 39(1), pp. 1-63

Sheory, P.R., 1997, Empirical rock failure criterion, Rotterdam, Balkema

Silva, J., Worsey, T., Lusk, B., 2018, Practical assessment of rock damage due to blasting, International Journal of Mining Science and Technology, pp. 1-7

Singh, B., Villadkar, M.N., Samadhiya, N.K., Mehrotra, V.K., 1997, Rock mass strength parameters mobilized in tunnels, Tunneling and Underground Space Technology, 12(1), 47-54

Sjöberg, J., 1993, Design methods for stope and sill pillars with application to the Zinkgruvan Mine, Central Sweden, Rock Mechanics and Rock Engineering, 26(3), pp. 253-275

Sonmez, H., Gokceoglu, C., Ulusay, R., 2004, Indirect determination of the modulus of deformation of rock masses based on the GSI system, International Journal of Rock Mechanics and Mining Scinece, 41, pp. 849-857

Sonmez, H., Gokceoglu, C., Nefeslioglu, H.A., Kayabasi, A., 2006, Estimation of rock modulus: for intact rocks with an artificial neural network and for rock masses with a new empirical equation, International Journal of Rock Mechanics and Mining Scinece, 43, pp. 554-61

Sulistianto, B., Sulaiman, S.M., Wattimena, K.R., Ardianto, A., Matsui, K., 2009, Determination of stope geometry in jointed rock mass at Pongkor underground gold mine, International Journal of the JCRM, 5(2), pp. 63-68

Tahzibi, K., Nasiri, M., Mashoof, B., Lotfi, Sh., 2016, Experimental and analytical studies to achieve an optimized cemented backfill mix to be used in a cut -fill mining method, International Journal of Mining Engineering and Mineral Processing, 5(1), pp. 1-8

Tatiya, R.R., 2005, Surface and Underground Excavations – Methods, Techniques, and Equipment, Taylor & Francis Group, LLC, pp. 405-507

REFERENCES (continued)

Thibodeau, D., Yao, M., 2015, Post-pillar design for overhand cut and fill mining in moderate to high stress conditions: a case study, In: Proceedings of ISRM Congress, International Symposium on Rock Mechanics,

Trueman, R., 1988, An evaluation of strata supports techniques in dual life gate roads, PhD thesis, University of Wales, Cardiff, In Basarir, H., 2006, Engineering geological studies and tunnel support design at Sulakyurt dam site, Turkey, Engineering Geology, 86, pp. 225-237

Vasarhelyi, B., Kovacs, D., 2017, Empirical methods of calculating the mechanical parameters of the rock mass, Periodica Polytechnica Civil Engineering, 61(1), pp. 38-50

Villaescusa E., 2014, Geotechnical Design for Sublevel Open Stoping, Taylor& Francis Group,CRC Press, pp. 113-243

Wang, J,. Pakalnis, R., Milne, D., and Lang, B., 2000, Empirical underground entry-type excavation span design modification, 53rd Annual Conference of the Canadian Geotechnical Society, p8

Yager, R.R., 1978, Fuzzy decision making including unequal objectives, Fuzzy Sets and Systems 1, pp. 87-95

Yavuz, M., Iphar, M., Once, G., 2008, The optimum support design selection by using AHP method for the main haulage road in WLC Tuncbilek colliery, Tunneling and Underground Space Technology, 23(2), pp. 111-119

Yavuz, M., 2015, The application of the analytic hierarchy process (AHP) and Yager's method in underground mining method selection problem, International Journal of Mining, Reclamation and Environment, 29(6), pp. 453-475

Yang, Zh., Zhai, Sh., Gao, Qian., Li, Maohi., 2015, Stability analysis of large scale stope using stage subsequent filling mining method in Sijiaying iron mine, Journal of Rock Mechanics and Geotechnical Engineering, 7: pp. 87-94

Yudhbir, W.L., Prinzl, F., 1983, An empirical failure criterion for rock masses, In: Proceedings of 5th International Congress on rock mechanics, Madras, pp. B1-B8

Yugo, N., Shin, W., 2015, Analysis of blasting damage in adjacent mining excavations, journal of Rock Mechanics and Geotechnical Engineering, 7, pp. 282-290

Zadeh, L.A., 1973, Outline of a new approach to the analysis of complex systems and decision process, IEEE Transactions, SMC 3, pp. 28-44

REFERENCES (continued)

Zhang, Y., Mitri, S.H., 2008, Elastopplastic stability analysis of mine haulage drift in the vicinity of mined stopes, International Journal of Rock Mechanics and Mining Science, 45, pp. 574-593

Zhang, L., 2010, Estimating the strength of jointed rock masses, Rock Mechanics and Rock Engineering, 43(4), pp. 391-402

Zhang, Z.X., 2017, Rock Mechanics related to Mining Engineering, 3rd Nordic Rock Mechanics Symposium, Johansson & Raasakka (eds), Helsink, Finland, pp. 39-64

Zhou, N., Yan, H., Jiang, Sh., Sun, Q., Ouyand, Sh., 2019, Stability analysis of surrounding rock in paste backfill recovery of residual room pillars, Sustainability - Open Access Journal, 11: pp. 1-13

APPENDIXES

Appendix A. Underground mining method selection for Trepça underground mine

Appendix B. FLAC^{3D} numerical analysis results of maximum principal stress to UCS ratio

Appendix C. FLAC^{3D} numerical analysis results of pillar yield ratio (PYR)

APPENDIX –A

Underground mining method selection for Trepça underground mine

Selection of an appropriate method for ore recovery is the basis of an underground mining operation. In this study, a numerical ranking mining method selection technique and two simple suitable multiple attribute decision-making methods are applied. The UBC, AHP, and FMADM techniques with "n" criteria have been employed to select the optimal mining method for Trepça mineral deposit in Stan Trg, Kosovo.

UBC solution technique

The UBC method was developed by (Miller-Tait et al. 1995), this technique it’s an online computer based version of the Nicholas method (EduMine, 2019). UBC is a numerical ranking mining method selection technique. The technique includes summation and rating of mathematical values related to ore body characteristics. The working principle of the UBC technique is pointing out the rightness of a mining method to the available parameters. Estimating all the scoring will result in a final score; the mining method scoring the highest will be ranked highest and is considered most appropriate (Kabwe, 2017).

In order to determine the valid alternatives for studied mine site considering the geotechnical parameters given in Table 3.1 and Table 3.5 suitable underground mining methods can be selected using online computer based version EduMine, (2019), as shown in Figure A.1. Ranking for all underground mining method alternatives is given in parenthesis. Furthermore, applying UBC rating window requires estimation of the rock mass rating (RMR) according to (Bieniawski, 1989) and rock substance strength (RSS) of the ore body and its host rock masse which specifically targets underground mining methods Peskens (2013). The rock substance strength (RSS) values were calculated dividing the uniaxial compressive strength (UCS) of the geological units to principal stress, as given in equation (E.1) and results are tabulated in Table A.1.

$$RSS = \frac{\sigma_c}{\sigma_1} \tag{E.1}$$

The principal stress values were determined by multiplying each unit weight for ore body and its host rock mass with an average depth of 600 below the ground surface. Determined RSS values are presented in Table A.1.

Table A.1. Rock substance strength (RSS) at a depth of 600 m below the ground surface.

Depth, m	Geological units	Rock substance strength (RSS)
600	Hanging wall	3.7
	Ore body	3.6
	Footwall	3.8

The final ranking is accomplished with the application of the UBC mining method selector provided by EduMine, (2019) which apply the original method by Miller-Tait et al. (1995). The mining depth at Trepça mine is more than 600 below the ground surface.

Thus, the results are presented in Figure A.1 and showing the ranking and the scored points for each mining method. It is clearly seen that the Block caving mining method is ranked number 1. Hence, block caving is the most appropriate mining method for Trepça mine when using the UBC mining method selection tool. Nevertheless, since the UBC technique is adjusted for Canadian hard rock mine so it cannot be precisely suited to Trepça underground mine.

Applicable alternatives presented in Figure A.1 can be included or excluded from the alternatives set considering either the rating given for alternatives or engineering experience. The underground mining method selection process for the mine studied site, AHP, and Fuzzy MADM techniques were performed by excluding block caving and square set stoping methods. However, four other available alternatives such as cut-and-fill stoping, sublevel caving, sublevel stoping, and top slicing were being considered.

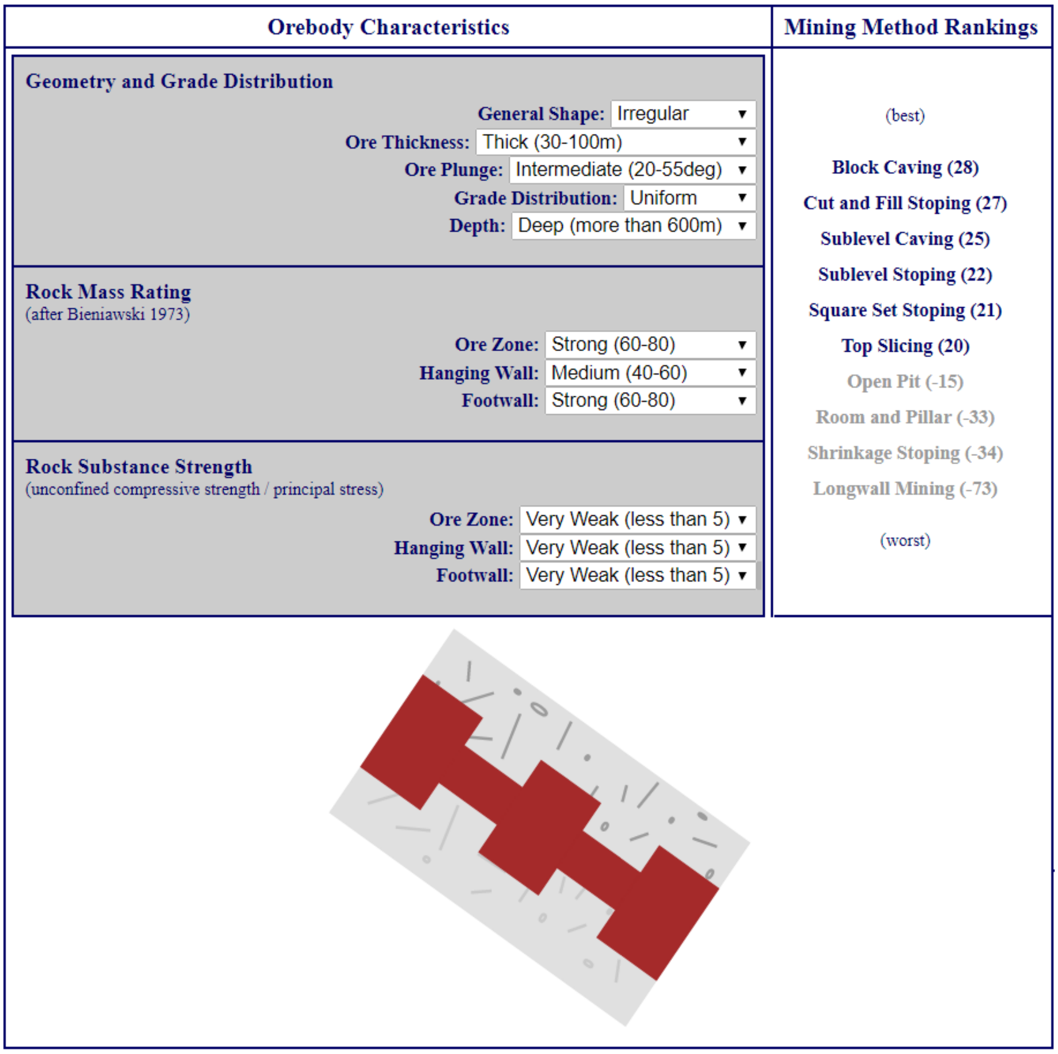

Orebody Characteristics

Mining Method Rankings

Geometry and Grade Distribution

General Shape: Irregular
Ore Thickness: Thick (30-100m)
Ore Plunge: Intermediate (20-55deg)
Grade Distribution: Uniform
Depth: Deep (more than 600m)

Rock Mass Rating
(after Bieniawski 1973)

Ore Zone: Strong (60-80)
Hanging Wall: Medium (40-60)
Footwall: Strong (60-80)

Rock Substance Strength
(unconfined compressive strength / principal stress)

Ore Zone: Very Weak (less than 5)
Hanging Wall: Very Weak (less than 5)
Footwall: Very Weak (less than 5)

(best)

Block Caving (28)
Cut and Fill Stoping (27)
Sublevel Caving (25)
Sublevel Stoping (22)
Square Set Stoping (21)
Top Slicing (20)
Open Pit (-15)
Room and Pillar (-33)
Shrinkage Stoping (-34)
Longwall Mining (-73)

(worst)

Figure A.1. UBC ranking tool for depth > 600m at Trepça underground mine (EduMine, 2019).

The AHP and FMADM solution techniques

In order to optimize the mining method selection process to be able to control the wide spectrum of mineral deposit new techniques were implemented. These techniques are based on Multiple Criteria Decision Making (MCDM) and are called AHP and FMADM approaches.

Additionally, in this thesis, the AHP and FMADM approaches will be used on the different available stoping method given in Figure A.1. The methods which can be applied for this underground mine were determined by the experts.

Those are given below:

1. Cut-and-Fill stoping method (C&F)
2. Sublevel caving method (SC)
3. Sublevel stoping method (ST)
4. Top slicing method (TS)

The criteria were also determined by the experts and clustered into main groups and their subgroups as given below:

1. Production criteria (C_1)
    a. Mechanization possibilities (C_{11})
    b. Flexibility (C_{12})
    c. Method changing (C_{13})

2. Technological criteria (C_2)
    a. Concentration (C_{21})
    b. Selectivity (C_{22})
    c. Ore winning (C_{23})
    d. Dilatation (C_{24})

3. Management criteria (C_3)
    a. Organizations (C_{31})
    b. Safety (C_{32})

4. Economic criteria (C_4)
    a. Investment cost (C_{41})
    b. Production cost (C_{42})

The AHP solution technique

In order to start solving the problem with the AHP approach, the problem was structured in a hierarchy of different levels comprising of goal, criteria, and alternative, as shown in Figure A.2. After structuring the hierarchy, the pair-wise comparison matrix for each level was constructed. For the pair-wise comparison values, a simple scale is used given in Table 3.12. All main criteria affecting underground mining method selection were compared to each other by the experts and the pair-wise comparison matrix is given in Table A.2 was constructed.

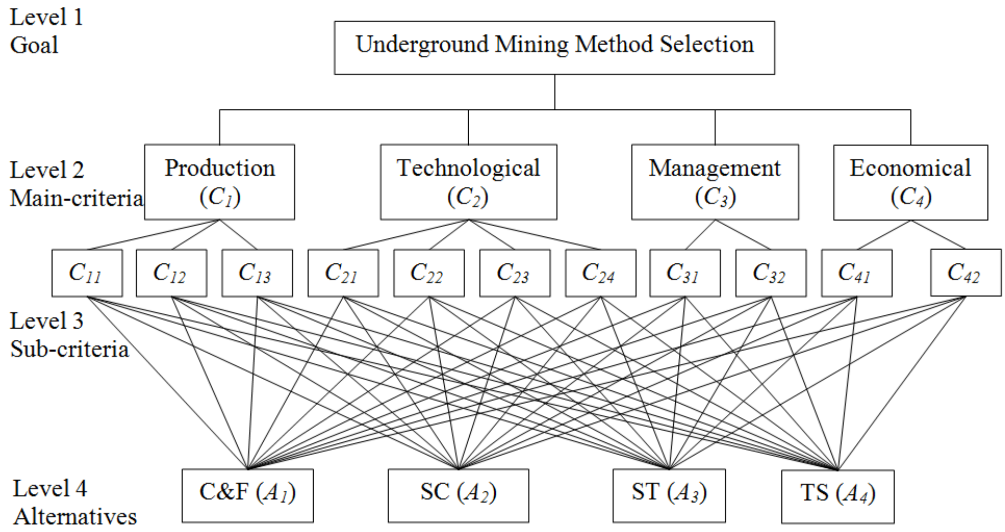
Level 1
Goal
Underground Mining Method Selection
Level 2
Main-criteria
Production (C_1)
Technological (C_2)
Management (C_3)
Economical (C_4)
C_{11}
C_{12}
C_{13}
C_{21}
C_{22}
C_{23}
C_{24}
C_{31}
C_{32}
C_{41}
C_{42}
Level 3
Sub-criteria
Level 4
Alternatives
C&F (A_1)
SC (A_2)
ST (A_3)
TS (A_4)

Figure A.2.The hierarchy structure of the problem

It is obvious that the Economic criterion is the most important criteria (with a rating of 0.440) and it is followed by the technological criterion.

Table A.2.Pair-wise comparison matrix of main criterion.

	C_1	C_2	C_3	C_4	W
C_1	1	1/3	3	1/2	0.190
C_2	3	1	2	1/3	0.268
C_3	1/3	1/2	1	1/4	0.102
C_4	2	3	4	1	0.440
$\lambda_{max} = 4.226; CR = 0.084 \leq 0.1$					

After comparing the main criteria, a similar procedure was also performed for all their sub-group criteria by the experts and the following comparison matrices are given in Table A.3, A.4, A.5, and A.6, respectively were constructed.

Table A.3. Pair-wise comparison matrix of sub-group criteria of production criterion.

	C_{11}	C_{12}	C_{13}	W
C_{11}	1	2	3	0.540
C_{12}	1/2	1	2	0.297
C_{13}	1/3	1/2	1	0.163
$\lambda_{max} = 3.009; CR = 0.008 \leq 0.1$				

At the next step, the pair-wise comparison of the alternatives based on each sub-criterion should be performed. Hence, eleven matrices were formed. As there are four Alternatives, the matrix order is (4×4).

Table A.4.Pair-wise comparison matrix of sub-group criteria of technological criterion.

	C_{21}	C_{22}	C_{23}	C_{24}	W
C_{21}	1	1/2	1/3	2	0.160
C_{22}	2	1	1/2	3	0.278
C_{23}	3	2	1	4	0.467
C_{24}	1/2	1/3	1/4	1	0.095
$\lambda_{max} = 4.031; CR = 0.011 \leq 0.1$					

Table A.5. Pair-wise comparison matrix of sub-group criteria of management criterion.

	C_{31}	C_{32}	W
C_{31}	1	2	0.667
C_{32}	1/2	1	0.333
$\lambda_{max} = 2; CR = 0 \leq 0.1$			

Table A.6. Pair-wise comparison matrix of sub-group criteria of economical criterion.

	C_{41}	C_{42}	W
C_{41}	1	1/2	0.333
C_{42}	2	1	0.667
$\lambda_{max} = 2; CR = 0 \leq 0.1$			

One example of comparison matrices (e.g. flexibility) is presented in Table A.7. Table A.8 shows overall priorities estimated for the sub-criteria of the main criterion production. It is easily observed from Table A.8 that the most appropriate mining method selection is cut-and-fill stoping method when adjusted by the criterion of production.

Table A.7.Pair-wise comparison matrix of alternatives based on flexibility sub-criterion.

	C&F	SC	ST	TS	W
C&F	1	3	5	7	0.564
SC	1/3	1	3	5	0.263
ST	1/5	1/3	1	3	0.118
TS	1/7	1/5	1/3	1	0.055
$\lambda_{max} = 4.117; CR = 0.043 \leq 0.1$					

Table A.8.Overall priorities of production main criterion.

	C_{11}	C_{12}	C_{13}	W
C&F	0.467	0.564	0.472	0.497
SC	0.278	0.263	0.285	0.275
ST	0.160	0.118	0.170	0.149
TS	0.095	0.055	0.073	0.080

The overall rating of each alternative is calculated by summing the product of the relative priority of each criterion and the relative priority of the alternative considering the corresponding criteria. Thus, the overall rating of alternative ‘cut-and-fill stoping method’ is estimated as; $(0.467 \times 0.540) + (0.564 \times 0.297) + (0.472 \times 0.163) = 0.497$. The final matrix is presented in Table A.9.

Table A.9.Overall results/final matrix.

	C_1	C_2	C_3	C_4	Overall
C&F	0.497	0.473	0.149	0.471	0.443
SC	0.275	0.240	0.238	0.242	0.247
ST	0.149	0.205	0.397	0.133	0.182
TS	0.080	0.083	0.217	0.153	0.127
Main	0.190	0.268	0.102	0.440	

Since the comparisons are based on the subjective evaluation, consistency ratios CR were estimated using equation (3.5), ensuring the selection accuracy. Hence, the results show that the maximum Eigen values (λ_{max})were near to the size of the corresponding matrices and the CR values for all matrices were less than 0.10. However, overall results in Table A.9 shows that the alternative 'cut-and-fill stoping method' should be selected as the optimum underground mining method for Trepça mine due to the priority of this alternative (0.443) is the highest value compared with the other alternatives.

The FMADM solution approach

In Fuzzy MADM solution the set of possible alternatives is A = {*C&F*, *SC*, *ST*, *TS*}and the set of selection criteria is C = {C_{11}, C_{12}, C_{13}, C_{21}, C_{22}, C_{23}, C_{24}, C_{31}, C_{32}, C_{41}, C_{42}}. For this method, the decision maker was asked to define the membership levels of each criterion after conferring with the experts. Table A.10 shows the membership levels of each criterion. The respective weights of the criteria were obtained by using Fuzzy MADM approach. Those are given in Table A.11.The final eigenvector corresponds to the weights to be associated with the memberships of each criterion. The exponential weighting was consequently defined from each criterion as: α_1= 0.102, α_2= 0.056, α_3= 0.031, α_4= 0.043, α_5= 0.075, α_6= 0.125, α_7= 0.026, α_8= 0.068, α_9= 0.034, α_{10}= 0.147, α_{11}= 0.293.

Table A.10. Membership level of each criterion.

	Alternatives			
	Cut-and-Fill stoping	Sublevel caving	Sublevel stoping	Top slicing
C_{11}	0.80	0.60	0.40	0.20
C_{12}	0.95	0.60	0.40	0.05
C_{13}	0.65	0.50	0.45	0.20
C_{21}	0.80	0.60	0.60	0.40
C_{22}	0.95	0.80	0.65	0.60
C_{23}	0.80	0.60	0.60	0.40
C_{24}	0.40	0.60	0.80	0.20
C_{31}	0.40	0.60	0.80	0.20
C_{32}	0.20	0.60	0.60	0.80
C_{41}	0.80	0.60	0.40	0.80
C_{42}	0.60	0.80	0.40	0.20

Table A.11.Eigenvalues of criteria.

Main	Sub	Eigenvector		
		Sub	Main	Final
C_1	C_{11}	0.540	0.190	0.102
	C_{12}	0.297		0.056
	C_{13}	0.163		0.031
C_2	C_{21}	0.160	0.268	0.043
	C_{22}	0.278		0.075
	C_{23}	0.467		0.125
	C_{24}	0.095		0.026
C_3	C_{31}	0.667	0.102	0.068
	C_{32}	0.333		0.034
C_4	C_{41}	0.333	0.440	0.147
	C_{42}	0.667		0.293

According to Yager (1978), the membership decision function was determined for each alternative and they are given in Table A.12.

Table A.12. Membership decision function of each criterion by Yager's method.

	Alternatives			
	Cut-and-Fill Stoping	Sublevel Caving	Sublevel Stoping	Top Slicing
C_{11}	0.977	0.949	0.910	**0.848**
C_{12}	0.997	0.972	0.950	0.845
C_{13}	0.987	0.979	0.976	0.951
C_{21}	0.990	0.978	0.978	0.961
C_{22}	0.996	0.984	0.968	0.963
C_{23}	0.972	**0.938**	0.938	0.892
C_{24}	0.977	0.987	0.994	0.960
C_{31}	0.940	0.966	0.985	0.896
C_{32}	0.947	0.983	0.983	0.992
C_{41}	**0.968**	0.928	0.874	0.968
C_{42}	0.861	0.937	**0.764**	0.624
Min	0.861	0.928	0.764	0.624

Applying the max-min Bellman and Zadeh, (1970) principle, the final set is determined as shown and bellow yielding the result are;

$$\mu D(A) = \left\{\frac{C\&F}{0.968}, \frac{SC}{0.938}, \frac{ST}{0.764}, \frac{TS}{0.848}\right\} \quad \text{(E.2)}$$

The optimal solution is;

$$\mu D(A*) = max\big(\mu D(A1)\big) = 0.968 \quad \text{(E.3)}$$

The results obtained from equation (E.3), shows that the Cut-and-Fill Stoping Method (A1) is the most desired one.

APPENDIX –B

FLAC^{3D} numerical analysis results of maximum principal stress to UCS ratio

Table B.1. Numerical results of maximum principal stress to UCS and pillar width to height ratio using hydraulic filling material.

Depth (m)	Stoping parameters			Stoping height (m)	Total stages	Pillar no.	$\frac{w_p}{h_p}$	$\frac{\sigma_{max}}{UCS}$
	R_{MAX} (%)	$w_p(m)$	$w_o(m)$					
453	70	13	10	4	8	HW1	3.25	23.56/78 = 0.30
						HW2	3.25	22.85/78 = 0.29
						HW3	3.25	23.61/78 = 0.30
						FW1	3.25	32.21/78 = 0.41
						FW2	3.25	33.39/78 = 0.43
						FW3	3.25	31.89/78 = 0.40
453	75	12	12	4	8	HW1	3.0	25.95/78 = 0.33
						HW2	3.0	24.33/78 = 0.31
						HW3	3.0	25.95/78 = 0.33
						FW1	3.0	34.24/78 = 0.43
						FW2	3.0	36.34/78 = 0.46
						FW3	3.0	34.25/78 = 0.43
453	80	10	14	4	8	HW1	2.5	26.31/78 = 0.33
						HW2	2.5	23.84/78 = 0.30
						HW3	2.5	26.30/78 = 0.33
						FW1	2.5	37.25/78 = 0.47
						FW2	2.5	40.92/78 = 0.52
						FW3	2.5	37.24/78 = 0.47
453	90	7	15	4	8	HW1	1.75	22.28/78 = 0.28
						HW2	1.75	20.71/78 = 0.26
						HW3	1.75	22.53/78 = 0.29
						FW1	1.75	31.45/78 = 0.40
						FW2	1.75	32.15/78 = 0.41
						FW3	1.75	31.56/78 = 0.40
573	70	13	10	4	8	HW1	3.25	29.12/78 = 0.37
						HW2	3.25	27.41/78 = 0.35
						HW3	3.25	29.25/78 = 0.37
						FW1	3.25	39.05/78 = 0.50
						FW2	3.25	40.87/78 = 0.52
						FW3	3.25	38.62/78 = 0.49
573	75	12	12	4	8	HW1	3.0	31.40/78 = 0.40
						HW2	3.0	28.33/78 = 0.36
						HW3	3.0	31.42/78 = 0.40
						FW1	3.0	41.67/78 = 0.53
						FW2	3.0	45.16/78 = 0.57
						FW3	3.0	41.67/78 = 0.53

Table B.1. Numerical results of maximum principal stress to UCS and pillar width to height ratio using hydraulic filling material (continued).

Depth (m)	Stoping parameters			Stoping height (m)	Total stages	Pillar no.	$\frac{w_p}{h_p}$	$\frac{\sigma_{max}}{UCS}$
	RMAX (%)	$w_p(m)$	$w_o(m)$					
573	80	10	14	4	8	HW1	2.5	30.70/78 = 0.39
						HW2	2.5	27.26/78 = 0.34
						HW3	2.5	30.70/78 = 0.39
						FW1	2.5	45.95/78 = 0.58
						FW2	2.5	51.44/78 = 0.65
						FW3	2.5	45.95/78 = 0.58
573	90	7	15	4	8	HW1	1.75	25.75/78 = 0.33
						HW2	1.75	23.59/78 = 0.30
						HW3	1.75	25.56/78 = 0.32
						FW1	1.75	35.35/78 = 0.45
						FW2	1.75	36.16/78 = 0.46
						FW3	1.75	35.48/78 = 0.45
693	70	13	10	4	8	HW1	3.25	33.71/78 = 0.43
						HW2	3.25	31.29/78 = 0.40
						HW3	3.25	34.01/78 = 0.44
						FW1	3.25	46.49/78 = 0.59
						FW2	3.25	48.86/78 = 0.63
						FW3	3.25	45.76/78 = 0.58
693	75	12	12	4	8	HW1	3.0	35.79/78 = 0.46
						HW2	3.0	31.87/78 = 0.41
						HW3	3.0	35.78/78 = 0.46
						FW1	3.0	50.17/78 = 0.64
						FW2	3.0	54.17/78 = 0.69
						FW3	3.0	50.17/78 = 0.64
693	80	10	14	4	8	HW1	2.5	34.34/78 = 0.44
						HW2	2.5	30.33/78 = 0.39
						HW3	2.5	34.36/78 = 0.44
						FW1	2.5	55.60/78 = 0.71
						FW2	2.5	63.19/78 = 0.81
						FW3	2.5	55.61/78 = 0.71
693	90	7	15	4	8	HW1	1.75	28.67/78 = 0.37
						HW2	1.75	26.19/78 = 0.34
						HW3	1.75	28.48/78 = 0.36
						FW1	1.75	39.05/78 = 0.50
						FW2	1.75	39.87/78 = 0.51
						FW3	1.75	39.15/78 = 0.50
813	70	13	10	4	8	HW1	3.25	37.63/78 = 0.48
						HW2	3.25	34.63/78 = 0.44
						HW3	3.25	38.13/78 = 0.49
						FW1	3.25	53.78/78 = 0.69
						FW2	3.25	56.05/78 = 0.72
						FW3	3.25	52.99/78 = 0.67

Table B.1. Numerical results of maximum principal stress to UCS and pillar width to height ratio using hydraulic filling material (continued).

Depth (m)	Stoping parameters			Stoping height (m)	Total stages	Pillar no.	$\frac{w_p}{h_p}$	$\frac{\sigma_{max}}{UCS}$
	R_{MAX} (%)	$w_p(m)$	$w_o(m)$					
933	70	13	10	4	8	HW1	3.25	41.11/78 = 0.53
						HW2	3.25	37.62/78 = 0.48
						HW3	3.25	41.68/78 = 0.53
						FW1	3.25	60.62/78 = 0.78
						FW2	3.25	63.46/78 = 0.81
						FW3	3.25	59.57/78 = 0.76
933	75	12	12	4	8	HW1	3.0	42.18/78 = 0.54
						HW2	3.0	37.87/78 = 0.48
						HW3	3.0	42.20/78 = 0.54
						FW1	3.0	66.69/78 = 0.85
						FW2	3.0	74.06/78 = 0.95
						FW3	3.0	66.70/78 = 0.85

Table B.2. Numerical results of maximum principal stress to UCS and pillar width to height ratio using cemented rock filling material

Depth (m)	Stoping parameters			Stoping height (m)	Total stages	Pillar no.	$\frac{w_p}{h_p}$	$\frac{\sigma_{max}}{UCS}$
	R_{MAX} (%)	$w_p(m)$	$w_o(m)$					
453	70	13	10	4	8	HW1	3.25	23.54/78 = 0.30
						HW2	3.25	22.78/78 = 0.29
						HW3	3.25	23.60/78 = 0.30
						FW1	3.25	32.10/78 = 0.41
						FW2	3.25	33.26/78 = 0.42
						FW3	3.25	31.78/78 = 0.40
573	70	13	10	4	8	HW1	3.25	29.10/78 = 0.37
						HW2	3.25	27.38/78 = 0.35
						HW3	3.25	29.24/78 = 0.37
						FW1	3.25	39.04/78 = 0.50
						FW2	3.25	40.75/78 = 0.52
						FW3	3.25	38.62/78 = 0.49
693	70	13	10	4	8	HW1	3.25	33.79/78 = 0.43
						HW2	3.25	31.38/78 = 0.40
						HW3	3.25	34.11/78 = 0.43
						FW1	3.25	46.59/78 = 0.59
						FW2	3.25	48.90/78 = 0.62
						FW3	3.25	45.86/78 = 0.58
813	70	13	10	4	8	HW1	3.25	37.87/78 = 0.49
						HW2	3.25	34.78/78 = 0.44
						HW3	3.25	38.34/78 = 0.49
						FW1	3.25	54.01/78 = 0.69
						FW2	3.25	56.21/78 = 0.72
						FW3	3.25	53.18/78 = 0.68
933	70	13	10	4	8	HW1	3.25	41.40/78 = 0.53
						HW2	3.25	37.75/78 = 0.48
						HW3	3.25	41.94/78 = 0.53
						FW1	3.25	60.91/78 = 0.78
						FW2	3.25	63.68/78 = 0.81
						FW3	3.25	59.8878 = 0.76

APPENDIX –C

FLAC^{3D} numerical analysis results of pillar yield ratio (PYR)

Table C.1. Numerical results of extent of failure zone (PYR) using hydraulic filling material

Depth (m)	R$_{MAX}$ (%)	Stoping height (m)	Total stages	Pillar no.	Pillar Yield Ratio (PYR)			Section view	Failure zone
					X-X	Y-Y	Z-Z		
453	70	4	8	HW1	11%	9%	**27%**	Z-Z	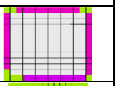
				HW2	11%	10%	**27%**	Z-Z	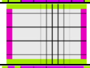
				HW3	11%	12%	**27%**	Z-Z	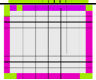
				FW1	14%	9%	**26%**	Z-Z	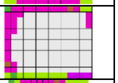
				FW2	19%	14%	**31%**	Z-Z	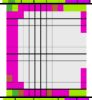
				FW3	14%	14%	**26%**	Z-Z	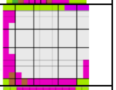
453	75	4	7	HW1	12%	11%	**30%**	Z-Z	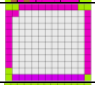
				HW2	12%	11%	**29%**	Z-Z	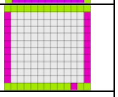
				HW3	12%	9%	**30%**	Z-Z	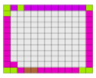
				FW1	16%	15%	**33%**	Z-Z	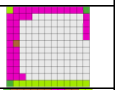
				FW2	20%	23%	**39%**	Z-Z	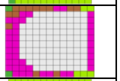
				FW3	16%	15%	**33%**	Z-Z	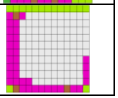

Table C.1. Numerical results of extent of failure zone (PYR) using hydraulic filling material (continued).

Depth (m)	R_{MAX} (%)	Stoping height (m)	Total stages	Pillar no.	Pillar Yield Ratio (PYR)			Section view	Failure zone
					X-X	Y-Y	Z-Z		
453	80	4	8	HW1	15%	11%	**35%**	Z-Z	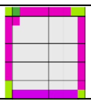
				HW2	15%	13%	**34%**	Z-Z	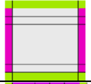
				HW3	15%	11%	**35%**	Z-Z	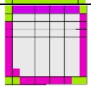
				FW1	30%	31%	**48%**	Z-Z	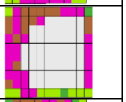
				FW2	40%	45%	**59%**	Z-Z	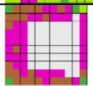
				FW3	30%	31%	**48%**	Z-Z	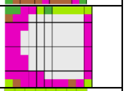
453	90	4	8	HW1	21%	15%	**42%**	Z-Z	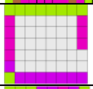
				HW2	21%	12%	**46%**	Z-Z	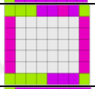
				HW3	21%	12%	**42%**	Z-Z	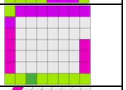
				FW1	57%	**62%**	57%	Y-Y	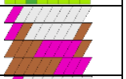
				FW2	58%	**62%**	58%	Y-Y	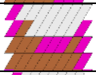
				FW3	57%	**62%**	57%	Y-Y	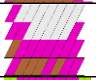
573	70	4	8	HW1	11%	12%	**28%**	Z-Z	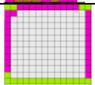
				HW2	11%	12%	**28%**	Z-Z	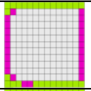
				HW3	11%	12%	**28%**	Z-Z	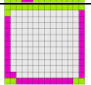
				FW1	22%	17%	**36%**	Z-Z	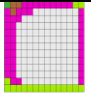
				FW2	25%	26%	**39%**	Z-Z	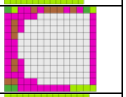
				FW3	20%	21%	**36%**	Z-Z	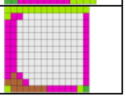

Table C.1. Numerical results of extent of failure zone (PYR) using hydraulic filling material (continued).

Depth (m)	R_{MAX} (%)	Stoping height (m)	Total stages	Pillar no.	Pillar Yield Ratio (PYR)			Section view	Failure zone
					X-X	Y-Y	Z-Z		
573	75	4	8	HW1	12%	13%	**30%**	Z-Z	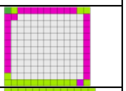
				HW2	12%	13%	**30%**	Z-Z	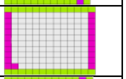
				HW3	12%	13%	**30%**	Z-Z	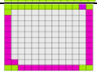
				FW1	27%	28%	**44%**	Z-Z	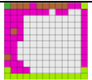
				FW2	33%	34%	**52%**	Z-Z	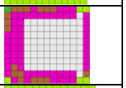
				FW3	27%	28%	**44%**	Z-Z	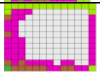
573	80	4	8	HW1	17%	15%	**35%**	Z-Z	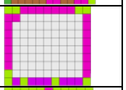
				HW2	15%	13%	**34%**	Z-Z	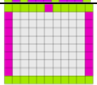
				HW3	17%	15%	**35%**	Z-Z	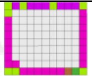
				FW1	45%	45%	**59%**	Z-Z	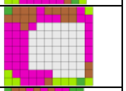
				FW2	60%	52%	**67%**	Z-Z	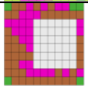
				FW3	45%	45%	**59%**	Z-Z	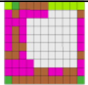
573	90	4	8	HW1	26%	35%	**46%**	Z-Z	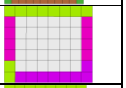
				HW2	21%	35%	**46%**	Z-Z	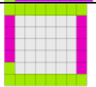
				HW3	25%	35%	**44%**	Z-Z	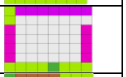
				FW1	60%	62%	**62%**	Z-Z	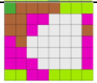
				FW2	67%	65%	**71%**	Z-Z	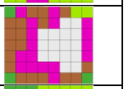
				FW3	62%	62%	**64%**	Z-Z	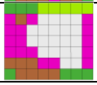

Table C.1. Numerical results of extent of failure zone (PYR) using hydraulic filling material (continued).

Depth (m)	R_{MAX} (%)	Stoping height (m)	Total stages	Pillar no.	Pillar Yield Ratio (PYR)			Section view	Failure zone
					X-X	Y-Y	Z-Z		
693	70	4	8	HW1	15%	14%	**29%**	Z-Z	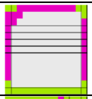
				HW2	11%	12%	**28%**	Z-Z	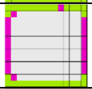
				HW3	15%	14%	**29%**	Z-Z	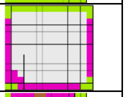
				FW1	27%	32%	**45%**	Z-Z	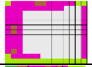
				FW2	32%	36%	**47%**	Z-Z	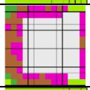
				FW3	27%	29%	**44%**	Z-Z	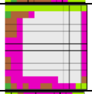
693	75	4	8	HW1	19%	13%	**31%**	Z-Z	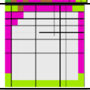
				HW2	12%	13%	**30%**	Z-Z	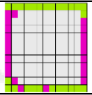
				HW3	19%	13%	**31%**	Z-Z	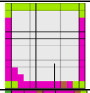
				FW1	31%	35%	**51%**	Z-Z	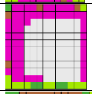
				FW2	42%	42%	**59%**	Z-Z	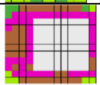
				FW3	31%	35%	**51%**	Z-Z	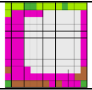
693	80	4	8	HW1	25%	16%	**36%**	Z-Z	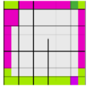
				HW2	20%	16%	**35%**	Z-Z	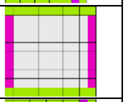
				HW3	25%	16%	**36%**	Z-Z	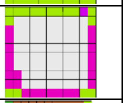
				FW1	57%	52%	**67%**	Z-Z	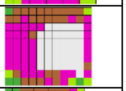
				FW2	65%	66%	**72%**	Z-Z	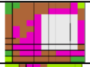
				FW3	57%	52%	**68%**	Z-Z	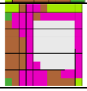

Table C.1. Numerical results of extent of failure zone (PYR) using hydraulic filling material (continued).

Depth (m)	R_{MAX} (%)	Stoping height (m)	Total stages	Pillar no.	Pillar Yield Ratio (PYR)			Section view	Failure zone
					X-X	Y-Y	Z-Z		
693	90	4	8	HW1	34%	28%	**46%**	Z-Z	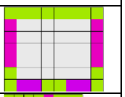
				HW2	28%	22%	**46%**	Z-Z	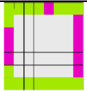
				HW3	32%	25%	**46%**	Z-Z	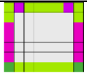
				FW1	66%	66%	**73%**	Z-Z	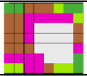
				FW2	71%	69%	**79%**	Z-Z	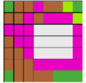
				FW3	68%	66%	**73%**	Z-Z	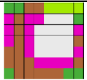
813	70	4	8	HW1	17%	14%	**30%**	Z-Z	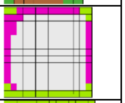
				HW2	13%	14%	**31%**	Z-Z	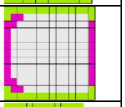
				HW3	18%	14%	**30%**	Z-Z	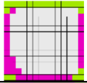
				FW1	35%	36%	**49%**	Z-Z	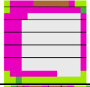
				FW2	38%	41%	**55%**	Z-Z	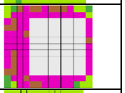
				FW3	35%	36%	**49%**	Z-Z	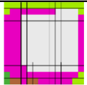
933	70	4	8	HW1	19%	14%	**31%**	Z-Z	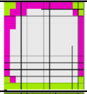
				HW2	18%	14%	**30%**	Z-Z	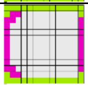
				HW3	19%	14%	**32%**	Z-Z	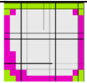
				FW1	35%	41%	**54%**	Z-Z	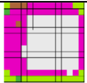
				FW2	43%	46%	**55%**	Z-Z	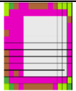
				FW3	34%	37%	**52%**	Z-Z	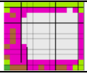

Table C.1. Numerical results of extent of failure zone (PYR) using hydraulic filling material (continued).

Depth (m)	R_{MAX} (%)	Stoping height (m)	Total stages	Pillar no.	Pillar Yield Ratio (PYR)			Section view	Failure zone
					X-X	Y-Y	Z-Z		
933	75	4	8	HW1	23%	15%	**35%**	Z-Z	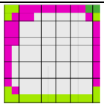
				HW2	16%	15%	**33%**	Z-Z	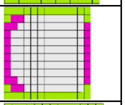
				HW3	23%	15%	**35%**	Z-Z	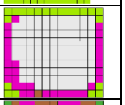
				FW1	39%	44%	**63%**	Z-Z	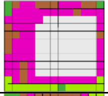
				FW2	54%	52%	**69%**	Z-Z	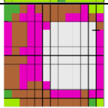
				FW3	39%	44%	**63%**	Z-Z	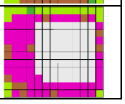

Table C.2. Numerical results of extent of failure zone (PYR) using cemented rock filling material.

Depth (m)	R_{MAX} (%)	Stoping height (m)	Total stages	Pillar no.	Pillar Yield Ratio (PYR)			Section view	Failure zone
					X-X	Y-Y	Z-Z		
453	70	4	8	HW1	11	9	**28**	Z-Z	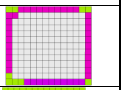
				HW2	11	11	**27**	Z-Z	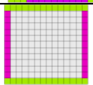
				HW3	11	9	**28**	Z-Z	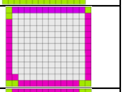
				FW1	14	11	**27**	Z-Z	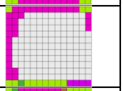
				FW2	14	14	**32**	Z-Z	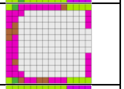
				FW3	14	11	**26**	Z-Z	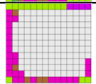
573	70	4	8	HW1	12	13	**28**	Z-Z	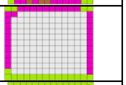
				HW2	12	13	**29**	Z-Z	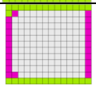
				HW3	12	13	**28**	Z-Z	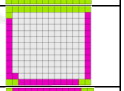
				FW1	21	20	**36**	Z-Z	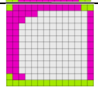
				FW2	25	23	**41**	Z-Z	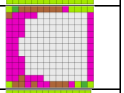
				FW3	21	20	**36**	Z-Z	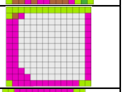
933	70	4	8	HW1	19	14	**32**	Z-Z	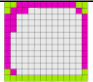
				HW2	19	14	**32**	Z-Z	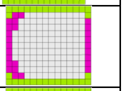
				HW3	19	14	**33**	Z-Z	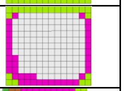
				FW1	36	39	**53**	Z-Z	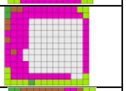
				FW2	43	46	**55**	Z-Z	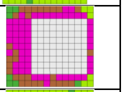
				FW3	35	38	**52**	Z-Z	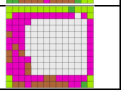

CURRICULUM VITAE

PERSONAL INFORMATION

Surname, Name: Ibishi, Gzim
Nationality: Albanian
Data and Place of Birth: 08 October 1988, Mitrovica/Kosovo
Marital Status: Engaged
Contact details: E-mail: gzim-ibishi@hotmail.com
Phone: +383 (0) 44176357

EDUCATION

Degree	Institution	Year of Graduation
Master of Science	University of Prishtina Mining Engineering Department	2014
Bachelor of Science	University of Prishtina Mining Engineering Department	2011
High School	Professional High School "Latif Berisha"	2008

WORK EXPERIENCE

Year	Place	Enrollment
2014 - Present	Public University of Mitrovica	Research Assistant

FOREIGN LANGUAGES

English, Turkish

HOBBIES

Playing table tennis, Photography, Movies.